

**Paleoseismology and Neotectonics
of the Central and Eastern Garlock Fault, California**

**Dissertation by
Sara Hanley Fagerson McGill**

**In Partial Fulfillment of the Requirements
for the Degree of Doctor of Philosophy**

California Institute of Technology

Pasadena, California

1992

(Submitted September 13, 1991)

Moreover, when God gives anyone wealth and possessions, and enables her to enjoy them, to accept her lot and to be happy in her work-- this is a gift from God.

Ecclesiastes 5:19

Dedicated to John McGill

ACKNOWLEDGMENTS

This work was supported by the U. S. Geological Survey's National Earthquake Hazards Reduction Program, grants #14-08-0001-G1789 and #14-08-0001-G1370 and by the Koons Field Research Fellowship. Topographic maps and trench logs were surveyed with a Wild TC-2000 total station purchased with funds from the W. M. Keck Foundation and from U. S. Geological Survey Earthquake Hazards Reduction Program grant #14-08-0001-G1177.

I thank the China Lake Naval Weapons Center for allowing access to the portion of the fault within the Naval Weapons Center and for permitting the excavations discussed in Chapter 2. Allan Katzenstein, Glenn Roquemore, and John Zellmer assisted in relations with Naval Weapons Center.

Captain Michael Williams, Sergeant Michael O'Brian, and a number of others assisted with access to the portion of the fault in Fort Irwin Military Reservation.

I thank the Bureau of Land Management, Ridgecrest Office, for granting permission to excavate the site discussed in Chapter 4 and Joe Liebhauser for coordinating relations with the BLM.

Special thanks go to everyone who helped out with the field work: Heidi Anderson, Laura Birkett, Steve Bryant, Chris Campo, Joe Cheng, Dana Coyle, Lisa Grant, Greg Holk, Wei-Shi Huang, Laura Jones, Tanya Kurosky, Eric Lange, Everett Lee, Linda Maepa, John McGill, Carol Prentice, Helen Qian, Glenn Roquemore,

Mike Slates, Rob Speiler, Pierre St. Amand, Lauren Western, and Eric Wilmanns.

I thank Malcolm Clark for lending me U.S.G.S. aerial photographs flown for his Garlock fault investigations.

Thanks go to George I. Smith for sharing his unpublished mapping of and dates for deposits of Searles Lake, and for many helpful discussions of the history of Searles Lake and the Garlock fault.

Lee Silver assisted with the search for shell fragments in the beach deposits discussed in Chapter 2.

Jan Mayne and Lisa Grant assisted with drafting of figures.

Malcolm Clark, Dana Coyle, Ken Hudnut, Craig Jones, Phil Pearthree, Tom Rockwell, and Jon Spencer provided helpful reviews of Chapter 3.

I thank Eugene Rivers for encouraging me to enter graduate school and my family, especially John McGill and my parents, for moral support.

I especially thank Kerry Sieh for all that he has taught me and for making graduate school enjoyable.

ABSTRACT

The Garlock fault is one of the major active faults in California. Although it has not produced any large earthquakes during historic times, abundant fault scarps in Holocene deposits and offset geomorphic features attest to the occurrence of large, prehistoric earthquakes on this fault. In an effort to better characterize the seismic hazard associated with the Garlock fault, I have measured the slip rate of the fault in southeastern Searles Valley, documented the left-lateral displacement associated with past earthquakes on the central and eastern portions of the fault, estimated the size and frequency of those earthquakes, and constrained the age of the most recent large earthquake on the portion of the fault in Searles Valley.

A latest-Pleistocene shoreline at the overflow-level of Searles Lake has been offset 82 to 106 meters (best estimate = 90 m) along the Garlock fault, in southeastern Searles Valley. Radiocarbon dates from both surface and subsurface units indicate that the most recent highstand of Searles Lake ended sometime between 10,000 and 13,800 radiocarbon years ago (Stuiver and Smith, 1979; Benson and others, 1990; Bard and others, 1990). The maximum slip rate of the Garlock fault in southeastern Searles Valley is thus 10.6 mm/ $^{14}\text{C-yr}$. If part of the offset of the shoreline is a remnant from older lakestands, then the slip rate may be somewhat less, but a channel that incised after the most recent highstand is offset 69 ± 2 m, indicating that the minimum slip rate is 5 mm/ $^{14}\text{C-yr}$. Subjective evaluation of the constraints on the offset and on the age of the shoreline suggest that the slip rate is

most likely between 6 and 8 mm/ $^{14}\text{C-yr}$ at this site. If Bard and others' (1990) calibration of the radiocarbon timescale is correct, then the true slip rate of the Garlock fault is between 4 and 9 mm/yr and most likely between 5 and 7 mm/yr.

This slip rate is consistent with the 7^{+1}_{-2} mm/ $^{14}\text{C-yr}$ rate determined by Clark and Lajoie (1974) at Koehn Lake. Considering the Quaternary, west-northwestward extension that has occurred north of the Garlock fault, one might expect the slip rate of the Garlock fault to decrease eastward (Davis and Burchfiel, 1973). The slip rate determined in southeastern Searles Valley indicates that no eastward decrease in the Garlock fault slip rate is required between Koehn Lake and Searles Lake, but an eastward decrease of up to 3 mm/yr is plausible.

Geomorphic features offset along the central and eastern Garlock fault record the amount of left-lateral surface slip associated with prehistoric earthquakes. Along the easternmost 90 km of the fault, the smallest offsets cluster around 2-3 m, apparently associated with the most recent rupture of this portion of the fault. Larger offsets along this part of the fault, especially in Pilot Knob Valley, cluster around values consistent with 2 to 4 m of slip in each of the past several events. Farther west, south of El Paso Mountains, offset geomorphic features suggest that each of the past two earthquakes on this stretch of the Garlock fault was produced by about 7 m of slip, whereas the third event back resulted from about 4 m of slip.

Vertical displacements of geomorphic features range from 0% to 30% of the left-lateral offsets. Within Pilot Knob Valley (along the southern side of the Slate Range) vertical displacements are consistently up on the northern side, whereas within the Avawatz Mountains both north- and south-side-up displacements are present.

On the basis of the geomorphic offsets, the geometry of the Garlock fault, and the precedents set by historical strike-slip earthquakes elsewhere, a number of different rupture patterns are plausible. These range from rupture of the entire Garlock fault in a single event with a maximum magnitude of about $M_w=7.8$, to separate rupture of the western segment and of the central and eastern segments combined, with approximate magnitudes of $M_w<7.7$ and $M_w=7.5$, respectively, to separate rupture of even shorter segments, producing earthquakes of magnitudes $M_w=6.6$ to $M_w=7.5$.

In conjunction with available slip rates for the Garlock fault, the geomorphic offsets suggest that average recurrence intervals are probably within the range of 600-1200 yr south of El Paso Mountains, about 200-750 yr in Searles Valley, about 200-1300 yr in Pilot Knob Valley, and about 200-3000 yr near Leach Lake and in the Avawatz Mountains.

Stratigraphic relations exposed in two trenches across the Garlock fault in Searles Valley provide clear evidence for several Late Holocene, prehistoric faulting events. A radiocarbon date on detrital charcoal from one of the trenches indicates

that the most recent surface-faulting event on this portion of the Garlock fault occurred no more than 530 years ago. This earthquake probably had a magnitude in the range of $M_w = 7.2$ to $M_w \leq 7.8$. Historical evidence suggests that this event occurred more than about 90 years ago. Consideration of these constraints and of the average recurrence interval for this portion of the fault (200-750 yr) suggests that the next large earthquake on the Garlock fault in Searles Valley will occur within the next 660 yr and could, in fact, be overdue.

TABLE OF CONTENTS

Acknowledgments.....	iv
Abstract.....	vi
List of figures, tables.....	xiii
Chapter 1: Introduction	
Location, geometry and total displacement.....	1
Tectonic role.....	1
Aseismic creep.....	4
Historical seismicity.....	5
Earthquake potential.....	7
Organization of the dissertation.....	7
References.....	9

Chapter 2: Latest Quaternary Slip Rate of the Garlock Fault in Southeastern Searles Valley

Abstract.....	14
Introduction.....	15
Description of site.....	18
Offset of the shoreline.....	29
Offset across the southern fault zone.....	29
Possible offset between Trenches 3 and 4... .	55
Possible offset between Trenches 4 and 11..	58
Offset across the north-central	
shear zone.....	58
Offset across the northern fault zone.....	73

Correlation of shoreline features north of the northern fault zone.....	83
Possible offset away from the main fault zone.....	99
Total offset of the shoreline.....	100
Age of the shoreline and slip rate of the Garlock fault.....	103
Discussion.....	113
Conclusions.....	115
References.....	117
 Chapter 3: Displacement, Magnitude and Frequency of Past Earthquakes on the Central and Eastern Garlock Fault	
Abstract.....	121
Introduction.....	122
Methodology.....	123
Data collection.....	125
Data presentation and analysis.....	132
 Garlock townsite and Highway 395 areas....	132
 Searles Valley.....	146
 Pilot Knob Valley.....	146
 Leach Lake area.....	165
 Avawatz Mountains.....	173
Discussion.....	181
 Segmentation of the Garlock fault.....	181

Probable sizes of earthquakes produced by the Garlock fault.....	190
Recurrence interval.....	195
Eastern termination of the Garlock fault..	200
Conclusions.....	202
References.....	204

**Chapter 4: Age of the Most Recent Slip Event along the
Garlock Fault in Searles Valley**

Abstract.....	211
Introduction.....	211
Description of site.....	214
Constraints on the age of the latest earthquake.....	222
Probable timing and size of the next large earthquake.....	227
Comparison of the western and central Garlock fault.....	230
Conclusions.....	231
References.....	233
Plates.....	in pocket

LIST OF FIGURES, TABLES AND PLATES**Figures:**

1-1. Reference map of the Garlock fault.....	3
2-1. Reference map of the Garlock fault showing location of offset shoreline.....	17
2-2. Lake level history of Searles Lake.....	21
2-3. Map of locations where Searles Lake shoreline crosses Garlock fault.....	23
2-4. Geologic map of offset shoreline of Searles Lake.	25
2-5. Stereo-pair aerial photographs of offset shoreline of Searles Lake.....	28
2-6. Map documenting offset of shoreline across southern fault zone.....	32
2-7. Cross sections of trenches on both sides of the southern fault zone: A. Explanation of symbols.....	34
B. Trench 1.....	36
C. Trench 17.....	38
D. Trench 9.....	40
E. Trench 18.....	42
F. Trench 10.....	44
G. Trench 3.....	46
H. Trench 4.....	48
2-8. Map documenting offset across the north-central shear zone.....	61

2-9. Cross sections of excavations within the north-central shear zone:	
A. Trench 11.....	63
B. Trench 12.....	65
C. Trench 19.....	67
2-10. Map documenting offset of the shoreline in the vicinity of Trench 19.....	71
2-11. Map documenting offset of the shoreline across the northern fault zone.....	75
2-12. Cross sections of excavations on both sides of the northern fault zone:	
A. Trench 13.....	77
B. Trench 5.....	79
C. Trench 14.....	81
2-13. Map showing locations of shoreline features north of the northern fault zone.....	85
2-14. Cross sections of excavations north of the northern fault zone:	
A. Trench 6.....	87
B. Trench 7.....	89
C. Trench 8.....	91
D. Trench 15 (northern portion).....	93
E. Trench 15 (central portion).....	95
2-15. Vertical displacement of the shoreline.....	98

3-1. Reference map of Garlock fault showing areas in which small offsets were measured.....	127
3-2. Sketch illustrating potential for erosional modification of an offset channel wall.....	131
3-3. Topographic map of abandoned channel.....	136
3-4. Topographic map of offset alluvial fan.....	138
3-5. Geomorphic offsets south of El Paso Mountains plotted as a function of distance along fault.....	141
3-6. Summation of Gaussian probability density functions for offset features south of El Paso Mountains.....	143
3-7. Geomorphic offsets in Searles Valley plotted as a function of distance along the fault.....	149
3-8. Summation of Gaussian probability density functions for offset features in Searles Valley.....	151
3-9. Geomorphic offsets in Pilot Knob Valley plotted as a function of distance along the fault.....	155
3-10. Summation of Gaussian probability density functions for offset features in Pilot Knob Valley.....	157
3-11. Topographic map of offset gully.....	162

3-12. Topographic map of offset terrace riser and gully.....	164
3-13. Geomorphic offsets near Leach Lake and in the Avawatz Mountains plotted as a function of distance along the fault.....	170
3-14. Summed Gaussian probability density functions for offset features near Leach Lake and in the Avawatz Mountains.....	172
3-15. Photograph of offset ridge.....	176
3-16. Topographic map of offset terrace riser and debris flow.....	178
3-17. Possible rupture patterns for the Garlock fault.....	186
4-1. Reference map showing the location of paleoseismic site on the Garlock fault in Searles Valley.....	213
4-2. Photo-geologic map of paleoseismic site.....	216
4-3. Cross section along Trench 1.....	219
4-4. Cross section along southern portion of Trench 1.....	221
4-5. Cross section along central portion of Trench 2.....	224

Tables:

2-1. Explanation of units in cross sections.....	49
2-2. Summary of offset of the Searles Lake shoreline across the north-central shear zone....	69
2-3. Summary of offset of the Searles Lake shoreline across the entire fault zone.....	101
2-4. Description of soil profile 18S-1.....	104
3-1. Geomorphic offsets south of El Paso Mountains...	133
3-2. Geomorphic offsets in Searles Valley.....	147
3-3. Geomorphic offsets in Pilot Knob Valley.....	152
3-4. Geomorphic offsets near Leach Lake and in the Avawatz Mountains.....	166
3-5. Possible rupture patterns and associated earthquake magnitudes.....	191
3-6. Estimated recurrence intervals for portions of the central and eastern Garlock fault.....	197

Plates:

Plate 1. Undrafted cross section of the eastern wall of Trench 2 from Searles Lake offset shoreline site (Chapter 2)....in pocket	
Plate 2. Undrafted cross section of the western wall of Trench 16 from Searles Lake offset shoreline site (Chapter 2)....in pocket	

Plate 3. Undrafted cross section of the western
wall of Trench 1 from the Searles
Valley paleoseismic site
(Chapter 4).....in pocket

Plate 4. Undrafted cross section of the western
wall of Trench 2 from the Searles
Valley paleoseismic site
(Chapter 4).....in pocket

Plate 5. Undrafted cross section of the eastern
wall of Trench 2 from the Searles
Valley paleoseismic site
(Chapter 4).....in pocket

CHAPTER 1: INTRODUCTION

Location, geometry and total displacement

The Garlock fault is one of the principal active faults of California. It separates the Tehachapi-Sierra Nevada province and the Basin and Range extensional province on the north from the Mojave block on the south. A total of 48 to 64 km of left-lateral displacement across the fault has been documented (Smith, 1962; Smith and Ketner, 1970; Davis and Burchfiel, 1973).

The fault is broadly arcuate over its 248-km length (Figure 1-1). From its intersection with the San Andreas fault it strikes northeasterly, but it curves to a more easterly strike toward its eastern end, at the southern end of Death Valley. A prominent stepover in the fault occurs in the vicinity of Koehn Lake, and a 15-degree bend in the fault is located south of the Quail Mountains. I refer to the segment of the fault that extends westward from the step-over in the Koehn Lake basin as the western Garlock fault, the segment between that step-over and the Quail Mountains as the central Garlock fault, and the segment that extends eastward from the Quail Mountains as the eastern Garlock fault.

Tectonic role

The tectonic role of the Garlock fault has been controversial. Hill and Dibblee (1953) viewed the left-lateral Garlock and Big Pine faults and the right-lateral San

Figure 1-1: Reference map of the region surrounding the Garlock fault. GF, Garlock fault; NBGF, North Branch Garlock fault; OL, Owens Lake; OLF, Owl Lake fault; PV, Panamint Valley; QM, Quail Mountains; SAF, San Andreas fault; SV Searles Valley.



Figure 1-1

Andreas fault as conjugate shears defining a regional strain pattern of north-south compression and east-west extension. Later workers (Davis and Burchfiel, 1973; Hamilton and Myers, 1966; and Troxel and others, 1972) interpreted the Garlock fault as an intracontinental transform fault that accommodates extension in the Basin and Range province, north of the fault, relative to the more stable Mojave block, south of the fault. Although the location of the Garlock fault suggests that it is related to Basin and Range extension, a simple transform model is inadequate to explain this relationship because the extension direction for the portion of the Basin and Range province north of the Garlock fault is not parallel to the fault (Wernicke and others, 1988; Minster and Jordan, 1987; Burchfiel and others, 1987; Stewart, 1983; Jones, 1987). It may be that the component of extension that is parallel to the Garlock drives the left-lateral slip on the fault and the component perpendicular to the fault (in conjunction with right-lateral shear in the Mojave Desert) has rotated the central and eastern Garlock fault clockwise (Dokka and Travis, 1990; Jones, 1987; Carter and others, 1987).

Aseismic creep

Several investigators have detected aseismic creep along the westernmost 60 km of the fault (Louie and others, 1985; Snay and Cline, 1980; Rodgers, 1979). Contrary to these observations, however, U. S. Geological Survey Quadrilaterals spaced at 15-km intervals along this portion of the fault have not detected any aseismic creep (Malcolm Clark, written communication, 1990). Similarly, creep has

never been detected on the central or eastern parts of the fault (Louie and others, 1985; Malcolm Clark, written communication, 1990).

Historical seismicity

Historical seismic activity has been most common along the westernmost 70 km of the fault (coinciding with the region that may be creeping aseismically) and along a 35-km-length of the fault within the dilational fault jog at Koehn Lake (Astiz and Allen, 1983). Instrumentally recorded earthquakes along the fault have been small ($M_L \leq 4.3$). No large or moderate historic earthquakes are known to have occurred on the Garlock fault. Although a number of earthquakes were felt in Bakersfield, the Kern River area, Tehachapi, Mojave, Barstow, and southernmost Owens Valley between 1868 and 1928 (Townley and Allen, 1939), it is difficult to determine whether any of these may have been produced by the Garlock fault. Several earthquakes with maximum Rossi-Forel intensities of VII and VIII (= Modified Mercalli intensity VI to VII) occurred during this time and had intensity distributions that could conceivably have been generated by earthquakes on the Garlock fault, but other source locations are possible and probably more likely for most of these events (Townley and Allen, 1939).

Two moderate, historical earthquakes for which the Garlock fault is a possible source occurred in 1916. One occurred near the eastern end of the Garlock fault on 10 November 1916. This event was recorded instrumentally at Reno, Berkeley and Mount Hamilton (Townley and Allen, 1939). Slemmons and others (1965) report the

event as $M=6.1$, located at 35.5° N, 116° W (about 40 km ESE of the eastern end of the Garlock fault), whereas Toppozada and others (1978) assign the event an $M=5.5$ magnitude and locate it at 36° N, 117° W (about 45 km north of the portion of the Garlock fault in the Quail Mountains). While the location of this event is very poorly constrained, the possibility that it may have occurred on the Garlock fault or on the nearby Owl Lake fault is intriguing. Another event, of magnitude 5.2, occurred on 23 October 1916 at the western end of the Garlock fault (Toppozada and others, 1978), but the San Andreas and other faults are also possible sources for this event.

A $M_L=5.4$ earthquake occurred on 10 June 1988 several km north of the Garlock fault and about 20 km east of its intersection with the San Andreas fault. This event may have been produced by slip on the North Branch of the Garlock fault or by slip on one of several northward-dipping faults imaged in seismic reflection data north of the Garlock fault (Goodman and others, 1989). The focal mechanism for this event is consistent with reverse and left-lateral slip on a plane striking $N82^\circ$ E and dipping 70° N (Wald and others, 1990). This plane projects to the surface about 1 km north of the North Branch of the Garlock fault, suggesting that that fault may have been the causative fault. In the few places where the North Branch of the Garlock fault is well exposed, it dips moderately northward (Sharry, 1981, p.123), consistent with the hypothesis that this fault produced the 1988 earthquake. The fairly linear trend of the fault on the ground surface, however, suggests that the North Branch of the Garlock fault is vertical or subvertical over much of its length

(Sharry, 1981), and thus may not project at depth to the hypocentral region of the 1988 earthquake.

Earthquake potential

Although the Garlock fault is not known to have produced large earthquakes during the period of historical record, abundant scarps and left-laterally offset geomorphic features of Holocene age indicate that the fault is active and that it has produced large earthquakes. Clark (1970, 1973) prepared a map of these features and suggested that 3 m of left-lateral slip had occurred in the most recent slip event along parts of the central and eastern Garlock fault. In addition, Holocene slip events have been documented by LaViolette and others (1980), Burke (1979), Burke and Clark (1978) and Roquemore and others (1982).

With respect to its earthquake potential, several questions about the Garlock fault have not been answered. Does the slip rate vary along strike? What size earthquakes does the fault produce? Which segments rupture during these events, and how large are the offsets during the earthquakes? How often do large events occur? When were the most recent ruptures? This dissertation will address these questions.

Organization of the dissertation

In Chapter 2 of this dissertation, I document the Latest Quaternary slip rate of the Garlock fault in southeastern Searles Valley, using an offset shoreline of

Searles Lake. In Chapter 3, I present measurements of left-laterally offset geomorphic features that constrain the amount of displacement in past large earthquakes on the central and eastern Garlock fault. I also use these estimates of the slip in past events to address the rupture lengths, magnitudes and frequency of past earthquakes on the fault. In Chapter 4, I constrain the age of the most recent faulting event on the Garlock fault in Searles Valley and discuss the implications of this date for the timing of future events along this part of the fault.

REFERENCES

Astiz, L. and C. R. Allen, Seismicity of the Garlock fault, California, *Bull. Seismol. Soc. Am.*, 73, 1721-1734, 1983.

Bard, E., B. Hamelin, R. G. Fairbanks, and A. Zindler, Calibration of the C-14 timescale over the past 30,000 years using mass-spectrometric U-Th ages from Barbados corals, *Nature*, 345, 405-410, 1990.

Benson, L. V., D. R. Currey, R.I. Dorn, K. R. Lajoie, C. G. Oviatt, S. W. Robinson, G. I. Smith, S. and Stine, Chronology of expansion and contraction of four Great Basin Lake systems during the past 35,000 years, *Palaeogeography, Palaeoclimatology, Palaeoecology*, 78, 241-286, 1990.

Burchfiel, B. C., K. V. Hodges, and L. H. Royden, Geology of Panamint Valley-Saline Valley pull-apart system, California: palinspastic evidence for low-angle geometry of a Neogene range-bounding fault, *J. Geophys. Res.*, 92, 10422-10426, 1987.

Burke, D. B., Log of a trench in the Garlock fault zone, Fremont Valley, California, *U. S. Geol. Surv. Map MF-1028*, 1979.

Burke, D. B., and M. M. Clark, Late Quaternary activity along the Garlock fault at Koehn Lake, Fremont Valley, California (abstract), *EOS, Trans. Am. Geophys. Union*, 59, 1126, 1978.

Carter, J. N., B. P. Luyendyk, and R. R. Terres, Neogene clockwise tectonic rotation of the eastern Transverse Ranges, California, suggested by paleomagnetic vectors, *Geol. Soc. Am. Bull.*, 98, 199-206, 1987.

Clark, M. M., Some characteristics of the most recently active traces of the Garlock fault, *Geol. Soc. Am., Abstracts with Programs*, 2, 82, 1970.

Clark, M. M., Map showing recently active breaks along the Garlock and associated faults, California, *U.S. Geol. Surv. Misc. Geol. Inv. Map, I-741*, 1973.

Clark, M. M. and K. R. Lajoie, Holocene behavior of the Garlock fault, *Geol. Soc. Am., Abstracts with Programs*, 6, 156-157, 1974.

Davis G. A., and B. C. Burchfiel, Garlock fault: an intracontinental transform structure, southern California, *Geol. Soc. Am. Bull.*, 84, 1407-1422, 1973.

Dokka, R. K., and C. J. Travis, Late Cenozoic strike-slip faulting in the Mojave Desert, California, *Tectonics*, 9, 311-340, 1990.

Goodman, E. D., P. E. Malin, E. L. Ambos, and J. C. Crowell, The southern San Joaquin Valley as an example of Cenozoic basin evolution in California, in R. A. Price, ed., *Origin and Evolution of Sedimentary Basins and Their Energy and Mineral Resources*, Am. Geophys. Union, Geophysical Monograph 48, IUGG Volume 3, pp. 87-107, 1989.

Hamilton, W. and W. B. Myers, Cenozoic tectonics of the western United States, *Rev. Geophys.* 4, 509-549, 1966.

Hill, M. L., and T. W. Dibblee, Jr., San Andreas, Garlock and Big Pine faults, California-- a study of the character, history, and tectonic significance of their displacements, *Geol. Soc. Am. Bull.* 64, 443-458, 1953.

Jones, C. H., Is extension in Death Valley accommodated by thinning of the mantle lithosphere beneath the Sierra Nevada, California?, *Tectonics*, 6, 449-473, 1987.

LaViolette, J. W., G. E. Christenson, and J. C. Stepp, Quaternary displacement on the western Garlock fault, southern California, in Fife, D. L. and A. R. Brown, eds., *Geology and Mineral Wealth of the California Desert*, Santa Ana, California, South Coast Geol. Soc., pp. 449-456, 1980.

Louie, J. N., C. R. Allen, D. C. Johnson, P. C. Haase, and S. N. Cohn, Fault slip in southern California, *Bull. Seismol. Soc. Am.*, 75, 811-833, 1985.

Minster, J. B., and T. H. Jordan, Vector constraints on western U.S. deformation from space geodesy, neotectonics, and plate motions, *J. Geophys. Res.*, 92, 4798-4804, 1987.

Rodgers, D. A., Vertical deformation, stress accumulation and secondary faulting in the vicinity of the Transverse Ranges of southern California, *Calif. Div. of Mines and Geol. Bull.* 203, 74 pp, 1979.

Roquemore, G. R., P. E. Smith, and E. W. Banks, Holocene earthquake activity of the eastern Garlock fault in Christmas Canyon, San Bernardino County, California, *Abstracts with Programs, Cordilleran Section, Geol. Soc. Am.*, 14, 228, 1982.

Sharry, J. The geology of the western Tehachapi Mountains, California, Ph.D. dissertation, Massachusetts Institute of Technology, 215 pp., 1981.

Slemmons, D. B., A. E. Jones, and J. I. Gimlett, Catalog of Nevada earthquakes, 1852-1960, *Bull. Seismol. Soc. Am.*, 55, 537-583, 1965.

Smith, G. I., Large lateral displacement on Garlock fault, California, as measured from offset dike swarm, *Bull. Am. Assoc. Petrol. Geol.*, 46, 85-104, 1962.

Smith, G. I., and K. B. Ketner, Lateral displacement on the Garlock fault, southeastern California, suggested by offset sections of similar metasedimentary rocks, *U.S. Geol. Surv. Profess. Paper 700-D*, D1-D9, 1970.

Snay, R. A., and M. W. Cline, Crustal movement investigations at Tejon Ranch California, *Natl. Oceanic and Atmosph. Adm. Technical Rept. 87*, 1980.

Stewart, J. H., Extensional tectonics in the Death Valley area, California: Transport of the Panamint Range structural block 80 km northwestward, *Geology*, 11, 153-157, 1983.

Stuiver, M., and G. I. Smith, Radiocarbon ages of stratigraphic units, in Smith, G. I., Subsurface stratigraphy and geochemistry of Late Quaternary evaporites, Searles Lake, California, *U. S. Geological Survey Professional Paper 1043*, 130 p., 1979.

Toppozada, T. R., D. L. Parke, and C. T. Higgins, Seismicity of California, 1900-1931. *Calif. Div. of Mines and Geol. Special Report 135*, 1978.

Townley, S. D., and M. W. Allen, Descriptive catalog of earthquakes of the Pacific Coast of the United States, 1769-1928, *Bull. Seismol. Soc. Am.*, 29, 1-297, 1939.

Troxel, B. W., L. A. Wright, and R. H. Jahns, Evidence for differential displacement along the Garlock fault zone, California, *Geol. Soc. Am., Abstracts with Programs* 4, 250, 1972.

Wald, L. A., D. D. Given, J. Mori, L. M. Jones, and L. K. Hutton, The southern California network bulletin January - December, 1988, *U. S. Geol. Surv. Open-File Rept 90-499*, 1990.

Wernicke, B., G. J. Axen, and J. K. Snow, Basin and Range extensional tectonics at the latitude of Las Vegas, Nevada, *Geol. Soc. Am. Bull.*, 100, p.1738-1757, 1988.

CHAPTER 2

**LATEST QUATERNARY SLIP RATE OF THE GARLOCK FAULT
IN SOUTHEASTERN SEARLES VALLEY, CALIFORNIA**

ABSTRACT

A latest-Pleistocene shoreline at the overflow-level of Searles Lake has been offset 82 to 106 meters (best estimate = 90 m) along the Garlock fault, at the southeastern corner of Searles Valley. Radiocarbon dates from both surface and subsurface units indicate that the most recent highstand of Searles Lake ended sometime between 10,000 and 13,800 ^{14}C -yr ago (Stuiver and Smith, 1979; Benson and others, 1990; Smith and Street-Perrott, 1983). The maximum slip rate of the Garlock fault in southeastern Searles Valley is thus 10.6 millimeters per carbon-14-year (mm/ ^{14}C -yr). If part of the offset of the shoreline is a remnant from older lakestands, then the slip rate may be somewhat less, but a channel that incised after the most recent highstand is offset 69 ± 2 m, indicating that the minimum slip rate is 5 mm/ ^{14}C -yr. Subjective evaluation of the constraints on the offset and on the age of the shoreline suggest that the slip rate is most likely between 6 and 8 mm/ ^{14}C -yr at this site. If Bard and others' (1990) calibration of the radiocarbon timescale is correct, then the calibrated slip rate of the Garlock fault is between 4 and 9 mm/yr and most likely between 5 and 7 mm/yr.

The slip rate in southeastern Searles Valley is compatible with the 7 ± 1 mm/ ^{14}C -yr slip rate at Koehn Lake (Clark and Lajoie, 1974; Clark and others,

1984). No extension is required north of the Garlock fault between Koehn Lake and southeastern Searles Valley, but up to 3 mm/yr of extension parallel to the Garlock fault is allowed.

INTRODUCTION

Several estimates of the slip rate of the Garlock fault have been made at various points along strike. LaViolette and others (1980) estimated a 1.6 to 3.3 mm/yr slip rate for the Garlock fault in Oak Creek Canyon (Figure 2-1) on the basis of the 0.3 km offset of several stream channels incised into a surface with a well-developed late Pleistocene soil. Clark and Lajoie (1974) obtained a slip rate of 7 ± 1 millimeters per carbon-14-year (mm/ ^{14}C -yr) from the offset of an \approx 11,000- ^{14}C -yr-old lacustrine bar of Koehn Lake. Carter (1980, 1982) calculated a 11-12 mm/yr minimum slip rate on the basis of Pleistocene alluvial fan gravels offset from their sources in El Paso Mountains. Smith (1975) estimated a slip rate of about 1 mm/yr at Christmas Canyon on the basis of the 8-m offset of a channel incised into ~10,000-yr-old lacustrine gravels. I regard this rate as a minimum, however, because the channel could have incised long after deposition of the ~10,000-yr-old gravels.

Better knowledge of the late Quaternary slip rate of the Garlock fault is important both for seismic hazard analysis and for improving our understanding of the Late Quaternary tectonics of the region surrounding the fault. Some estimates of the recurrence interval are dependent on accurate knowledge of the slip rate at several places along strike (McGill and Sieh, 1991; Chapter 3 of this dissertation).

FIGURE 2-1: Reference map shows locations mentioned in text. Carter, area in which Carter's (1980, 1982) 12 mm/yr slip rate was determined; CC, Christmas Canyon; Clark & Lajoie, site at which Clark and Lajoie's (1974) 7 mm/yr slip rate was determined; CR, Coso Range; DV, Death Valley; GF, Garlock fault; I WV, Indian Wells Valley; OL, Owens, Lake; OLF, Owl Lake fault; PKV, Pilot Knob Valley; PV, Panamint Valley; SAF, San Andreas fault; SR, Slate Range; SV, Searles Valley.



Knowledge of the Garlock fault slip rate at several places along strike is also critical for understanding the tectonic role of the Garlock fault and its relation to the Basin and Range Province north of the fault and to the proposed eastern California shear zone (Dokka and Travis, 1990). This knowledge is also important for understanding how motion between the North American and Pacific plates is distributed (e.g., Weldon and Humphreys, 1986).

I present evidence that the latest Quaternary slip rate of the central Garlock fault in southeastern Searles Valley is most likely between 6 and 8 mm/ $^{14}\text{C-yr}$, but that it could be as little as 5 mm/ $^{14}\text{C-yr}$ or as large as 10.6 mm/ $^{14}\text{C-yr}$. These estimates are based on the offset of the latest Quaternary high shoreline of Searles Lake and on the offset of a channel incised into that shoreline. This slip-rate determination does not completely resolve the questions presented above, but it is an additional constraint on the solution to those questions.

DESCRIPTION OF SITE

The slip-rate measurement presented in this paper is based on the offset of a latest-Pleistocene high shoreline of Searles Lake. Pleistocene Searles Lake was part of a chain of lakes that was fed by waters from the eastern flank of the Sierra Nevada via the Owens River (Gale, 1914; Smith, 1979). At times when water from the Owens River filled Owens Lake, the lake overflowed into the Indian Wells Valley to form China Lake, which in turn overflowed into Searles Lake. At times when Searles Lake was filled to an elevation of 678 m, it coalesced with China Lake

(Benson and others, 1990), and when it filled to about 690 m, it overflowed through Pilot Knob Valley into Panamint Valley (U. S. Geological Survey, 1984). The lake in Panamint Valley, in turn, may have overflowed into Death Valley to form Lake Manly.

Lacustrine sedimentation in Searles Valley began 3.18 million years ago, and lakes have occupied the valley intermittently since that time (Smith and others, 1983). During the late Pleistocene epoch, lakes occupying Searles Valley have reached the overflow level several times between about 10,000 and 24,000 $^{14}\text{C-yr}$ B.P. (Figure 2-2; Stuiver and Smith, 1979; Benson and others, 1990; G. I. Smith, unpublished data). Searles Lake also overflowed between about 120 and 135 thousand years (ka) ago and possibly around 50 ka (G. I. Smith, unpublished data). For reasons discussed below, I believe that the shoreline features studied in this paper probably formed during one of the most recent highstands, between about 10,000 and 24,000 $^{14}\text{C-yr}$ B.P.

The overflow shoreline of Searles Lake crosses the Garlock fault in several places (Figure 2-3). The intersection of this shoreline and the fault is best preserved near the outlet of the lake, at the southwestern corner of the Slate Range. At this site, an abrasion platform and sea cliff have been cut by wave action into older alluvium and older lacustrine sediments. A 0- to 2-m-thick veneer of nearshore, lacustrine sands was deposited on this platform during the most recent highstands, and pinches out against the sea cliff (Figure 2-4).

FIGURE 2-2: Lake-level history of Searles Lake (from Benson and others [1990, Figure 11a]). C1 and C3 refer to highstands discussed in the text.

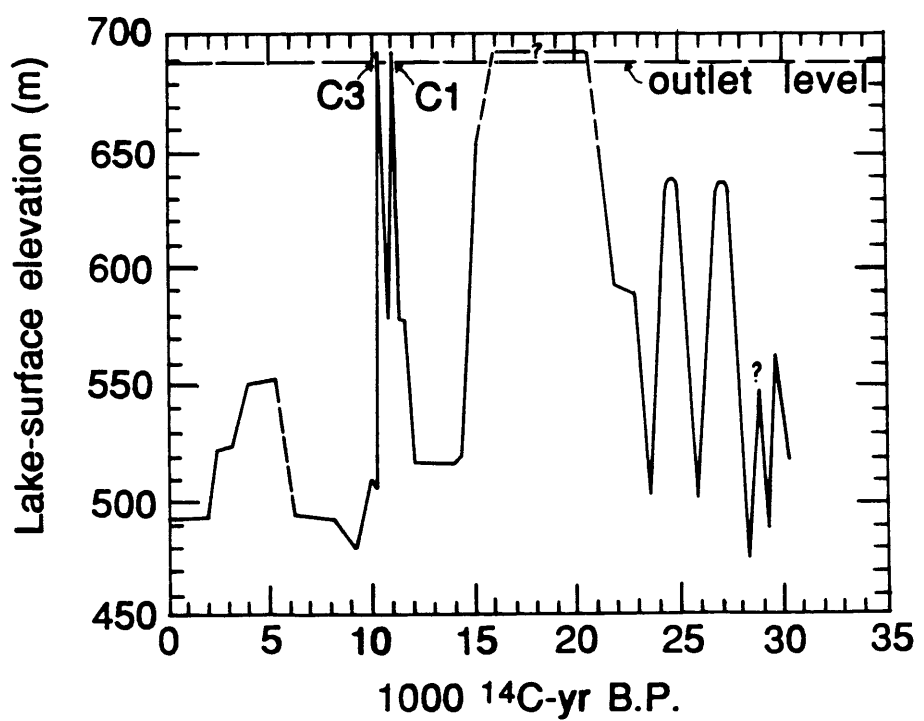


Figure 2-2

FIGURE 2-3: Map shows locations where the overflow shoreline of Searles Lake crosses the Garlock fault.

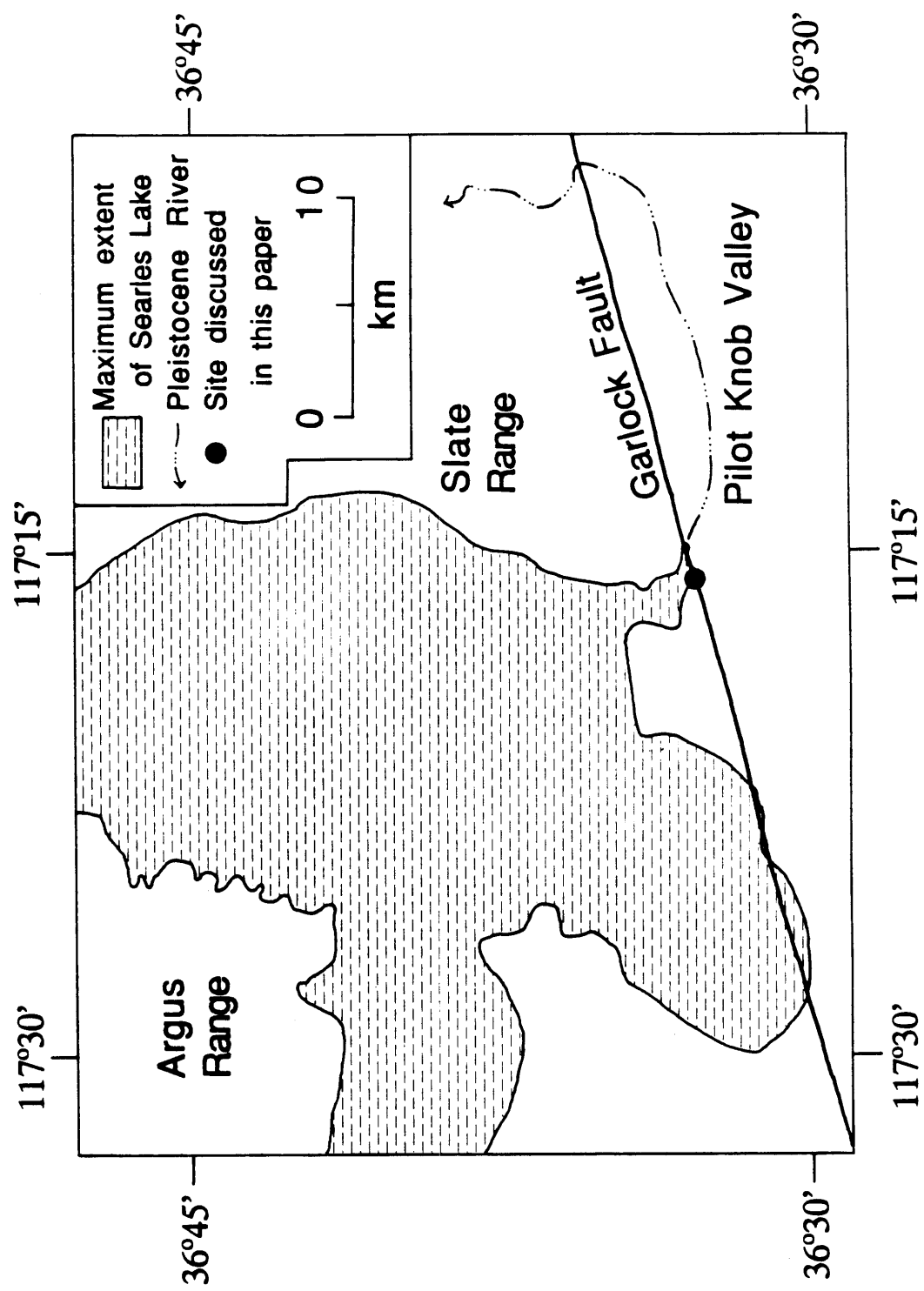


Figure 2-3

FIGURE 2-4: Geologic map of site and locations of trenches. Late Pleistocene shoreline is along southwestern limit of Late Quaternary beach and nearshore lacustrine sand. Note left-lateral offset of shoreline across the two major fault strands. Also note left-lateral offset of the western wall of the northward-flowing, incised channel on the right side of the map. Topography is from photogrammetry by Aerial Photometrics, Fresno, CA. Geologic mapping by S. McGill and G. Roquemore.

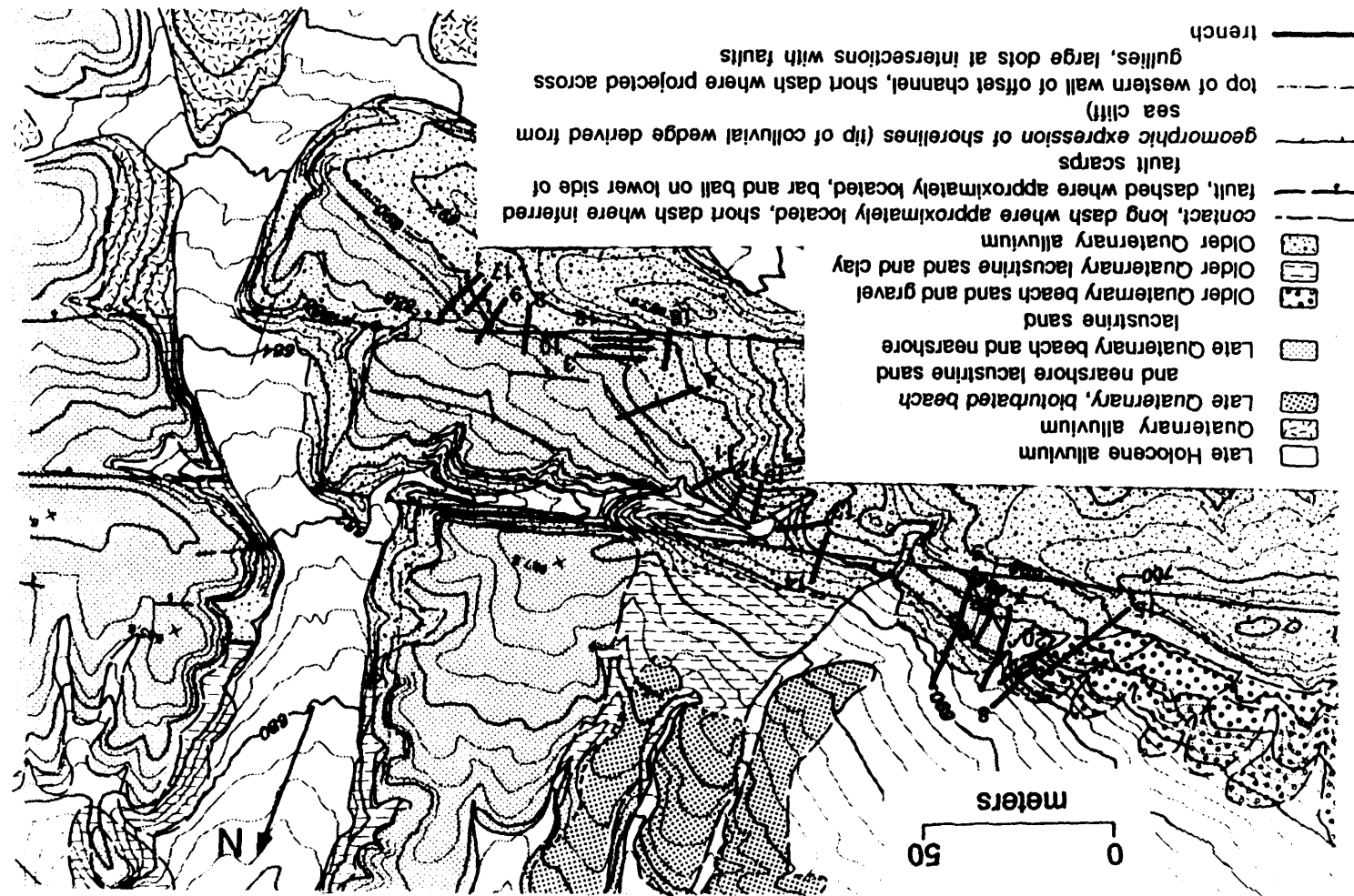


Figure 2-4

25b

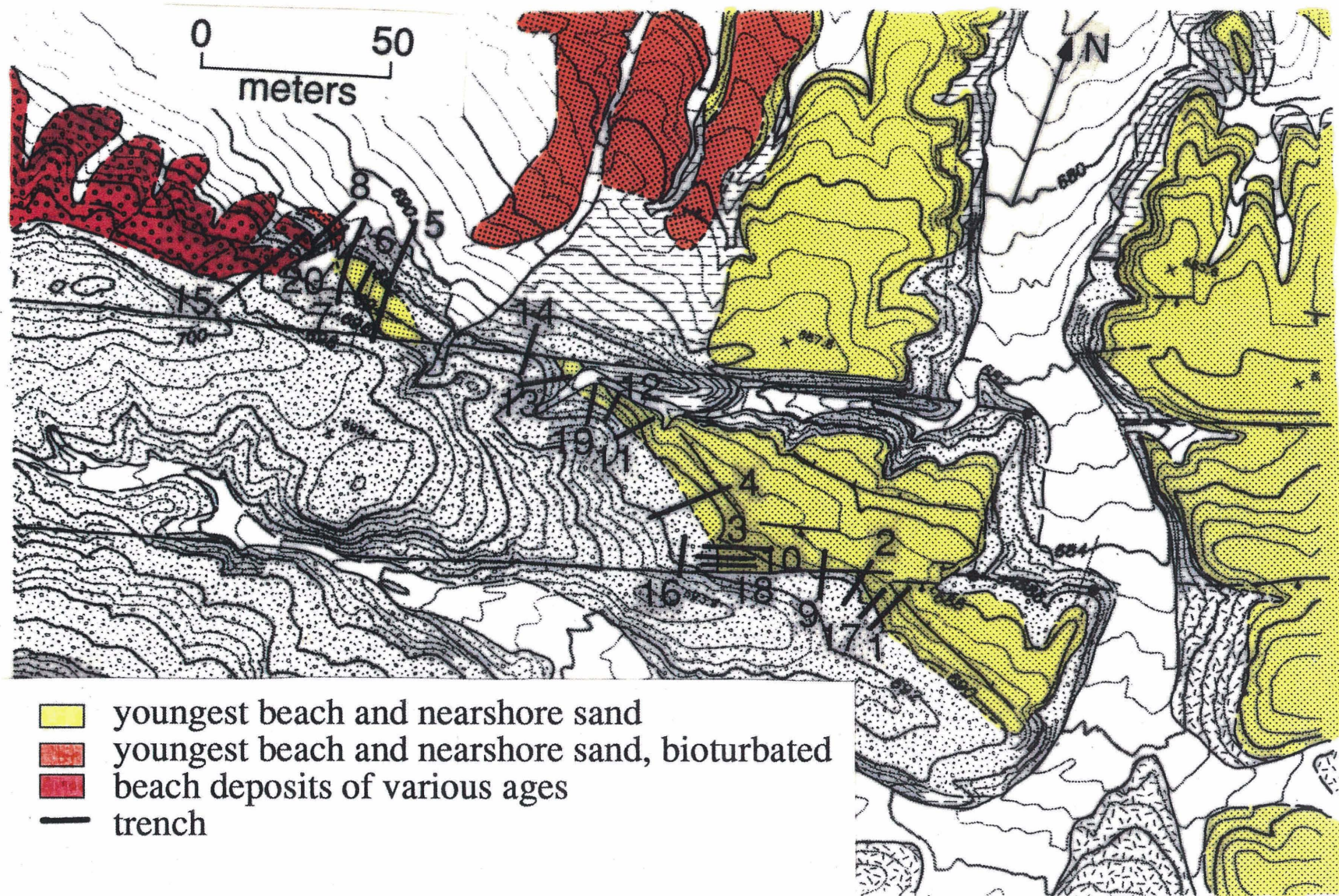


Figure 2-4

The shoreline angle, that linear feature formed by the intersection of the sea cliff and the abrasion platform, is left-laterally and vertically offset across two subparallel fault traces (Figures 2-4, 2-5), but the offset is difficult to measure precisely because the shoreline angle has been buried by colluvium. For this reason, I had 20 backhoe trenches dug to locate the shoreline and the fault strands precisely (Figure 2-4). The relationships in the trench walls were documented by mapping the exposures at a scale of 1:20. The mapping was controlled by surveying to nails placed along the important contacts. Both walls of most trenches were mapped, but only one wall of each trench is shown here. Undrafted, field cross sections of trenches 2 and 16 (not shown as figures in this chapter) can be found on plates 1 and 2. After mapping the trench walls, we excavated by hand along the shoreline to find the precise intersection of the shoreline with most of the major fault strands (Figure 2-4). The three-dimensional excavations were mapped at a scale of 1:10, with control again provided by a number of surveyed points within each excavation. Only one map of a three-dimensional excavation is shown in detail here (Figure 2-10).

The points surveyed in all trenches were combined in a common, three-dimensional coordinate system. The absolute elevation of this coordinate system was determined by traversing to the site from a benchmark about 3.5 km south of the site. The absolute elevation of points surveyed at the site is probably correct to within ± 10 cm (1σ). The uncertainty in the relative elevations of various points at the offset shoreline site is less than this.

FIGURE 2-5: Stereo-pair aerial photographs of a latest-Pleistocene shoreline of Searles Lake offset by two major strands of the Garlock fault zone. In right-hand photo, shoreline is indicated by dots; fault strands are indicated by lines. Also shown is an offset channel, which has incised the shoreline. Area shown corresponds to part of the area of Figure 2-4. Taken from U.S.G.S. photos supplied by Malcolm Clark.

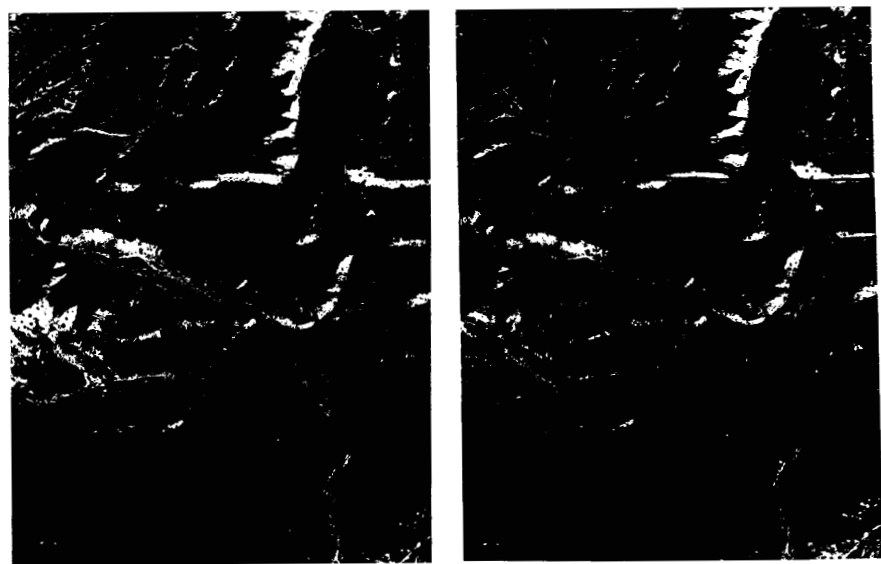


Figure 2-5

Most trenches across the shoreline revealed moderately sorted to well-sorted, unconsolidated to poorly consolidated, medium to very coarse sand that pinches out against a sea cliff cut into older alluvium or that interfingers with colluvium derived from a sea cliff. In most cases the upper part of these beach deposits (and occasionally the entire thickness) is poorly sorted because of bioturbation, which has mixed colluvium and aeolian silt with the well-sorted beach sands.

The shoreline is offset a total of 82 to 106 m (best estimate = 90 m) across the fault zone, and the details of this measurement are discussed in the following section. A channel incised into the wave-cut cliff and platform is also left-laterally offset about 69 ± 2 m across the fault zone (Figures 2-4 and 2-5). This channel presumably formed shortly after initiation of desiccation of the lake, in response to lowering of the base level.

OFFSET OF THE SHORELINE

Offset across the southern fault zone

The buried shoreline is exposed south of the southern fault zone in Trenches 1 and 17 and north of the southern fault zone in Trenches 3, 10 and 18 (Figure 2-6). In Trench 9 the shoreline is within the southern fault zone but is south of the main Holocene fault trace within that zone. The characteristics of the shoreline and the beach deposits in these 6 trenches are similar, indicating that the shoreline exposed in Trenches 1, 17 and 9 correlates with the one exposed in Trenches 3, 10 and 18 (Figure 2-7 and Table 2-1). These similarities are:

- (1) In all six of these trenches the dominant grain sizes of the beach deposits

are medium and coarse sand.

(2) In Trenches 1, 17, 18, 10 and 3, the beach sands are locally moderately to well sorted, but they grade upward and toward the sea cliff into more poorly sorted deposits, because of mixing of the beach sands with colluvial material through bioturbation and infiltration of aeolian silt. In Trench 9, well-sorted sands are exposed north of and in fault contact with the main fault strand in the southern fault zone, but the beach deposits exposed within the southern fault zone (that is, the deposits that I correlate with those near the sea cliff in Trench 18) are poorly sorted (Figure 2-7D). The poorly sorted sands exposed within the fault zone in Trench 9 are inferred to be bioturbated beach deposits because they are more poorly consolidated and finer grained than the underlying alluvium and because they pinch out southwestward against a cliff cut into the older alluvium. The poor sorting of the beach deposits within the fault zone in Trench 9 is consistent with the poor sorting of the beach deposits within 1-m of the sea cliff in Trench 18 (Figure 2-7E).

(3) In Trenches 1, 18 and 10 there is a lag deposit of rounded and subrounded cobbles at the base of the beach deposits, which extends lakeward from a point 4-5 m lakeward of the sea cliff. (The westernmost cobbles in Trench 18 are east of the eastern end of the cross section in Figure 2-7E). These cobbles were probably derived from the underlying older alluvium and were too large to be transported by wave action in the lake. The lack of a cobble lag deposit at the base of the bioturbated beach deposits within the fault zone in Trench 9 is consistent with lack of such a lag deposit within 4-5 m of the wave-cut cliff trenches 1, 17, 18 and 10.

FIGURE 2-6: Map documents offset of the shoreline across the southern fault zone and possible offset between Trenches 3 and 11. Offset across southern fault zone is most likely 37 m (P3 to P5), but could be as little as 36 m (P3 to P4) or as large as 38 m (P3 to P5 plus P1 to P2). Offset of the shoreline between Trenches 3 and 4 is most likely 0 m, but could be up to about 3 m (P6 to P7). Offset of the shoreline between Trench 4 and the excavation southeast of Trench 11 is most likely 2 m but could be 0 m. See text for explanation of piercing points P1 to P10. Tic marks along the sides of trenches correspond to tic marks along the tops and bottoms of cross sections in Figure 2-7.

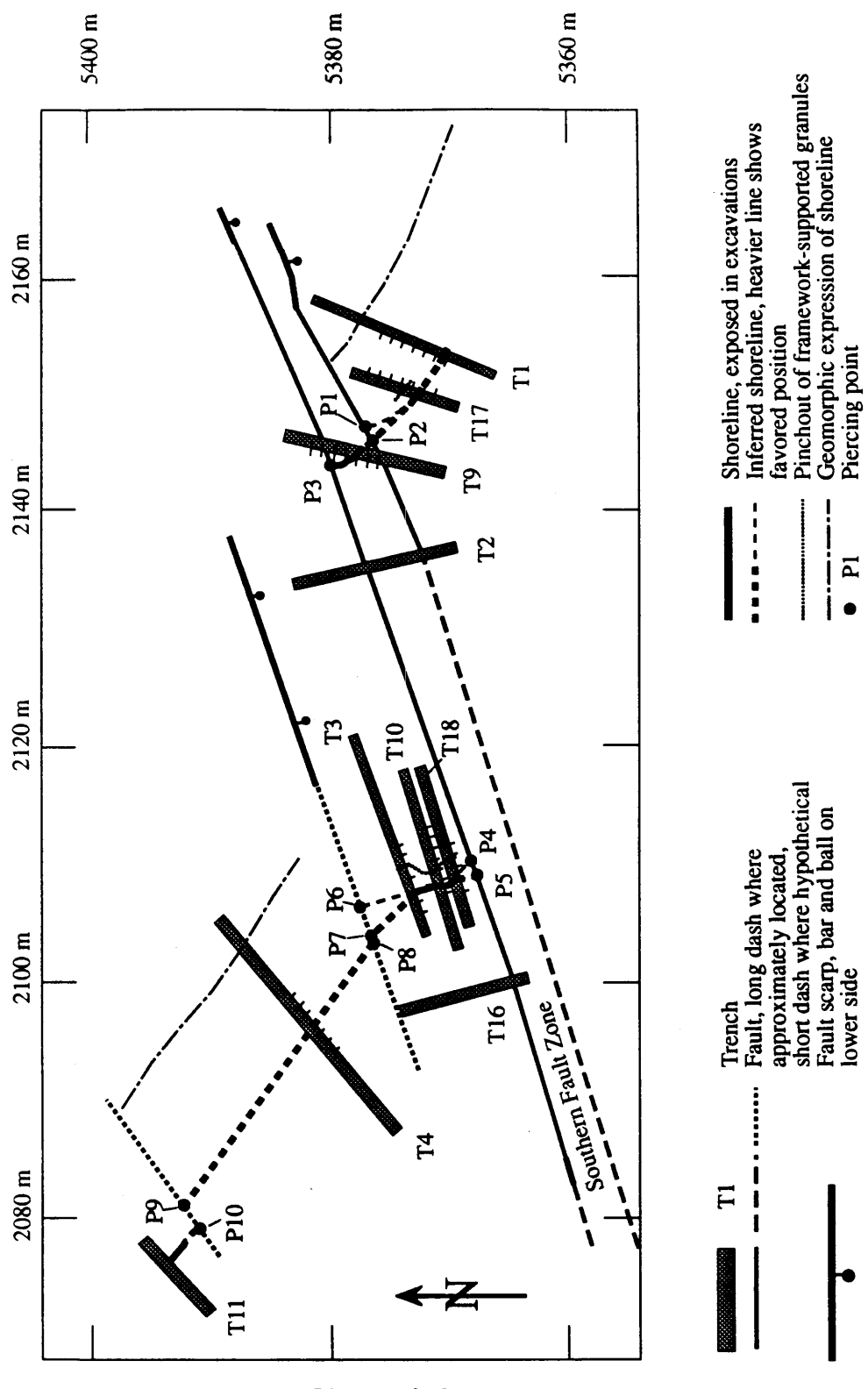


Figure 2-6

FIGURE 2-7: Cross sections of excavations on both sides of the southern fault zone. Tic marks on top and bottom of cross sections are spaced 1 meter apart and correspond to tic marks along the sides of trenches in Figure 2-6. Elevations labelled on the sides of cross sections are in meters above sea level. Cross sections of the western walls of Trenches 1 and 9 have been reversed for easier comparison to other cross sections. See Table 2-1 for explanation of units in cross sections. Both walls of most trenches were logged, but only one wall of each trench is shown here.

FIGURE 2-7A: Explanation of symbols used in cross sections

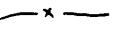
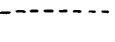
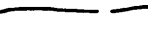
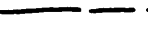
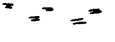
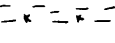
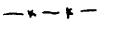
	cobbles, to scale
	pebbles
	granules: massive
	bedded
	coarse and massive
	very coarse sand: bedded
	fine to medium sand: massive
	bedded
	silt: massive
	laminated
	clay
	calcium carbonate
	ash
	shells or shell fragments
	contact
	contact, gradational over x cm
	inferred contact
	boundary of beach deposits, dashed where gradational
	fault, long dash where less certain, short dash where inferred
	pervasive fractures
	shear zone
	strongly developed platy soil structure
	weakly developed platy soil structure
	0.5- to 2-cm-thick layers, very weakly cemented by CaCO ₃
uc	unconsolidated
pc	poorly consolidated
mc	moderately consolidated
wc	well-consolidated
vwc	very well-consolidated

Figure 2-7A

FIGURE 2-7B: Cross section along western wall of Trench 1. Irregular bodies of well-sorted sand (Qb) are probably liquefaction structures. The sea cliff extends from the lowest sand layer at right edge of cross section upward along the inferred contact between older alluvium (Qoa₁) and colluvium (Qc) derived from the sea cliff. Logged by G. Roquemore and S. McGill.

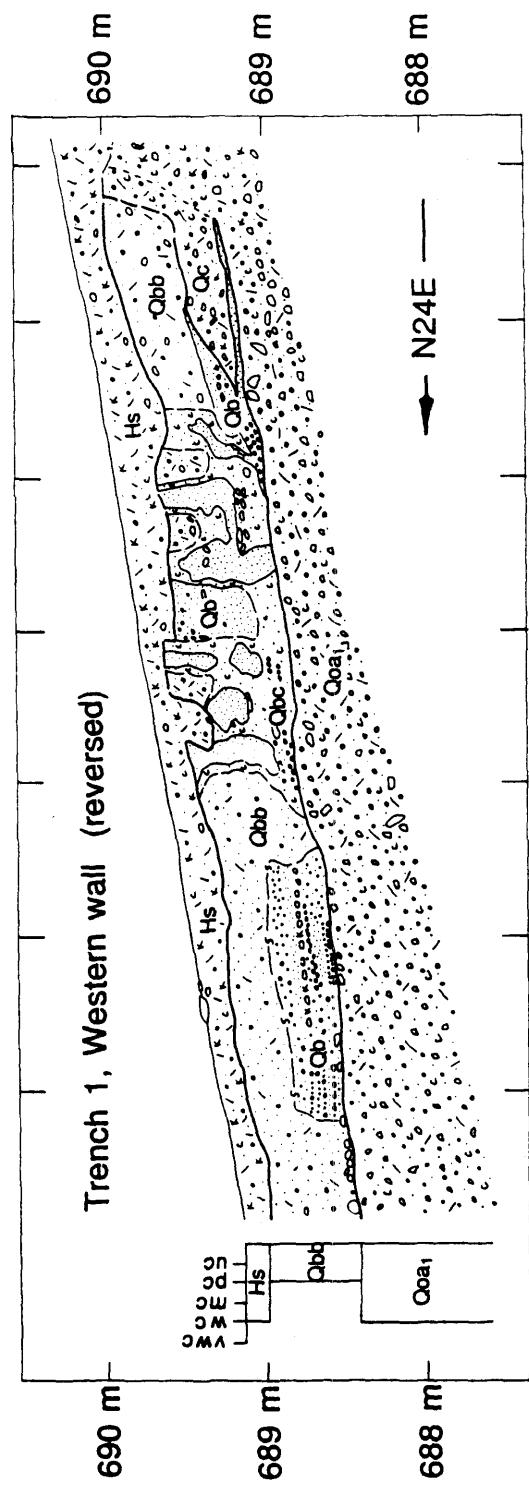


Figure 2-7B

FIGURE 2-7C: Cross section along eastern wall of Trench 17 shows thin layers of beach sand (Qb) interfingering with colluvium (Qc) derived from the sea cliff. Shoreline angle is at southwestern end of lowest sand layer. Note bed of framework-supported granules that terminates about 1.5 m northeast of the shoreline angle. This bed probably correlates with similar beds in Trenches 18 and 10. As in trench 1 (Figure 2-7B), the well-sorted sand (Qb) has probably been disrupted by liquefaction. Logged by S. McGill.

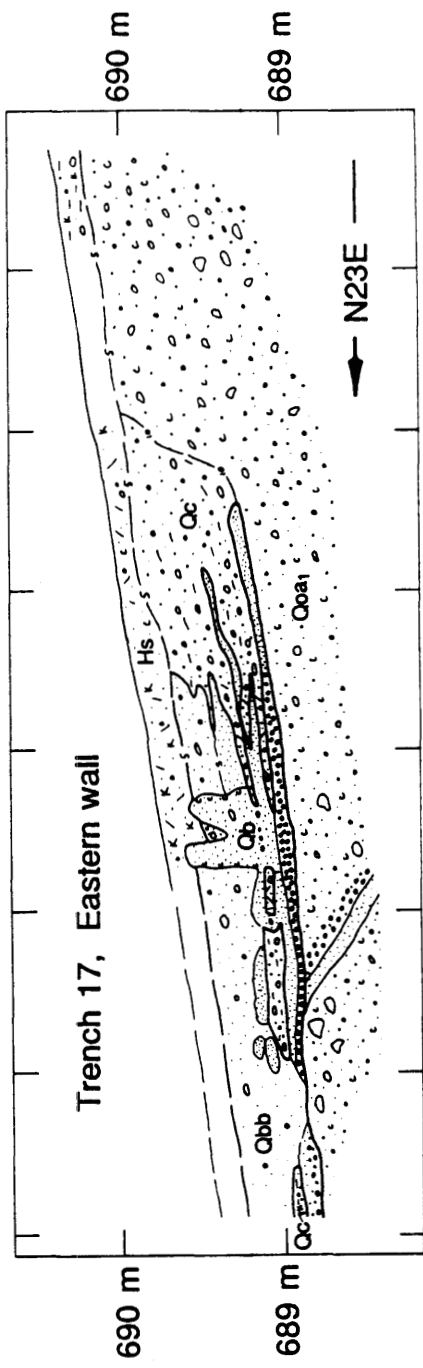


Figure 2-7C

FIGURE 2-7D: Cross section along western wall of Trench 9 shows well-sorted beach sands (Qb) truncated by fault 9A at the northern edge of the southern fault zone. Bioturbated beach deposits (Qbb) are exposed within the southern fault zone. The shoreline angle is about 20 cm north of fault 9J. Logged by S. McGill and M. Slates.

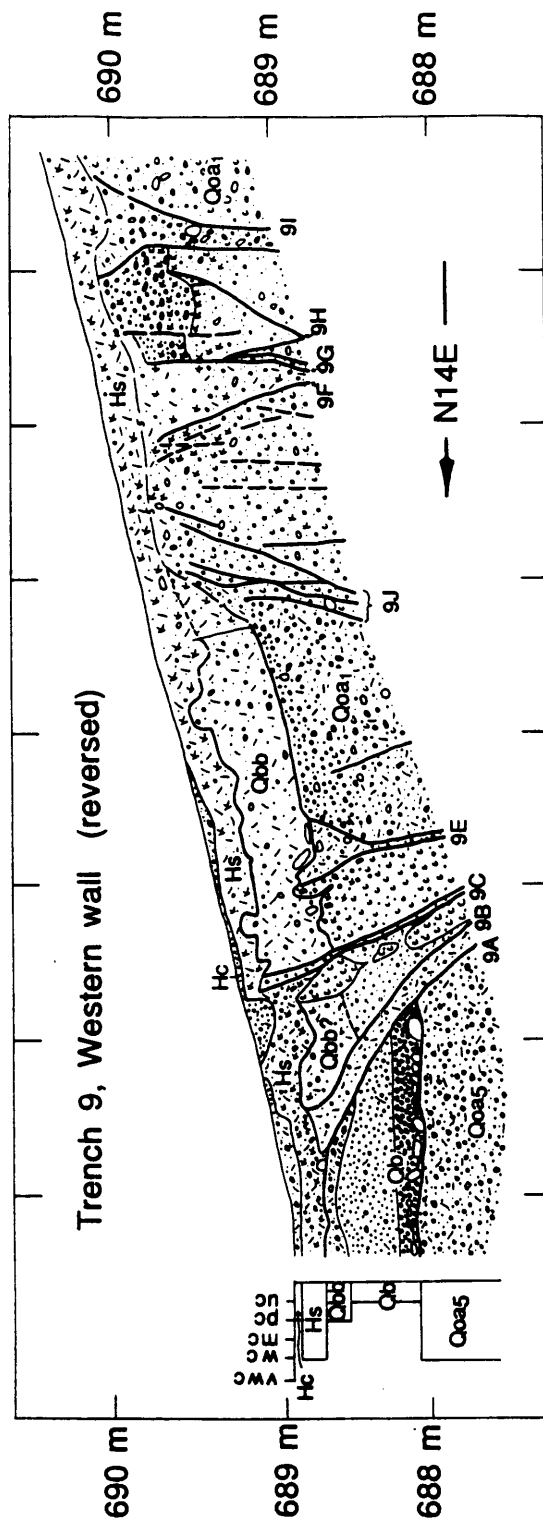


Figure 2-7D

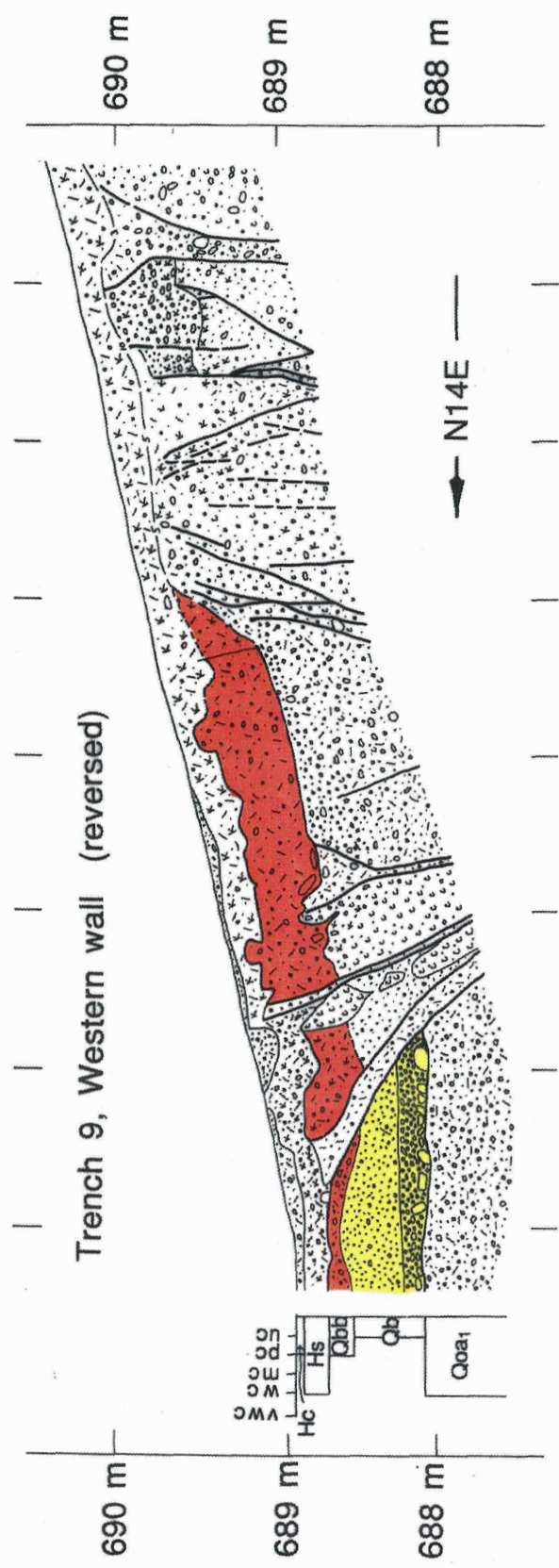


Figure 2-7D

FIGURE 2-7E: Cross section along southern wall of Trench 18 shows beach deposits (Qb) interfingering with colluvium (Qc) derived from the sea cliff. Shoreline angle is at western end of lowest sand layer. Note bed of framework-supported granules that pinches out about 2 m east of the shoreline angle. This bed probably correlates with similar beds in Trenches 17 and 10. A lag deposit of rounded and subrounded cobbles extends eastward from just beyond the eastern end of the cross section.

Logged by M. Slates.

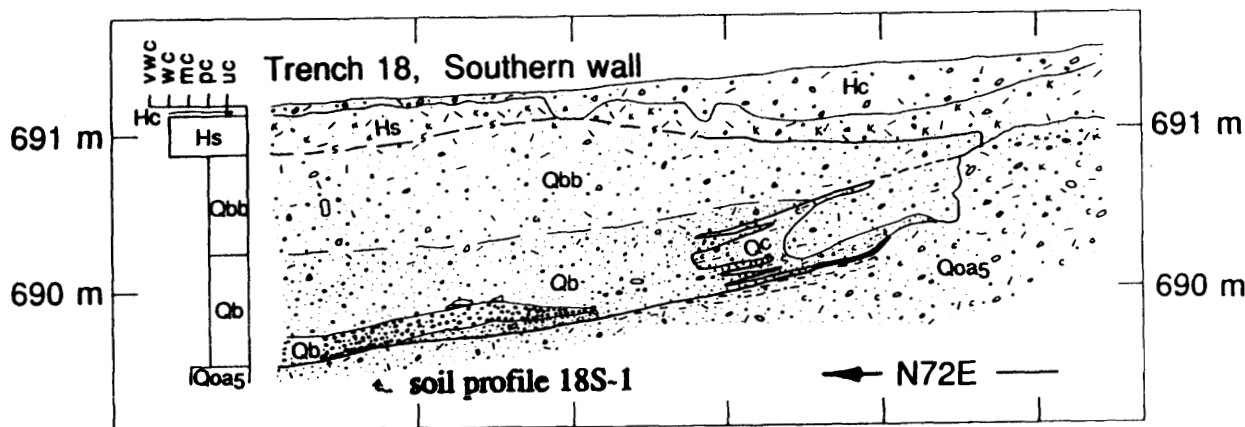


Figure 2-7E

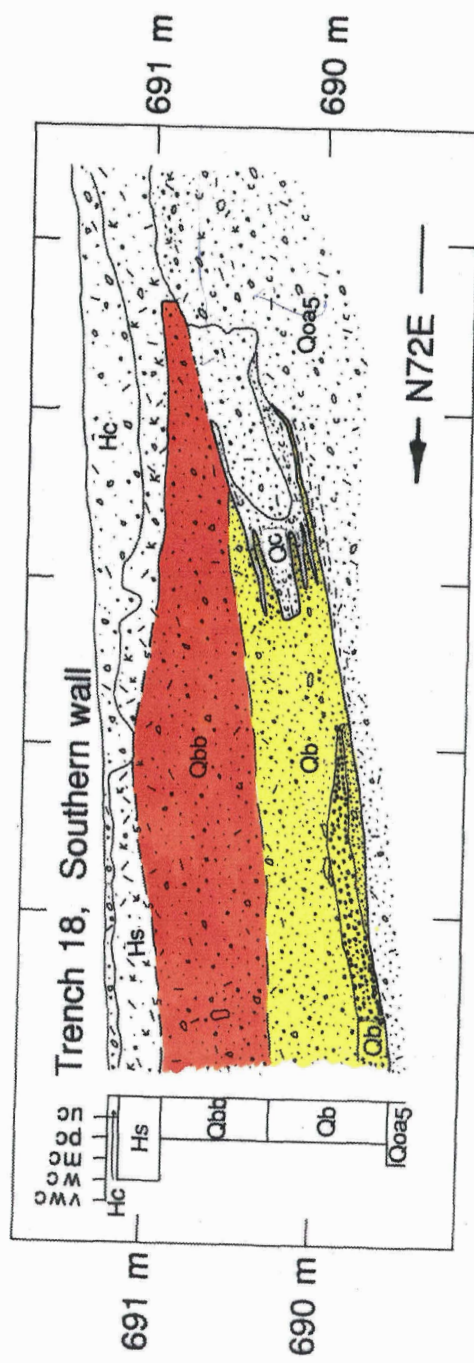


Figure 2-7E

FIGURE 2-7F: Cross section along southern wall of Trench 10 shows poorly consolidated, bioturbated beach deposits (Qbb) interfingering with colluvium (Qc) derived from the sea cliff. Shoreline angle is at lower, western corner of Qbb deposit. Note bed of framework-supported granules that pinches out about 1.5 m west of shoreline angle. This bed probably correlates with similar beds in Trenches 17 and 18. Also note lag deposit of rounded and subrounded cobbles that extends eastward from a point about 4 m east of the shoreline angle. Logged by S. McGill and M. Slates.

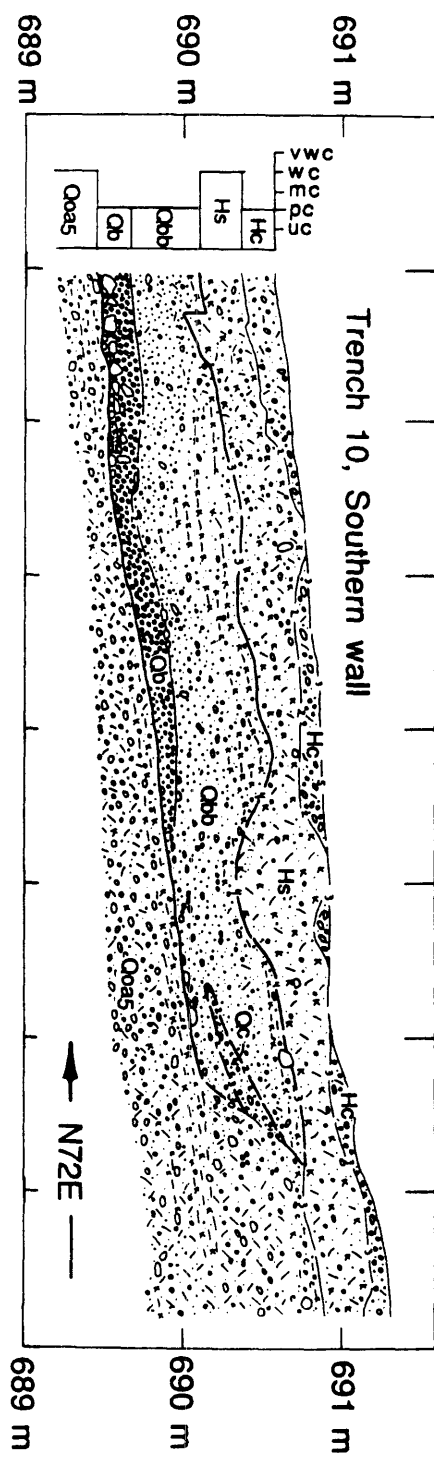


Figure 2-7F

FIGURE 2-7G: Cross section along the southern wall of Trench 3. There is no sea cliff in this exposure; beach deposits (Qb, Qbc) and bioturbated beach deposits (Qbb) pinchout along a gently sloping lake floor. Logged by S. McGill and M. Slates.

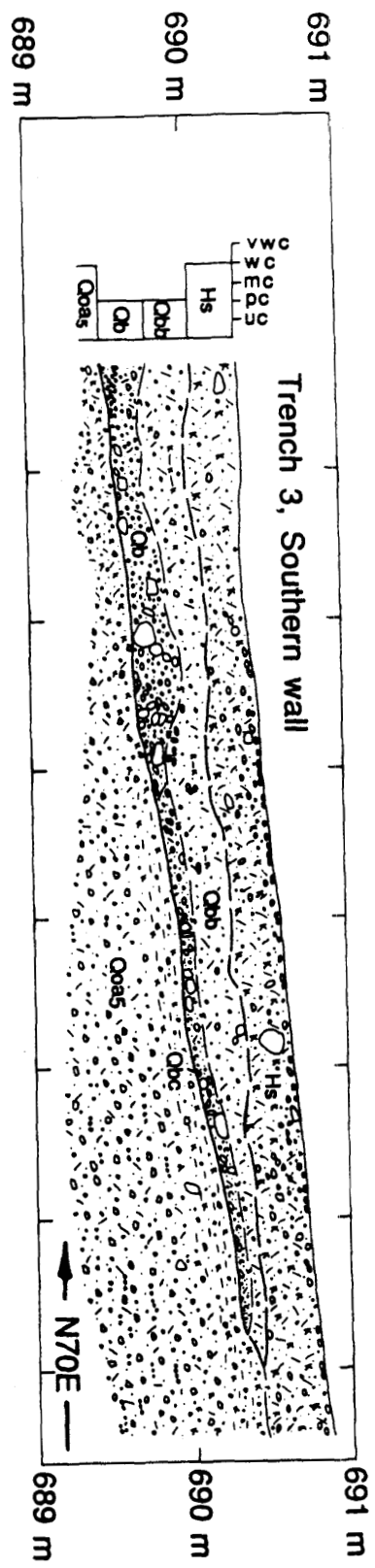


Figure 2-7G

FIGURE 2-7H: Cross section along southeastern wall of Trench 4. Gravel layer containing rounded and subrounded cobbles (Qob₃) was probably deposited during one of the older lakestands (possibly the 120-135 ka highstand) on the basis of 1-mm-thick calcium-carbonate coatings on the cobbles. Radiocarbon analyses of snail shells from this layer will test this hypothesis. The sea cliff associated with the most recent highstand is inferred to be along the poorly defined contact between moderately consolidated, massive, sandy gravel inferred to be bioturbated beach deposits (Qbb) and very well-consolidated, sandy gravel with crude, subhorizontal bedding inferred to be older alluvium (Qoa₀). The stronger soil development in the western two-thirds of the cross section is also consistent with the inferred position of the sea cliff associated with the most recent highstand. Logged by S. McGill and M. Slates.

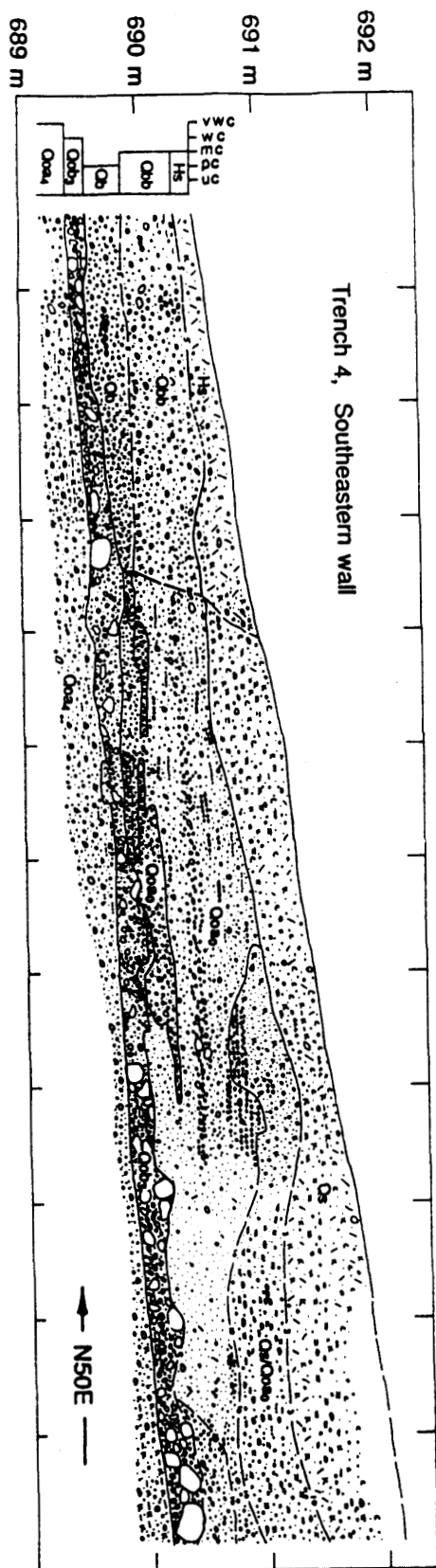


Figure 2-7H

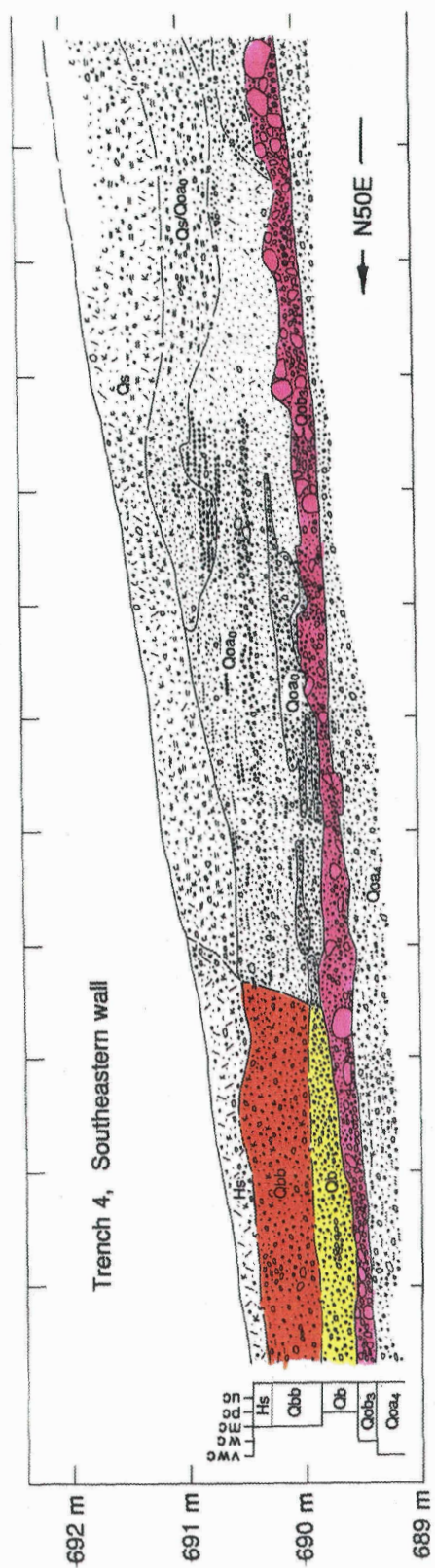


Figure 2-7H

TABLE 2-1. Explanation of units in cross sections

Hc: Holocene colluvium, deposited after Qb beach deposits. Poorly sorted, unstratified, pebbly, silty sand.

Hs: Holocene soil, produced by infiltration of aeolian silt and calcium-carbonate dust. Usually well-consolidated.

Qb: Quaternary beach and nearshore lacustrine deposits. Usually unconsolidated, moderately sorted to moderately well-sorted, fine to very coarse sand. Locally stratified, as shown in cross sections. Probably deposited during the most recent highstand of Searles Lake, which ended between about 10,000 and 13,800 ^{14}C -yr B.P. (Stuiver and Smith, 1979; Benson and others, 1990; Dorn and others, 1990; See section entitled "Age of the shoreline and slip rate of the Garlock fault.")

Qbb: Quaternary beach and nearshore lacustrine deposits that have been bioturbated and/or infiltrated by aeolian silt. Poorly consolidated, poorly sorted, unstratified, silty sand.

Qbc: Quaternary beach and nearshore lacustrine deposits that have been partially consolidated and reddened by clay. Clayey sand.

Qc: Quaternary colluvium, derived from a sea cliff and interfingering with the youngest beach deposits. Poorly sorted, pebbly sand.

Qob₁: Older Quaternary beach and nearshore lacustrine deposits. Mostly unconsolidated, moderately to poorly sorted coarse sand and granules. Stratified and locally cemented by calcium carbonate where exposed in the

Table 2-1 (continued)

northern end of Trench 15 (Figure 2-14D). Also exposed in trenches 7 (Figure 2-14B) and 20 (not shown). Relative elevations suggest that this deposit is older than Qb, but comparable soil development suggests that it is not much older than Qb. Qob₁ was probably deposited during one of the highstands of Searles Lake that occurred between 10,000 and 24,000 ¹⁴C-yr B.P. (Stuiver and Smith, 1979; Benson and others, 1990), but prior to the most recent highstand.

Qobb₁: Older Quaternary beach and nearshore lacustrine deposits that have been bioturbated and/or infiltrated by aeolian silt. Poorly sorted, silty sand, granules and pebbles. Exposed in trenches 7, 15 and 20.

Qob₂: Older Quaternary beach and nearshore lacustrine deposits. Interbedded, clast-supported pebbles, and moderately well-sorted granules and sand. Mostly unconsolidated, but locally cemented by calcium carbonate. Exposed in the central portion of trench 15 (Figure 2-14E). The coarseness and thickness of this unit is unlike any of the other beach deposits exposed in the trenches. Probably older than Qob₁, on the basis of their relative elevations, but not much older, because of the lack of a well-developed soil profile on Qob₂. Qob₂ may have been deposited during one of the highstands of Searles Lake that occurred between 10,000 and 24,000 ¹⁴C-yr B.P. (Stuiver and Smith, 1979; Benson and others, 1990), but most likely prior to deposition of Qb and Qob₁.

Table 2-1 (continued)

Qobb₂: Older Quaternary beach and nearshore lacustrine deposits that have been bioturbated and/or infiltrated by aeolian silt. Probably older than Qobb₁, on the basis of their relative elevations. Poorly sorted, pebbly, silty sand. Exposed in the central portion of trench 15.

Qu: Poorly consolidated, poorly sorted, unstratified, pebbly, silty sand of unknown origin. Underlies Qob₂.

Qol₁: Older Quaternary lacustrine(?) deposits. White, cemented, silty, fine-grained sandstone. Exposed in trench 15 (Figures 2-14D and 2-14E)

Qs: Soil developed on deposits older than Qb.

Qoa₀: Older Quaternary alluvium. Very well-consolidated, crudely stratified sandy gravel. Exposed in trench 4 (Figure 2-7H). Truncated to the northeast by an inferred sea cliff against which younger beach sediments (Qb, Qbb) have been deposited. The relative degree of soil development on Qoa₀ and Qbb also confirm that Qoa₀ is older than Qb and Qbb.

Qob₃: Older Quaternary beach and nearshore lacustrine deposits. Well-consolidated, cobble gravel. Exposed in trench 4 (Figure 2-7H). Contains fossil freshwater snail shells including Lymnaeidae *Stagnicola* sp., Lymnaeidae *Lymnaea* sp., and Planorbidae *Helisoma (Carinifex)* sp. Stratigraphic position indicates that this unit predates Qoa₀. Degree of soil development on Qoa₀ suggests that Qoa₀ and hence Qob₃ are considerably older than Qob₁ and Qob₂. Qob₃ may have been deposited during the highstand of Searles Lake that occurred about

Table 2-1 (continued)

120 and 135 ka ago (G. I. Smith, unpublished U-series dates).

Qoa₅: Older Quaternary alluvium. Well-consolidated sandy gravel. Exposed in trenches 2, 9, 18, 10 and 3, between the northern and southern fault strands. Stratigraphic position indicates this unit is older than Qb and Qbb. Less consolidated than but may correlate with Qoa₄ in trench 4.

Qoa₄: Older Quaternary alluvium. Very well-consolidated sandy gravel. Exposed in trench 4 (Figure 2-7H). Stratigraphically below Qob₃.

Qoa₃: Older Quaternary alluvium. Very well-consolidated gravel with some cobbles and boulders that disintegrate easily. Exposed in trenches north of the northern fault.

Qoa₂: Older Quaternary alluvium. Well-consolidated pebbly gravel. Exposed in trenches 11, 12, 19 and 13, within the north-central shear zone and between that zone and the northern fault. Stratigraphic position indicates this unit is older than Qb, but the age of this unit relative to other units older than Qb is uncertain.

Qol₂: Older Quaternary lacustrine deposits. Well-sorted claystone, siltstone and fine-grained sandstone. May include interbedded fluvial deposits. Where visible (in Trench 13), bedding has an apparent dip of 30-45° northeastward. Stratigraphic relations indicate that this unit is older than Qb, but its age relative to other units older than Qb is uncertain.

Table 2-1 (continued)

Qoa₁: Older Quaternary alluvium. Well-consolidated, sandy, clayey gravel. Bedding has an apparent dip of about 20° southwestward. Exposed in trenches 1, 17, 9 and 2, south of the southern fault. Stratigraphic relations indicate that this unit is older than Qb, but its age relative to other units older than Qb is uncertain.

(4) In Trenches 17, 18, 10 and 3 there is a 10- to 30-cm-thick layer of well-sorted, framework-supported granules that pinches out 1-2 m from the sea cliff. The lack of such a granule layer in Trench 9 is also consistent with the lack of such a layer within 2 m of the sea cliff in Trench 18.

There are a few differences in the shoreline features on either side of the southern fault. First, the beach deposits in Trench 18 are about twice as thick as those within the fault zone in Trench 9. This may be due to greater erosion of the beach sediments in Trench 9 than of those in Trench 18. Perhaps colluvium from the scarp along the southern fault quickly buried the beach deposits in Trench 18, protecting them from erosion. Second, in Trench 18 the beach sediments interfinger with clay-rich colluvium near the sea cliff, whereas in Trench 9 the beach deposits are buttressed against the cliff without any interfingering colluvium.

Although the southern fault zone is 4-5 m wide in Trenches 9 and 2, significant offset of the shoreline has occurred only along the northernmost fault within this zone. The other fault strands must have become inactive prior to deposition of the beach deposits of the youngest lakestand (Qb). In both Trenches 9 and 2, well-sorted sands (nearshore lacustrine deposits) are in fault contact with older alluvium along the northernmost strand within the southern fault zone. The trend of the shoreline angle (the pinchout of lacustrine sands at the base of the sea cliff) in Trenches 1, 17 and 9 suggests that the shoreline is not significantly offset along any of the fault strands exposed south of the shoreline in Trench 9. The shoreline may have been offset as much as about 1 m on these faults (P1 to P2 in

Figure 2-6), but any larger offset would require an unjustifiable and unlikely geometry of the shoreline. Three-dimensional hand-excavation of the sea cliff between the western wall of Trench 9 and the northernmost fault in the southern fault zone also indicates no left-lateral offset of the sea cliff on any of the faults between the shoreline in Trench 9 and the northernmost fault within the southern fault zone.

The three-dimensional hand-excavation along the sea cliff from the western wall of Trench 9 to the northernmost strand of the southern fault zone revealed the precise location of intersection of the base of the sea cliff with that fault (P3 on Figure 2-6). Projection of the base of the sea cliff from both walls of Trench 18 to the northernmost fault in the southern fault zone yields the piercing point P4, whereas projection of a visual best-fit line to the same feature as revealed in both walls of Trenches 10 and 18 yields the piercing point P5 (Figure 2-6). I prefer P5 to P4 because the trend of the best-fit line is less sensitive to the uncertainty in the location of the base of the sea cliff in any one trench wall and because the trend of the best-fit line is more consistent with the trend of the base of the sea cliff exposed in the three-dimensional excavation west of Trench 9. The preferred value for the left-lateral offset of the shoreline across the southern fault zone is 37 m (P3 to P5), but the offset could be as small as 36 m (P3 to P4) or as large as 38 m (P3 to P5 plus P1 to P2).

Possible offset between Trenches 3 and 4

The presence of a small (\approx 10-cm-high) fault scarp north of Trench 2 (Figures 2-4 and 2-6) suggests the possibility of additional offset of the shoreline between Trenches 3 and 4. The location and trend of the shoreline angle in Trenches 3 and 4, however, indicate that little or no lateral offset of the shoreline has occurred on this fault. In Trench 3, there is no sea cliff; the beach deposits thin and pinch out on a gently sloping lake floor. Because the base of the sea cliff is at an elevation of 690.1 m in Trench 10, I believe that the 690.1 m structure contour on the surface of the lake floor in Trench 3 correlates with the base of the sea cliff in Trenches 10 and 18. The projection of this structure contour intersects the projection of the small scarp at P7 (Figure 2-6). A reasonable eastern limit on the intersection of the shoreline with the projection of the small scarp is obtained by projecting the visual best-fit line through the shoreline in Trenches 10 and 18 northward to P6 (Figure 2-6).

In Trench 4, a 20- to 30-cm-thick gravel layer with rounded and subrounded cobbles extends from near the eastern end of the trench to beyond the western end of the trench and overlies well-consolidated, poorly sorted gravel (Figure 2-7H). I interpret the cobbly layer to be nearshore lacustrine gravels overlying older alluvium. The presence of 1-mm-thick calcium-carbonate coatings on many of the cobbles suggests that these lacustrine gravels were deposited during one of the older lakestands, perhaps the 120-135 ka highstand. A few dozen gastropod shells were collected from the rounded cobble layer. The collected shells included specimens of

Planorbidae *Helisoma (Carinifex)*, Lymnaeidae *Stagnicola*, and Lymnaea (Clif Coney, Los Angeles County Museum of Natural History, oral communication, 1991). Some of the shells appeared to be in growth position, affixed to the underside of cobbles. Future U-series and/or radiocarbon analyses of these shells may constrain the age of this layer.

In the western half of the trench, the rounded cobble layer is overlain by very well-consolidated alluvium with a well-developed soil profile. In the eastern half of the trench, however, the rounded cobble layer is overlain by poorly consolidated, moderately to poorly sorted sand and granules, which I interpret to be the beach deposits associated with the most recent highstand of Searles Lake. The soil profile in these deposits is much less developed than the profile in the western half of the trench. Apparently the lacustrine cobble layer from an older lakestand was buried by alluvium, and a soil began forming on that alluvium. Later, wave action during the most recent highstand of the lake eroded the alluvium that buries the older lake gravels from the eastern half of the trench and deposited beach sands on top of the older lake gravels. The presence of calcium-carbonate coatings up to 1-mm-thick on cobbles beneath the young beach sands indicates that waves during the most recent lakestand did not significantly rework the older, lacustrine cobble layer.

Uncertainty as to the precise location of the inferred sea cliff makes determination of the trend of that cliff impossible, so I assume a trend parallel to the geomorphic break in slope east of Trench 4 (Figure 2-6). This projects to the projection of the small scarp at P8, which lies very close to P7 and suggests that little

or no lateral offset of the shoreline has occurred on the small fault north of Trench 2 or on any concealed faults between Trenches 3 and 4. Because of the uncertainty in the location and trend of the shoreline in Trenches 3 and 4, however, the possibility of a few meters of slip in this zone can not be ruled out at this time (for example, 3 m from P6 to P8). Larger displacement is unlikely, given that the channel wall about 70 m to the east is not noticeably offset in this zone.

Possible offset between Trenches 4 and 11

There are no faults visible at the surface between Trenches 4 and 11, but projection of the shoreline northwestward from Trench 4 and southeastward from a hand-excavation southeast of Trench 11 suggests that conceivably the shoreline could have been offset a few meters on concealed faults between these two trenches (P9 to P10, Figure 2-6). Any concealed faults are probably not far southeast of Trench 11 because the geomorphic break in slope northeast of Trench 4 is not offset. The ~2-m- possible offset suggested by this projection is poorly constrained because of uncertainty in the location and trend of the shoreline in Trench 4 and in the trend of the shoreline between Trenches 4 and 11. There may well have been no offset of the shoreline between these two trenches.

Offset across the north-central shear zone

A zone of many, closely spaced faults that offset the shoreline lies about 6 to 14 m south of the northern fault zone. The relationships exposed in Trenches 11, 12,

13 and 19 and in the three-dimensional hand-excavations from these trenches place constraints on the displacement of the shoreline across this zone (Figure 2-8).

In the southeastern wall of Trench 11, very well-sorted beach sands pinch out against a sea cliff cut into older alluvium (Figure 2-9A). Three-dimensional hand-excavations revealed that the sand pinchout is offset 0.7 m across a fault exposed in and nearly parallel to the northwestern wall of Trench 11 (P12 to P13 in Figure 2-8) and is offset 0.1 m across a small fault north of Trench 11. The trend of the sand pinchout suggests that within 0.5 m north of the fault in the northwestern wall of Trench 11 and within 1.5 m south of that fault, the shoreline may have been warped left-laterally. If this is the case, then the 1 m of slip on discrete faults is a minimum estimate of the total displacement across this fault zone. Projection of the sand pinchout from farther away from this fault zone suggests that up to 1.8 m of left-lateral displacement may have occurred in a combination of slip on discrete faults and warping (Figure 2-8, P11-P14).

The trends of the sand pinchout in three-dimensional excavations northwest of Trench 11 and east of Trench 12 suggest that 1.8 m of left-lateral slip may have occurred on unexposed faults between these two trenches (Figure 2-8, P15-P16). It is also possible, of course, that no offset has occurred in this area because a smooth curve connecting the shoreline in the two hand-excavations would not be an unreasonable initial geometry for the shoreline. Given the number of faults that offset the lake bottom in Trenches 11, 12 and 19 (Figure 2-9), however, some offset on unexposed faults between Trenches 11 and 12 is likely. Therefore, I use 1.8 m as

FIGURE 2-8: Map documents the 3.5- to 13.6-m-offset of the shoreline across the north-central shear zone. The location of the pinchout of well-sorted beach sand against a sea cliff was revealed in Trenches 11, 12, 19 and 13 and in three-dimensional hand-excavations from these trenches. 12A-12G label faults that are also shown in Figure 2-9B. 19A-19G label faults that are also shown in Figure 2-9C. Locations of faults 19A-19G are shown where they intersect a horizontal plane at 690 m, and fault 19H is shown at the elevation of the base of the trench. Tic marks along the sides of trenches correspond to tic marks along the top and bottom of cross sections in Figures 2-9 and 2-12. P11-P26 are piercing points discussed in text. See text for details of offset measurements across the north-central shear zone.

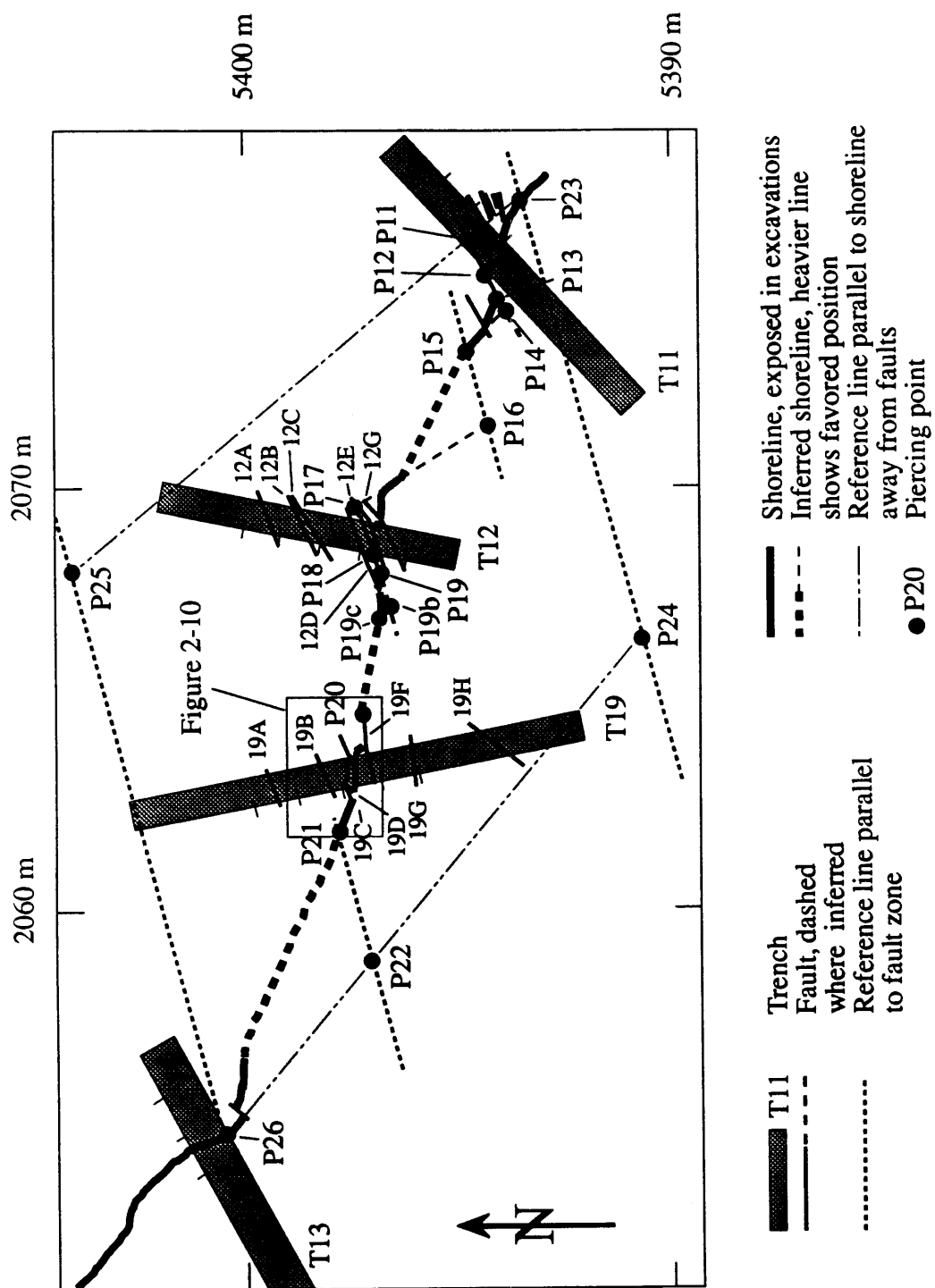


FIGURE 2-9: Cross sections of excavations within the north-central shear zone. Tic marks on top and bottom of cross sections are spaced 1 meter apart and correspond to tic marks along the sides of trenches in Figure 2-8. Elevations labelled on the sides of cross sections are in meters above sea level. Cross sections of the western walls of Trenches 12 and 19 have been reversed for easier comparison to other cross sections. See Figure 2-7A for explanation of symbols and Table 2-1 for explanation of units in cross sections.

FIGURE 2-9A: Cross section along southeastern wall of Trench 11 shows unconsolidated, well-sorted, coarse and very coarse beach sands (Qb) pinching out against a sea cliff. Logged by S. McGill and L. Maepa.

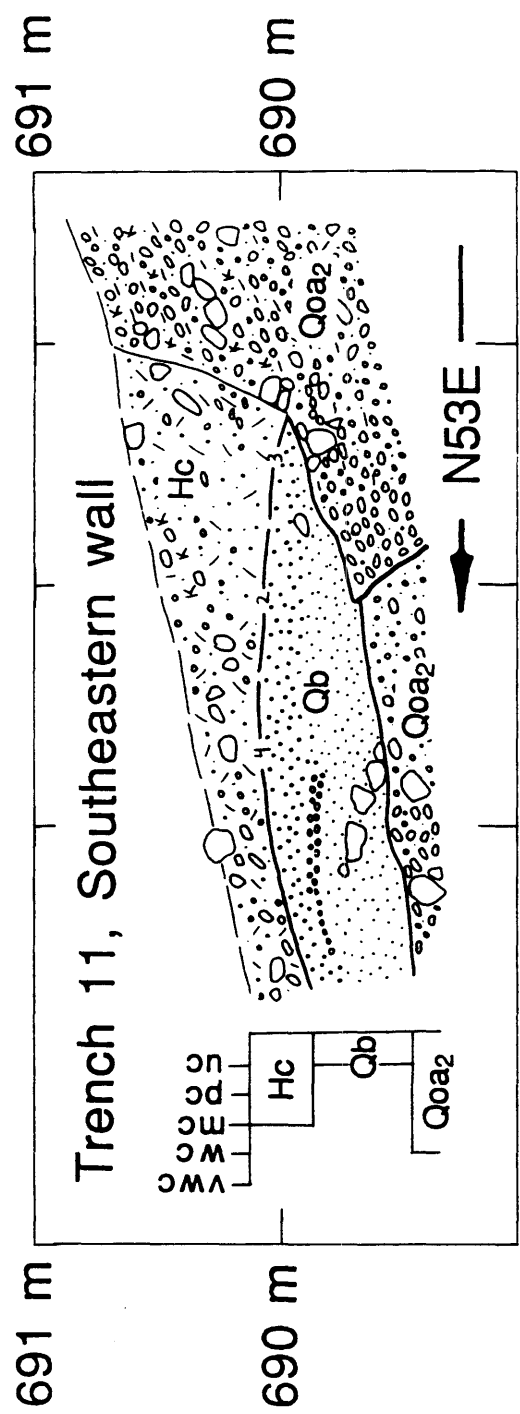


Figure 2-9A

FIGURE 2-9B: Cross section along western wall of Trench 12 shows unconsolidated, well-sorted, coarse and very coarse beach sands (Qb) truncated by fault 12E. Faults 12A-12G are shown in map view in Figure 2-8. Logged by S. McGill, M. Slates and S. Bryant.

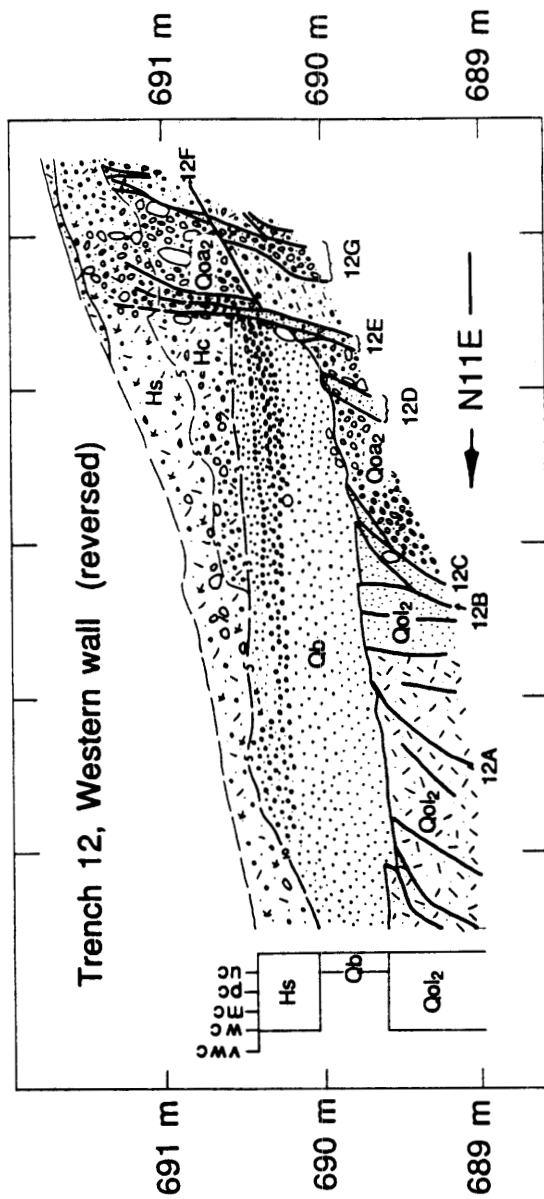


Figure 2-9B

FIGURE 2-9C: Cross section along western wall of Trench 19 shows poorly consolidated, well-sorted, coarse and very coarse beach sands (Qb) displaced along fault 19C and truncated by fault 19D. Faults 19A-19G are shown in map view in Figure 2-8. Logged by G. Roquemore, M. Slates and S. McGill.

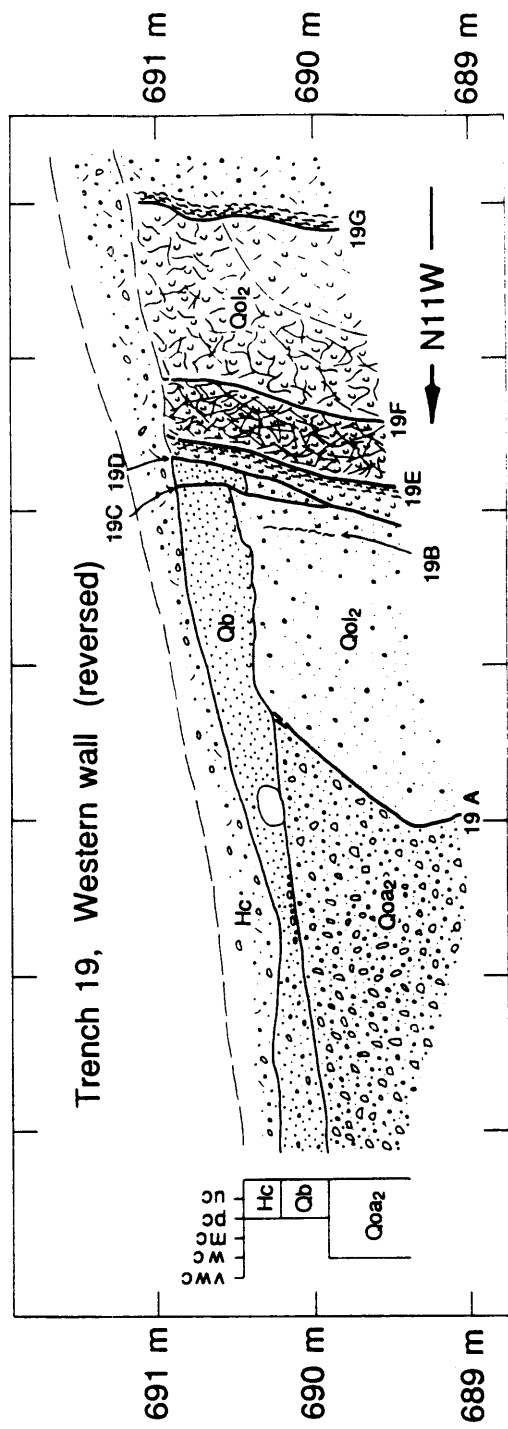


Figure 2-9C

a best estimate of the offset between Trenches 11 and 12 (Table 2-2).

In the western wall of Trench 12, very well-sorted beach sands are truncated by a near-vertical fault (fault 12E, Figure 2-9B). Projection of the sand pinchout in the western part of the hand-excavation east of Trench 12 indicates that about 0.7 m of left-lateral slip has occurred on faults 12E and 12G combined (P18-P19 in Figure 2-8). An additional 0.1 m offset of the shoreline has occurred on fault 12D. If the trends of the portions of the sand pinchout in the excavation west of Trench 12 and in the western part of the hand-excavation east of Trench 12 have been modified by warping, then a more complete estimate of the offset in this zone would be 2.8 m, from P17 to P19B, assuming that the original trend of the shoreline through this zone was parallel to the trend of the sand pinchout in the eastern part of the excavation east of Trench 12.

The shoreline may be offset the entire distance (about 2 m) between the excavations west of Trench 12 and east of Trench 19 along fault 19F (P19C to P20, Figure 2-8). Alternatively, it may not be offset at all in this area because the trend of the shoreline in the excavation west of Trench 12 projects directly to P20.

In the hand-excavation east of Trench 19, beach sands are truncated by fault 19F for a distance of at least 0.6 m (P20 to P27, Figure 2-10). A 15-cm-long segment of the shoreline is preserved between faults 19F and 19D, and the shoreline is offset 1.1 m along fault 19D (P28 to P29, Figure 2-10). The shoreline is offset about 0.2 m along fault C (P30 to P30B, Figure 2-10). The shoreline is thus offset a total of 1.9 m across discrete faults in the vicinity of Trench 19. If the shoreline has been

TABLE 2-2. Summary of offset across the north-central shear zone.

Area	Minimum offset (m)	Maximum offset (m)	Best estimate (m)
Trench 11 hand-excavations	0.8	1.8	0.8
Between hand-excavations			
from Trenches 11 and 12	0	1.8	1.8
Trench 12 hand-excavations	0.7	2.8	0.7
Between hand-excavations			
from Trenches 12 and 19	0	2.0	0
Trench 19 hand-excavations	1.9	2.1	1.9
Between hand-excavations			
from Trenches 19 and 13	0.1	3.1	0.1
TOTAL	3.5	13.6	5.3

FIGURE 2-10: Map documents 1.9- to 2.1-m-offset of shoreline in the vicinity of Trench 19. Sand-pinchout is offset at least 0.6 m along fault 19F (P20 to P27), about 1.1 m along fault 19D (P28 to P29) and about 0.2 m along fault 19C (P30 to P30b). An additional 0.2 m of left-lateral slip could conceivably have occurred as warping (P30b to P30c). Structure contour lines show the elevation of the lake floor in meters above sea level. Contour interval is 10 cm.

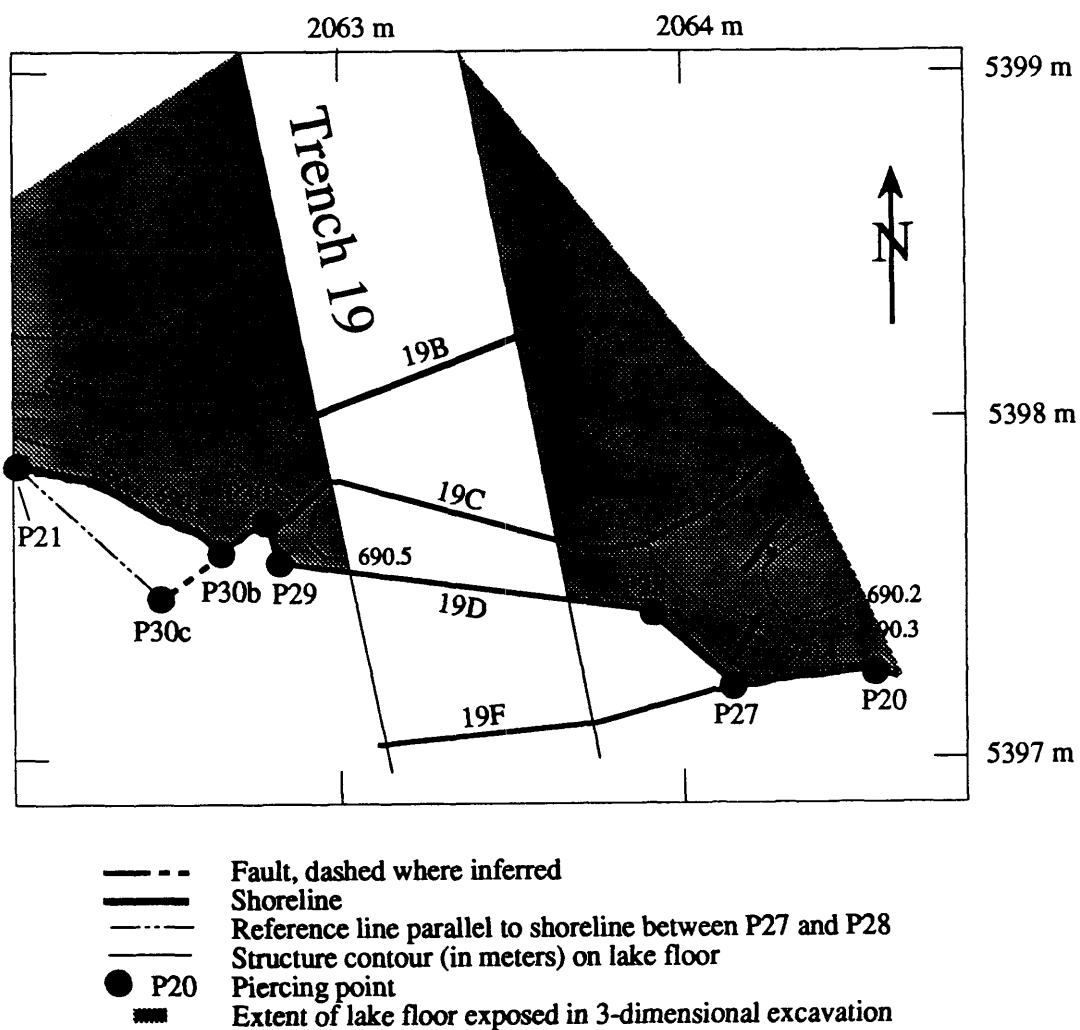


Figure 2-10

warped west of P30B, then an additional 0.2 m of slip may have occurred in this area (P30B to P30C, Figure 2-10).

The offset of the shoreline between the western edge of the hand-excavation west of Trench 19 and the southern wall of Trench 13 is between 0.1 m and 3.2 m. A smooth curve connecting the southern limit of the beach sands in the hand-excavations west of Trench 19 and south of Trench 13 would be reasonable geometry for the shoreline, suggesting that no offset may have occurred in this area (Figure 2-8). The structure contours on the sea cliff in the hand-excavation west of Trench 19 support a shoreline trend similar to that which would be consistent with no offset (Figures 2-8 and 2-10). If this is true, then the total offset between P21 and the southern wall of Trench 13 is 0.1 m, the offset on a minor fault exposed in the hand-excavation south of Trench 13. I use this value as a best estimate of the slip between P21 and P26. If the shoreline has been warped, however, the offset may be greater. An upper bound on the left-lateral displacement in this area is 3.1 m (P21 to P22, Figure 2-8). This is obtained from assuming a N50W original trend of the shoreline in this area (the trend of the shoreline away from any faults in the hand-excavation north of Trench 13) and a fault trend of N75E.

The total offset of the shoreline across the north-central shear zone is between 3.5 and 13.6 m (Table 2-2). The smaller value is the sum of measured offsets on discrete faults, whereas the larger value includes possible warping and possible slip on unexposed faults between the excavations. I use 5.3 m as a best estimate of the offset of the shoreline across the north-central shear zone. This value is the sum of

the measured offsets on discrete faults and the inferred 1.8 m offset that is strongly suggested by the projections of the shoreline northwest of Trench 11 and southeast of Trench 12.

An alternate method of estimating the left-lateral slip across the north-central shear zone is to project the trend of the shoreline on either side of the shear zone to a hypothetical fault trending N75E. Assuming an original shoreline trend of N40W (trend of sand pinchout in southeastern end of hand-excavation southeast of Trench 11) throughout the shear zone yields an offset of 13.7 m (P25 to P26 in Figure 2-8). Assuming an original trend of the shoreline throughout the shear zone of N50W (trend of sand pinchout in hand-excavation north of Trench 13) yields an offset of 10.7 m (P23 to P24 in Figure 2-8). These values are consistent with the range of offsets summarized in Table 2-2.

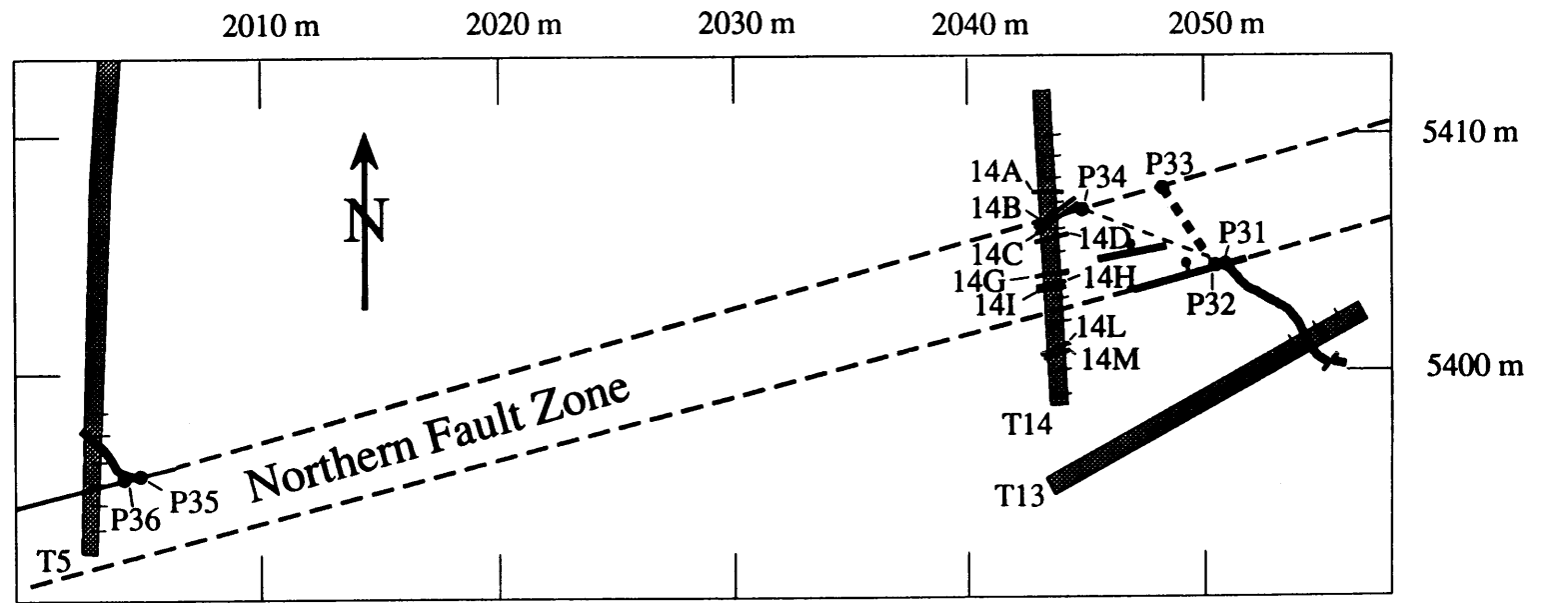
Offset across the northern fault zone

The characteristics of the shoreline and of the beach deposits in the hand-excavation north of Trench 13 are similar to those in the hand-excavation east of Trench 5, supporting the correlation of the shoreline between these two excavations (Figures 2-11 and 2-12). In both hand-excavations the beach deposits are 0.4 to 0.5 m thick and consist of moderately to well-sorted, coarse to very coarse sand. The trend of the shoreline in these two excavations is also similar (Figure 2-11).

The best estimate of the offset of the shoreline across the northern fault zone is 46 m. To obtain this estimate I project the shoreline to a line

FIGURE 2-11: Map documents 42- to 46-m-offset of the shoreline across the northern fault zone. The shoreline is probably warped within about 0.7 m north of the northern edge of the northern fault zone, in which case the offset is 46 m (P33 to P36 plus P31 to P32). The minimum offset is 42 m (P34 to P35 plus P31 to P32) and would apply if the current trend of the shoreline within 0.7 m north of the northern edge of the northern fault zone represents the original trend of the shoreline across the northern fault zone. Tic marks along the sides of trenches correspond to tic marks along the top and bottom of cross sections in Figure 2-12.

Figure 2-11



- - - Fault, dashed where approximately located
- - - Fault scarp, bar and ball on lower side
- - - Shoreline, dashed where inferred, heavier line shows favored position
- T5 Trench
- P31 Piercing point

FIGURE 2-12: Cross sections of excavations on both sides of and across the northern fault zone. Tic marks on top and bottom of cross sections are spaced 1 meter apart and correspond to tic marks along the sides of trenches in Figure 2-11. Elevations labelled on the sides of cross sections are in meters above sea level. Cross section of the northern wall of Trench 13 has been reversed for easier comparison to other cross sections. See Figure 2-7A for explanation of symbols and Table 2-1 for explanation of units in cross sections.

FIGURE 2-12A: Cross section along northern wall of Trench 13 shows poorly consolidated, well-sorted, coarse beach sands (Qb) pinching out against colluvium (Qc) derived from the sea cliff. Logged by S. McGill.

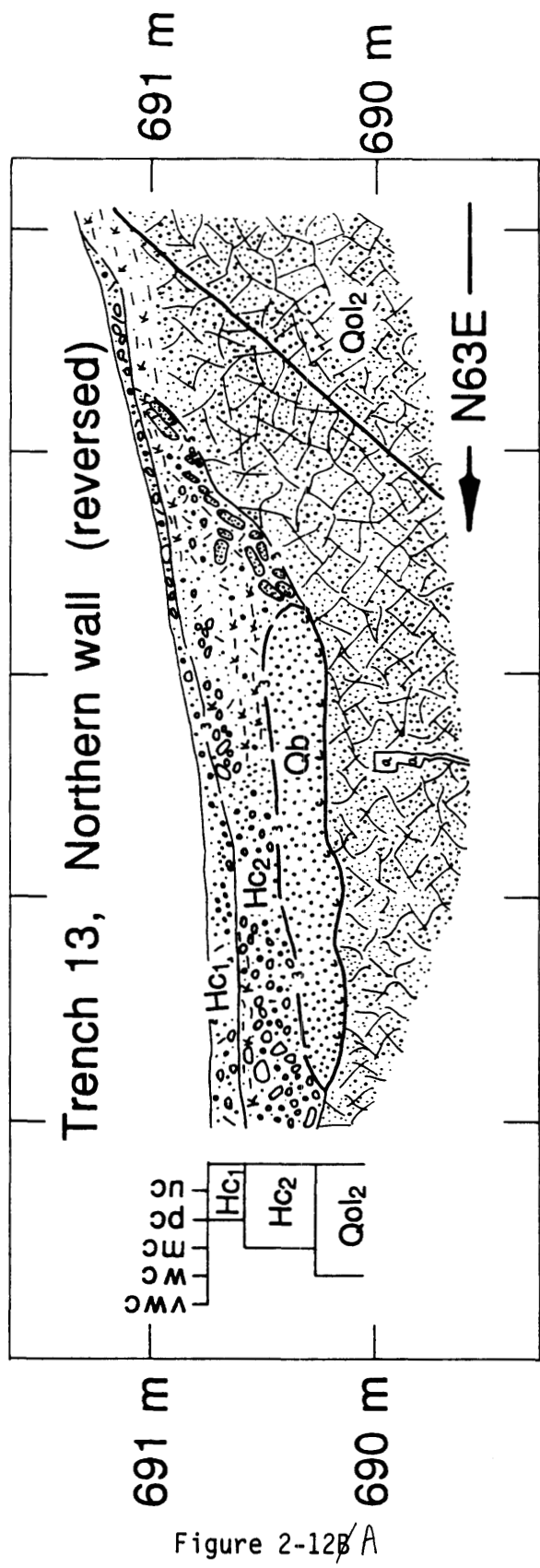


FIGURE 2-12B: Cross section along eastern wall of Trench 5 shows unconsolidated, well-sorted, coarse beach sands (Qb) pinching out against older alluvium (Qoa₃). Northern fault zone is exposed in the southern end of the cross section. Logged by S. McGill and M. Slates.

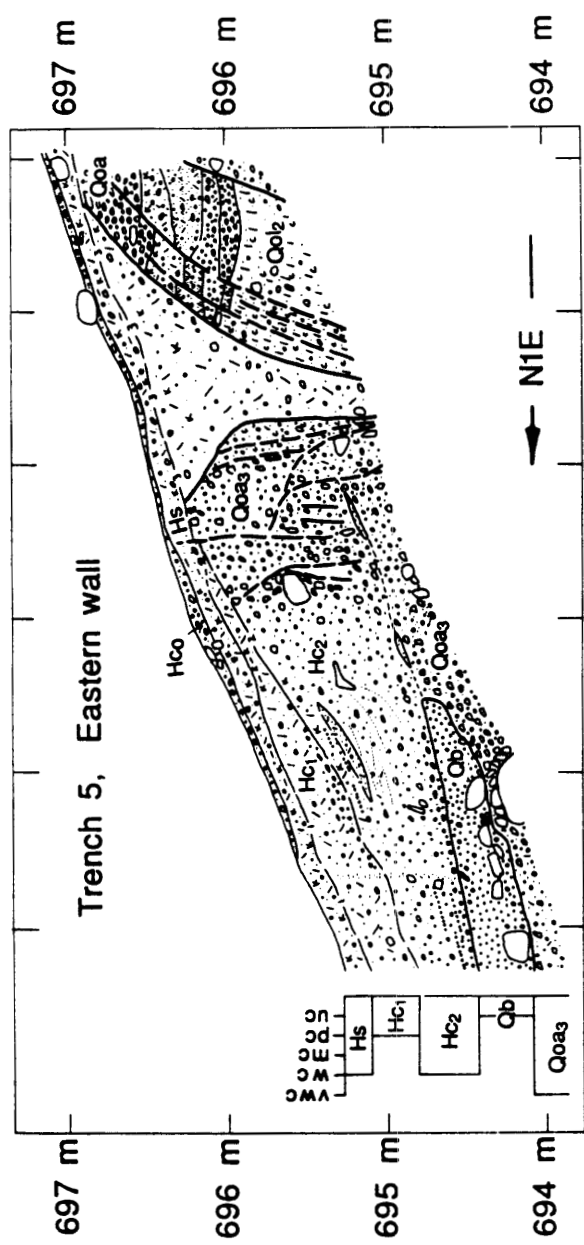


Figure 2-12B

FIGURE 2-12C: Cross section along eastern wall of Trench 14 shows the northern fault zone. Poorly consolidated, poorly sorted, sandy gravel that may be bioturbated beach deposits (Qbb?) are truncated by fault 14B. Faults 14B, 14C, 14D, 14E, 14F and 14G appear to be the most recently active strands within the northern fault zone. Faults 14A-14M are shown in map view in Figure 2-11. Logged by S. McGill, M. Slates and S. Bryant.

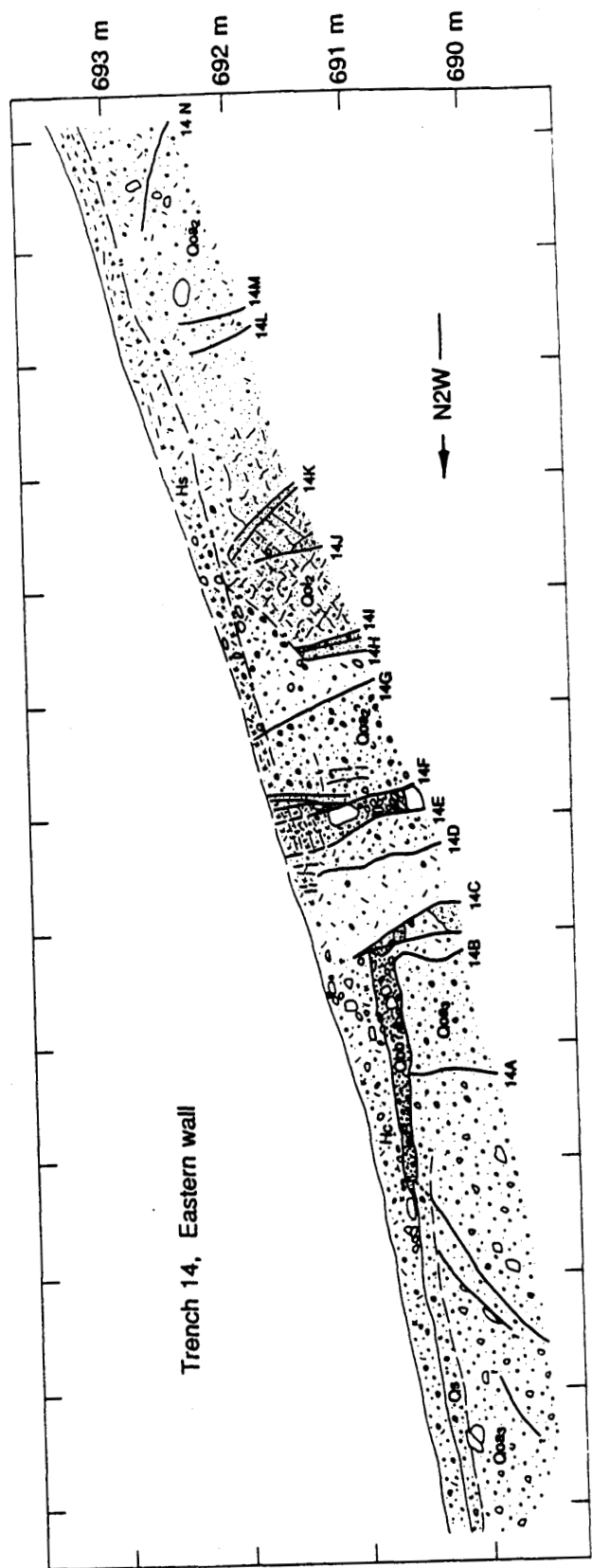


Figure 2-12C

connecting the northern edge of the northern fault zone in Trenches 5 and 14 (Figure 2-11). In Trench 14, fault 14A does not displace poorly consolidated, poorly sorted, pebbly sand that may be bioturbated beach deposits or alluvium burying the old lake floor (Figure 2-12C). These pebbly sands are truncated against fault 14B, however, so I use fault 14B as the northern limit of the northern fault zone in Trench 14, for the time period since the latest lake highstand. Although the trend of the northernmost fault in the hand-excavation east of Trench 5 and the trend of fault 14B are more northerly than the N75E-trend of the line connecting these two faults (Figure 2-11), these two fault strands are probably part of an *en echelon* fault pattern in which the trends of individual fault strands are not parallel to the trend of the fault zone as a whole.

To obtain a best estimate of the offset across the northern fault zone, I assume that the more easterly trend of the shoreline within about 0.7 m of the fault zone in the hand-excavation east of Trench 5 is due to warping (Figure 2-11). This is a reasonable assumption because the zone in which warping is inferred coincides with a zone in which the lake floor is displaced by minor faults with 3 to 25 cm of vertical separation. Furthermore, the \approx N35W trend of the shoreline immediately north of the zone of possible warping compares well with the trend of the shoreline in the northernmost part of the hand-excavation north of Trench 13. Projection of these parts of the shoreline to the northern edge of the northern fault zone yields an offset of 45.5 m (P33 to P36, Figure 2-11). When added to the 0.5 m offset measured across a minor fault in the hand-excavation north of Trench 13 (P31 to P32

in Figure 2-11), this gives a total of 46 m offset. If the shoreline is not warped near the fault zone in the hand-excavation east of Trench 5, and if the trend of the sand pinchout in this area represents the original trend of the shoreline across the fault zone (a hypothesis I regard as unlikely), then the offset could be as small as 42.1 m (P34 to P35 in Figure 2-11) plus the 0.5 m offset exposed in the hand-excavation north of Trench 13.

Correlation of shoreline features north of the northern fault zone

The sea cliff and beach deposits exposed in Trenches 6 and 7 are similar in thickness, grain size and sorting to those exposed in Trench 5 (Figures 2-13 and 2-14A,B). The location and trend of the shoreline in Trenches 5, 6 and 7 confirms the correlation of the shoreline between these three trenches (Figure 2-13). West of Trench 7, however, the correlation of shoreline features is less certain. Within Trenches 8, 15 and 20, three different sets of shoreline and nearshore deposits and features are exposed. In Trench 8 and in the northern half of Trench 20, a sea cliff is exposed, but there are no moderately or well-sorted sands (Figure 2-14C). The cliff and the inferred lake floor are buried by poorly sorted sand that may be alluvium or bioturbated beach deposits. In the southern half of Trench 20 and in the northern part of Trench 15 another possible shoreline is exposed. Very coarse sand and granules, moderately sorted in northern Trench 15 and poorly sorted in southern Trench 20, are present within a trough cut into the older alluvium (Figures 2-14D). Although the geometry of the deposit suggests that these may be alluvial sands, I

FIGURE 2-13: Locations of shoreline features in trenches north of the northern fault zone. There is no evidence of significant offset of the shoreline north of the northern fault zone, but up to about 3 m of left-lateral warping could conceivably have occurred (P37 to P38). Warping may be responsible for the more westerly trend of the shoreline angle in Trench 7.

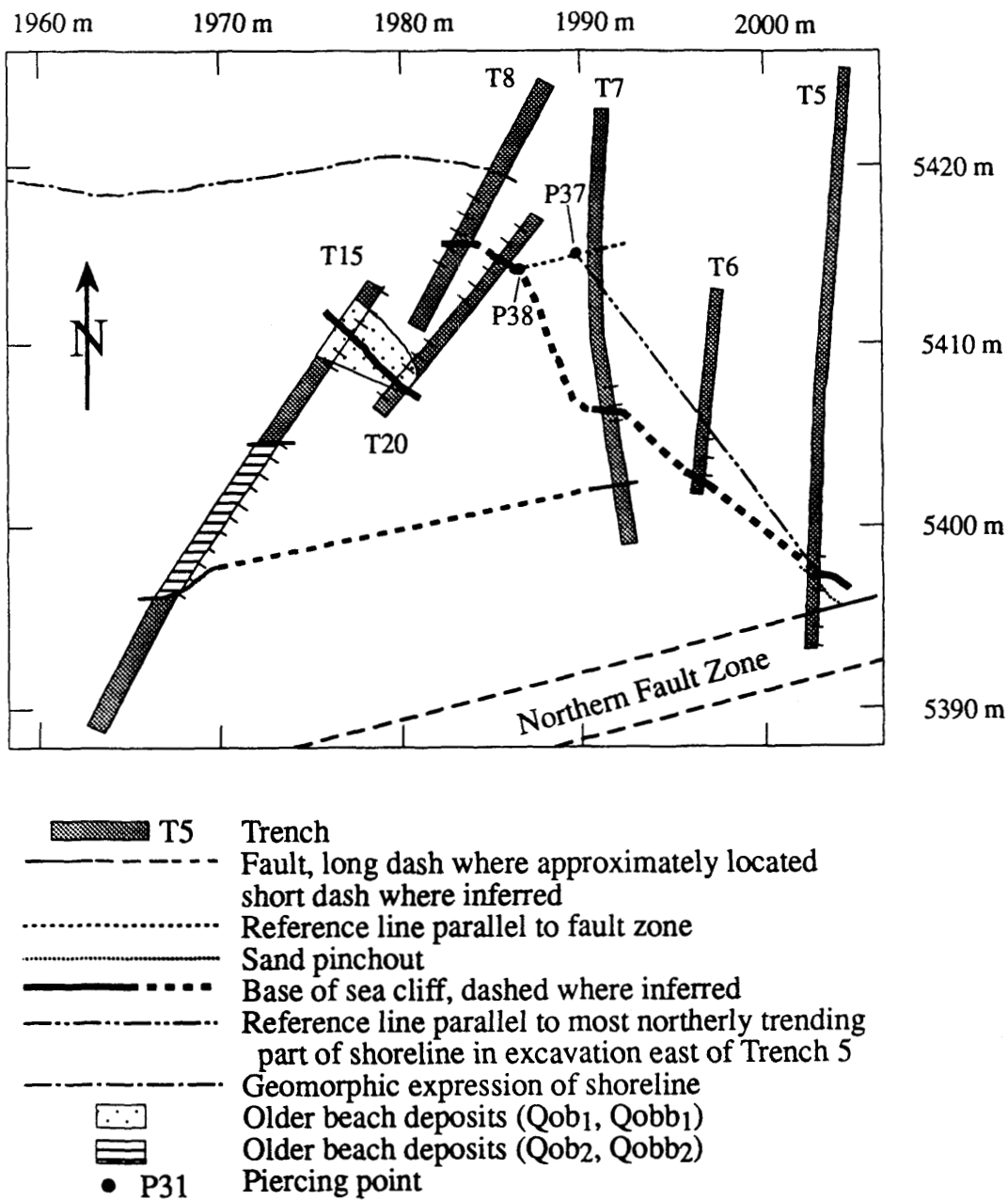


Figure 2-13

FIGURE 2-14: Cross sections of excavations north of the northern fault zone. Tic marks on top and bottom of cross sections are spaced 1 meter apart and correspond to tic marks along the sides of trenches in Figure 2-13. Elevations labelled on the sides of cross sections are in meters above sea level. Cross section of the western wall of Trench 8 has been reversed for easier comparison to other cross sections. See Figure 2-7A for explanation of symbols and Table 2-1 for explanation of units in cross sections.

FIGURE 2-14A: Cross section along eastern wall of Trench 6 shows clayey beach sands (Qbc) interbedded with colluvium (Qc) derived from sea cliff. Inferred contact between colluvium (Qc) and older alluvium (Qoa₃) shows probable location of sea cliff. Logged by S. McGill.

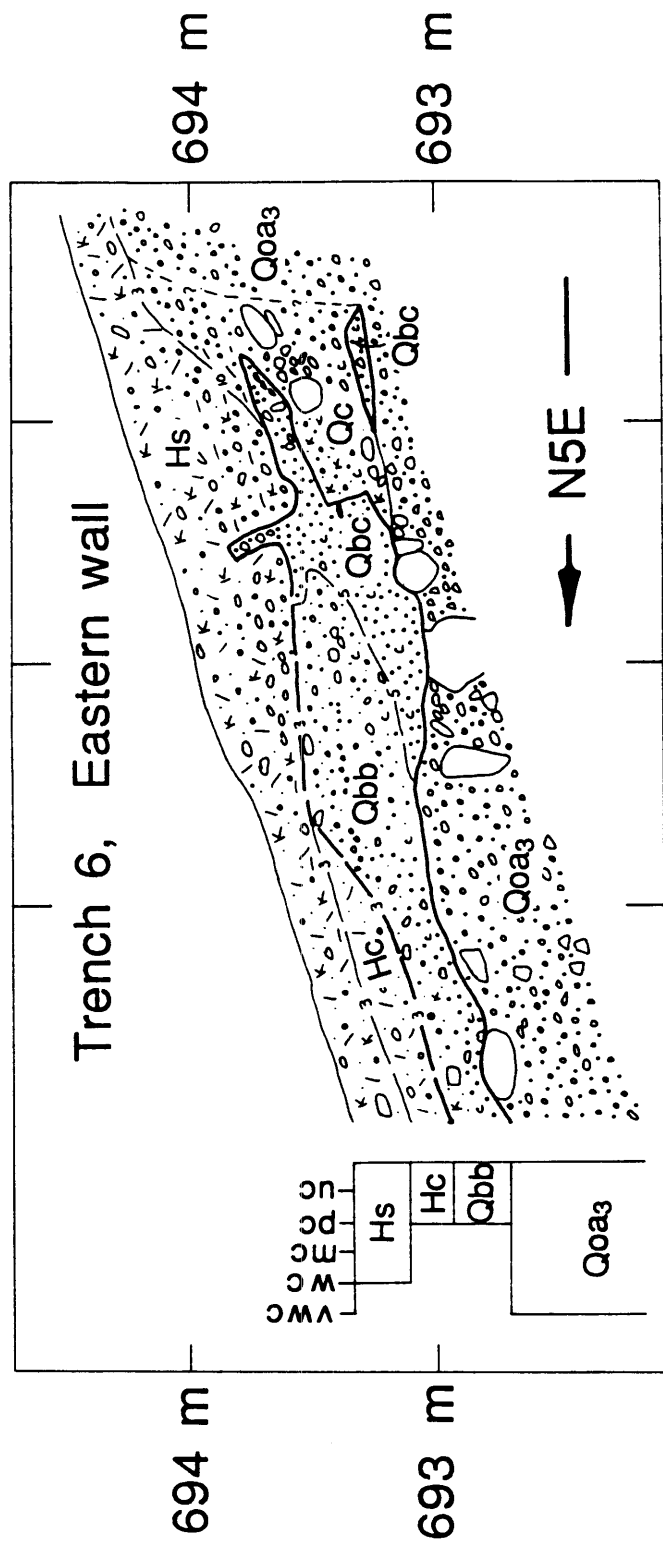


Figure 2-14A

FIGURE 2-14B: Cross section along eastern wall of Trench 7 shows beach sands (Qb, Qbc) deposited against a sea cliff. The beach sands are displaced several cm along a minor fault at the southern end of the cross section, but the matching stratigraphy of interbedded clayey sand and well-sorted sand on either side of this fault suggests that lateral offset has been minimal. Older beach deposits(?) (Qob₁ and Qobb₁) are truncated by this fault. Logged by S. McGill.

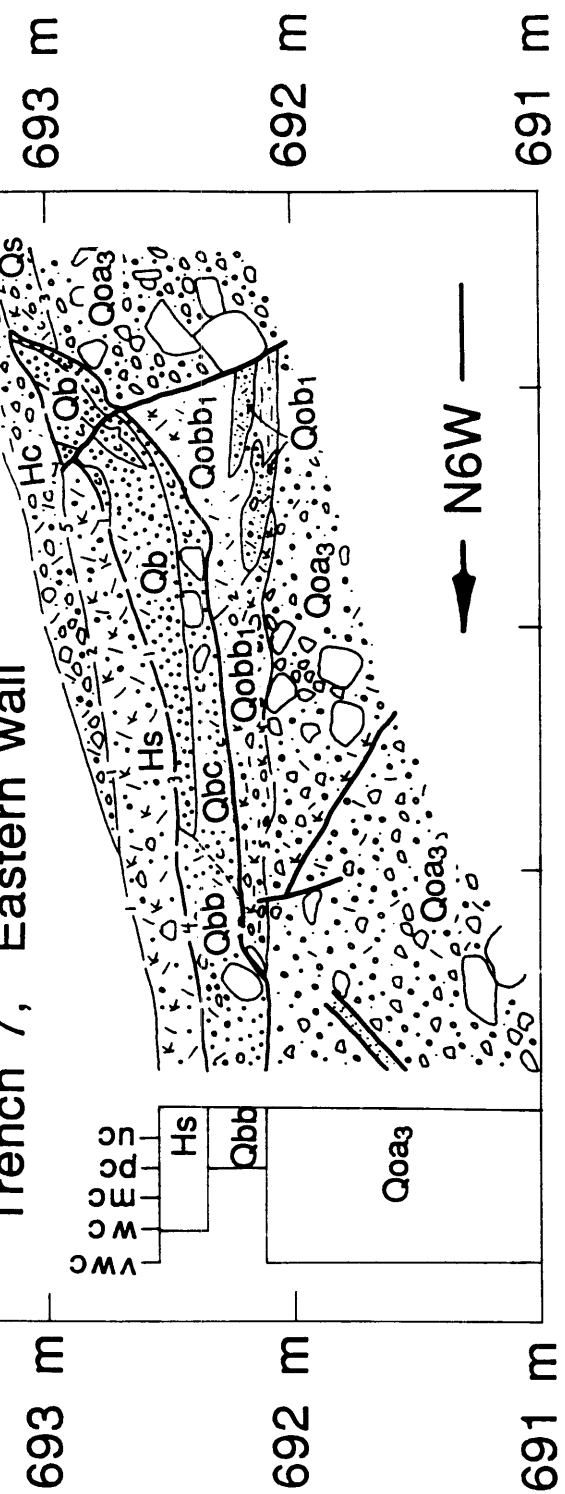


Figure 2-14B

FIGURE 2-14C: Cross section along northwestern wall of Trench 8. Poorly consolidated, poorly sorted sand (Qbb) pinches out against a sea cliff and may be bioturbated beach deposits from the latest lakestand or alluvium or colluvium burying the sea cliff. Logged by S. Bryant, M. Slates and L. Maepa.

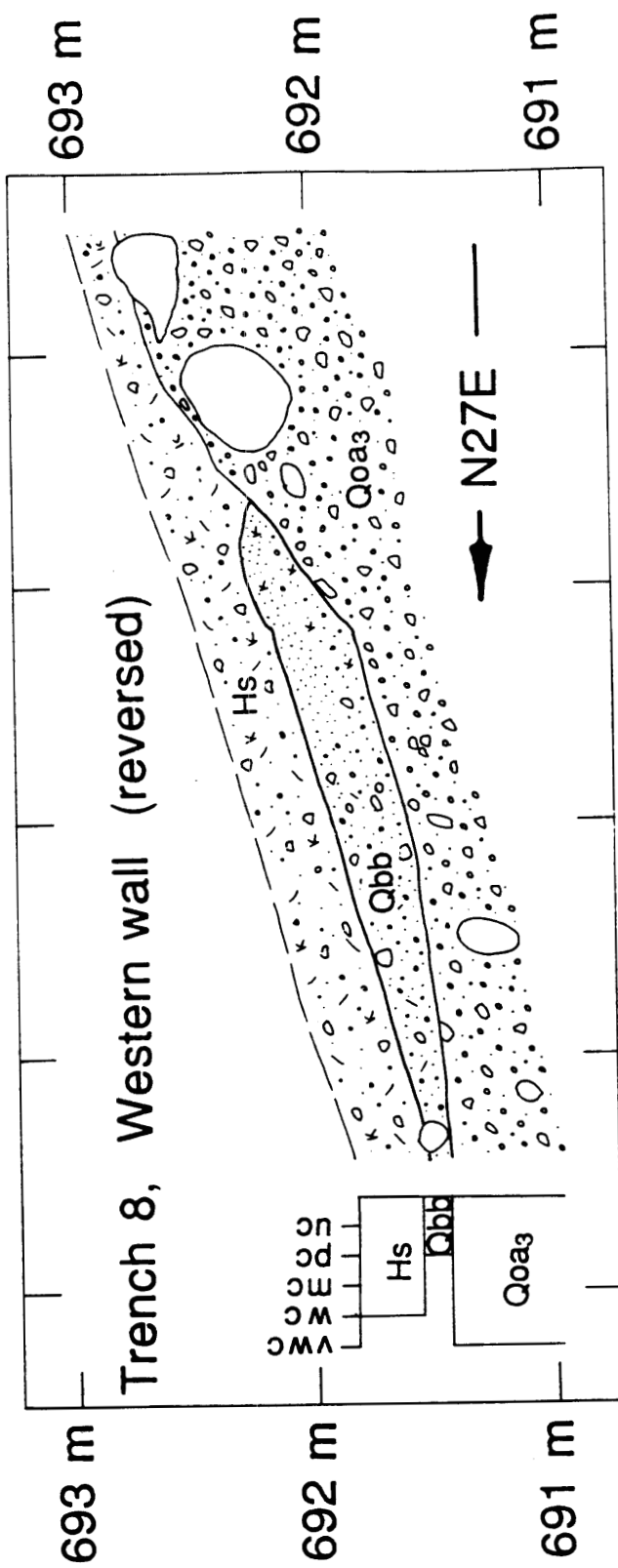


Figure 2-14C

FIGURE 2-14D: Cross section along the northern end of the eastern wall of Trench 15 shows moderately sorted beach deposits (Qob_1) filling a pre-existing channel. We interpret these deposits to be slightly older than the Qb beach deposits, for reasons discussed in the text. Logged by S. McGill.

Figure 2-14D

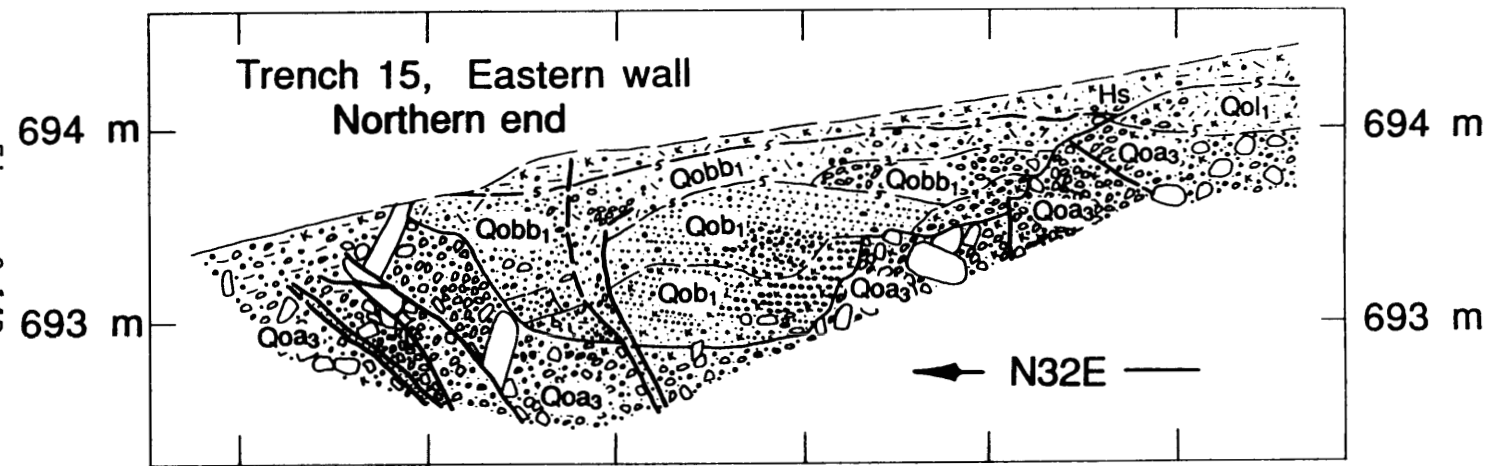


FIGURE 2-14E: Cross section along the central portion of the eastern wall of Trench 15 shows beach deposits (Qob_2) interpreted to be slightly older than the Qob_1 beach deposits for reasons discussed in the text. Logged by S. McGill and S. Bryant.

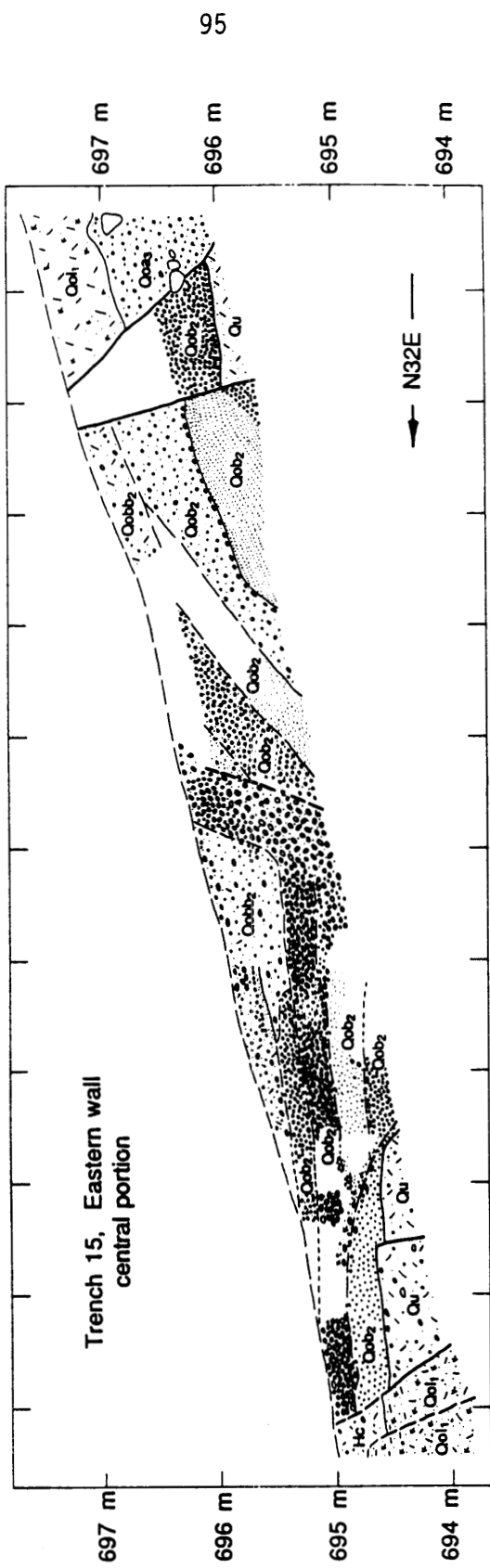


Figure 2-14E

interpret them as beach deposits filling a pre-existing channel because they are better sorted than most alluvium in this area. Evidence for a third set of beach deposits is found farther south in Trench 15 where poorly consolidated, well-sorted pebbles, granules and sands are exposed between two faults (Figure 2-14E). Although the sea cliff is not exposed in this cross section, these are undoubtably beach deposits.

The beach deposits in southern Trench 15 are much thicker and coarser than the beach deposits in Trenches 5, 6 and 7 and clearly do not correlate with them. Although the trend of the shoreline angle in Trench 7 suggests that it correlates with the southern shoreline in Trench 20 and the northern shoreline in Trench 15 (Figure 2-13), I suspect that it correlates instead with the sea cliff in Trench 8 and in northern Trench 20. Left-lateral warping, perhaps related to the minor fault that displaces the beach deposits in Trench 7, may explain the anomalous trend of the shoreline angle in Trench 7. There are no lower shorelines in Trenches 5, 6, and 7 with which the sea cliff in Trench 8 and northern Trench 20 could correlate. In addition, the elevation of the base of the sea cliff in northern Trench 20 is consistent with the decreasing elevation of the shoreline in Trenches 5, 6 and 7 northward from the northern fault (Figure 2-15). The shoreline angle in southern Trench 20 is farther from the northern fault than is the shoreline in Trench 7, but it is 1 m higher than the shoreline in Trench 7, which would represent a reversal in the trend of vertical warping if these two shorelines correlate.

I suspect that the beach deposits in southern Trench 20 and in Trench 15 are remnants from earlier highstands of Searles Lake. These two shorelines are several

FIGURE 2-15: Elevation of the shoreline angle (base of sea cliff) as a function of distance perpendicular to the fault zone. Dashes show elevation of Q_b shoreline; open triangles show elevation of Q_{ob_1} shoreline.

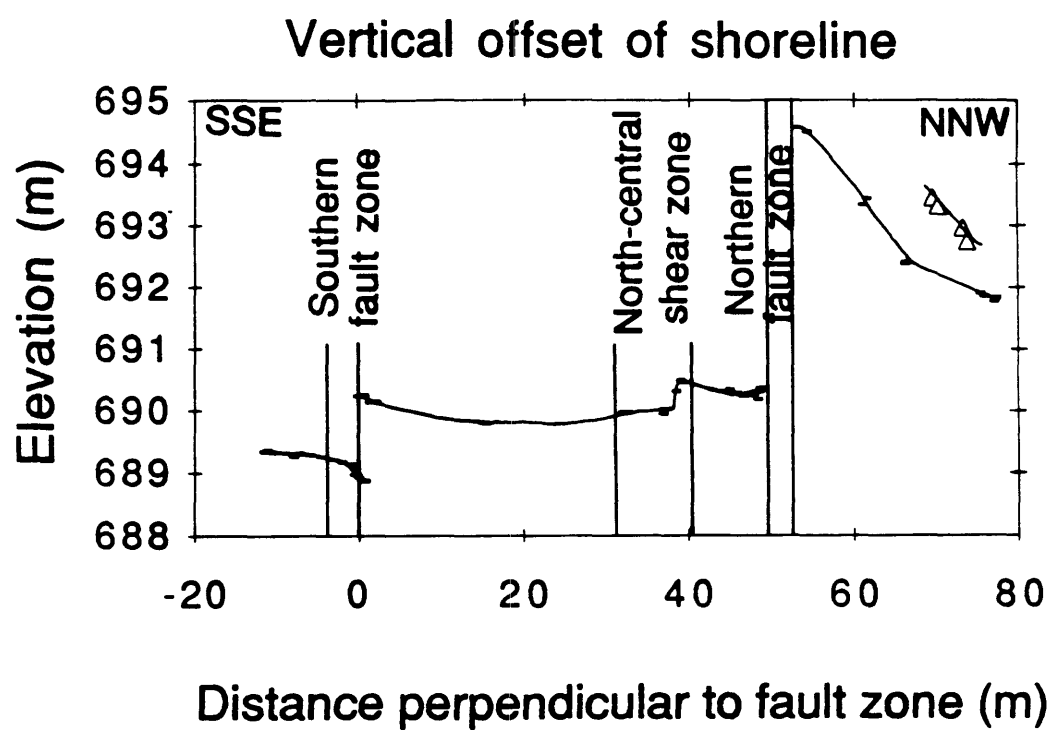


Figure 2-15

meters higher than the current elevation of the sill at the outlet to Searles basin (between 685 and 690 m, but probably just under 690 m; U. S. Geological Survey, 1984) and must have been uplifted after they formed. The fact that the shoreline exposed in Trenches 5, 6, and 7, has been warped upward towards the northern fault (Figure 2-15) indicates that older shorelines would have been warped upward to an even greater extent, as are the beach deposits in southern Trench 20 and in Trench 15. This uplift above the level of the sill (and thus above the level of wave action during younger lakestands) probably accounts for the preservation of remnants of older shorelines here and not elsewhere. The two older shorelines do not appear in Trenches 5 and 6, probably because they intersect the northern fault zone west of Trench 5. In Trench 7, sands (Qob_1 and $Qobb_1$) that may correlate with the beach deposits in southern Trench 20 and northern Trench 15 are located stratigraphically below the beach deposits (Qb) that correlate with those in Trenches 5 and 6 (Figure 2-14B). Although these are lower than the beach deposits in southern Trench 20 and northern Trench 15, they may be nearshore sediments associated with the same lakestand.

Possible offset away from the main fault zone

Significant offset of the shoreline on secondary faults north of the northern fault zone or south of the southern fault zone is unlikely. The incised channel east of the offset shoreline is not noticeably offset on any faults other than the two main fault zones. Although the beach deposits are faulted in Trench 7, the matching

stratigraphy of the beach deposits on either side of this minor fault suggests that little lateral offset has occurred on this fault since deposition of these beach sediments (Figure 2-14B). The agreement of the general trend of the shoreline between Trenches 5 and 7 with the local trend of the shoreline between the two walls of Trenches 5 and 6 also precludes large offset of the shoreline on discrete faults in this area (Figure 2-13). The fact that the shoreline has been warped vertically north of the northern fault, however, does suggest that it may also have been warped left-laterally. If any left-lateral warping has occurred north of the northern fault this would have rotated the shoreline to a more westerly trend. Because the shoreline between Trenches 5 and 8 trends more northerly than it does anywhere else at this site, significant left-lateral warping is unlikely. A subjective, but reasonable, upper bound on the amount of possible left-lateral warping and small offsets on discrete faults between Trenches 5 and 20 is about 3 m. This value is obtained by projecting a line parallel to the most northerly-trending part of the shoreline in the hand-excavation east of Trench 5 to a N75E-trending reference line (P37 to P38 in Figure 2-13).

Total offset of the shoreline

Summing the best estimates of the offsets across each part of the fault zone yields a total left-lateral offset of about 90 m (Table 2-3). Summing the minimum and maximum estimates of the offset across each part of the fault zone yields lower and upper bounds on the total offset of 82 m and 106 m, respectively. Although the

TABLE 2-3. Summary of offset across the entire fault zone.

Area	Minimum offset (m)	Maximum offset (m)	Best estimate (m)
Southern fault	36.0	38.0	37.0
Between Trenches 3 & 4	0	3.0	0
Between Trenches 4 & 11	0	2.0	2.0
North-central shear zone	3.5	13.6	5.3
Northern fault	42.1	46.0	46.0
North of Northern fault	0	3.0	0
TOTAL	81.6	105.6	90.3

upper and lower bounds on the offset across each part of the fault zone are subjective, it is unlikely that the true offset is close to the minimum offset, or close to the maximum offset, for *every* part of the fault zone. Thus, the probability that the true *total* offset lies within the upper and lower bounds for the total offset is greater than the probability that the true offset across any part of the fault zone lies within the upper and lower bounds for that part of the fault zone. Hence I view the maximum and minimum values as conservative limits.

The vertical offset of the shoreline across the main fault in the southern fault zone is about 1.3 m, north-side-up, but part of this is due to vertical warping near the fault (Figure 2-15). The net vertical offset across the southern fault zone is about 0.5 m, north-side-up, between Trenches 17 and 4. About 0.5 m of north-side-up displacement occurs between Trenches 12 and 19 in the north-central shear zone. The vertical displacement of the shoreline across the northern fault zone is about 4 m, north-side-up. However, the shoreline is warped upward toward the fault on the north side of the northern fault zone (Figure 2-15). The net elevation difference of the shoreline between Trench 13 and Trench 8 is about 1.5 m, north-side-up. The net vertical offset of the shoreline across the entire width of the fault zone is about 2.5 m, north-side-up, between Trenches 1 and 8. The vertical warping of the shoreline north of the northern fault may be an example of how some shutter ridges and "squeeze-ups" form.

AGE OF THE SHORELINE AND SLIP RATE OF THE GARLOCK FAULT

Lakes occupying Searles Valley have reached the overflow level several times between about 10,000 and 24,000 $^{14}\text{C-yr}$ B.P. (Figure 2-2; Stuiver and Smith, 1979; Benson and others, 1990; G. I. Smith, unpublished data). Searles Lake also overflowed between about 120 and 135 ka and possibly around 50 ka (G. I. Smith unpublished data).

The degree of soil development in the trenches across the offset shoreline suggests that the offset shoreline features studied in this paper formed during one of the most recent highstands, between about 10,000 and 24,000 $^{14}\text{C-yr}$ B.P. Soil samples spanning 10-cm depth intervals were collected from the southern wall of Trench 18, about 3 m east (lakeward) of the shoreline (Figure 2-7E). The samples from this profile (Profile 18S-1) were described by Oliver Chadwick (Table 2-4). The upper part of the profile is enriched in silt and clay relative to the parent material (below about 110 cm). The greatest enrichment in fine material occurs between 20 and 30 cm below the ground surface, corresponding to the layer mapped as Holocene soil (Hs) in Figure 2-7E. The amount of silt and clay in the profile gradually decreases downward through the unit mapped as bioturbated beach deposits (Qbb) until apparently unmodified beach deposits (Qb) are reached at about 110 cm depth (Figure 2-7E and Table 2-4). The source of the fine material is probably aeolian dust derived in part from the Searles Lake playa, about 20 km to the northwest.

If the offset shoreline had formed during the highstand of 120-135 ka, one would expect to see evidence of two generations of dust influx in the soil profile.

Table 2-4. Description of soil profile 18S-1

depth (cm)	texture (%clay)	dry con- sistence	structure	effe- rescence	carbonate stage	horizon
0-10	SL (10)	lo-so	indeterm.	es	---	A1k
10-20	SL(fSL)(14)	h	1msbk	es	I	A2k
20-30	L (18)	h	1f,msbk	es	I	Btk
30-40	SL (14)	h	1fsbk	es	I	Bk1
40-50	SL (10)	so	m	es+	I-II	Bk2
50-60	SL (8)	so	m	es+	I-II	Bk3
60-70	SL (8)	so	m	es+	I-II	Bk3
70-80	LS (6)	so	m-lo	es+	II	Bk4
80-90	LS (4)	so	lo	es+	I	Bk5
90-100	LS (6)	so	m-lo	es+	I-II	Bk6
100-110	LS (4)	so	lo	es	I	Bk7
110-120	S (3)	lo-so	lo	e	I	Bk8
120-130	S (2)	lo-so	lo	e	I	Bk9
130-140	S (2)	lo-so	lo	e-	I	Bk10
140-150	S (2)	lo-so	lo	e-	I	2Bk11

Description by Oliver Chadwick, Jet Propulsion Laboratory, Pasadena, CA.
Field description of dry consistence by Sally McGill.

Key to Abbreviations

texture: S, sand
 LS, loamy sand
 SL, sandy loam
 L, loam
 % clay was estimated, not measured.

dry consistence: lo, loose
 so, soft
 sh, slightly hard
 h, hard
 vh, very hard
 eh, extremely hard

Table 2-4 (continued)

structure: indeterm., indeterminate
1msbk, weak, medium, subangular blocky
1f,msbk, weak, fine to medium, subangular blocky
1fsbk, weak, fine, subangular blocky
m, massive
lo, loose

One episode of dust influx would have occurred when the playa was exposed between the 120-135 ka highstand and the most recent highstands (10-24 ka), and a second episode would have occurred after the most recent highstands. The dust that infiltrated during the first episode would have migrated deeper into the profile, would have weathered to clay and would have a stronger structure than the dust that infiltrated during the second episode. Unweathered dust from the second episode of influx would be concentrated near the top of the profile. The lack of moderately or strongly developed soil structure in Profile 18S-1, and the lack of evidence for two episodes of dust influx suggest that the offset shoreline formed during one of the most recent highstands, 10,000 to 24,000 years ago.

Furthermore, the texture and calcium-carbonate stage in Profile 18S-1 are comparable to and the structure is weaker than on profiles SL85-1a and SL85-2c on the lower part of alluvial fans draining towards Silver Lake, about 100 km east of the site discussed in this paper (Reheis and others, 1989). The latter two profiles are formed on fan surfaces estimated to be approximately 35,000 and 11,000 years old, respectively, on the basis of field relations with radiocarbon deposits, and on radiocarbon and cation-ratio dates on rock varnish (Reheis and others, 1989). This supports the correlation of the offset shoreline with one of the youngest highstands of Searles Lake, rather than with the 120-135 ka highstand.

The following field relations indicate that the shoreline features that are offset across the southern fault zone formed during the most recent one of these highstands (C3 in Figure 2-2). Lacustrine deposits attributed to highstand C3 can be traced to

an elevation of 695 m in northern Searles Valley (G. I. Smith, oral communication, 1991), indicating that this highstand reached the level of the offset shoreline discussed in this paper. (Some uplift of the shoreline in northern Searles Valley must have occurred relative to the area near the outlet of the lake, since the shoreline in northern Searles Valley is several meters higher than the shoreline discussed in this paper and than the current elevation of the outlet of the basin, which is just under 690 m.)

In addition, the offset channel east of the shoreline must have incised after the C3 highstand; otherwise, deposits from that lakestand would have filled the channel. Even if the most recent highstand (C3 in Figure 2-2) at this site was several meters lower than the offset shoreline (an unlikely hypothesis, given the 695 m elevation of deposits associated with the C3 highstand in northern Searles Valley), the most recent lake would have flooded the channel and filled or partially filled it with lacustrine sediments, had the channel existed at that time. Lacustrine sediments deposited on the western side of the channel and just north of either of the two main faults would be preserved from erosion by later stream flow in the channel. The lack of lacustrine sediments in the channel thus indicates that the channel incised after the most recent highstand of the lake.

The fact that the shoreline angle is offset the same amount across the southern fault as is the channel indicates that the shoreline features on either side of the southern fault must have formed during the most recent highstand and that the channel must have incised immediately (within one or two earthquake cycles)

after that shoreline was abandoned. Apparently the most recent highstand of the lake in this area reworked the beach deposits of earlier highstands and further incised the pre-existing sea cliff, thus obliterating the evidence of offset of any shoreline features from previous lakestands.

The offset of the shoreline across the northern fault zone and the north-central shear zone, however, is 10-20 m larger than the offset of the channel across those zones (Table 2-3 and Figure 2-4). (The north-central shear zone probably merges with the northern fault in the vicinity of the offset channel, or is located beneath the small channel parallel to the northern fault). This suggests that the shoreline features on either side of the northern fault strand may have formed during an earlier highstand and were not completely reworked by the youngest highstand. Perhaps the sea cliff exposed in the three-dimensional excavation north of Trench 13 and east of Trench 5 was cut during an earlier highstand of the lake and was offset several meters prior to the most recent highstand. When the lake reoccupied this shoreline during the C3 highstand, it would have had a fault-parallel segment of its shoreline initially. If the most recent highstand had a brief duration, then the waves may have cut into the fault zone only a few tens of cm, leaving an essentially fault-parallel segment of the shoreline that could be misinterpreted as offset that had occurred since the latest lakestand. For this reason I use the offset of the channel (69 ± 2 m) as a lower bound on the slip across the entire Garlock fault zone since the most recent highstand.

Several other explanations for the discrepancy between the offset of the

shoreline and the offset of the channel across the northern fault zone and the north-central shear zone are possible. (1) If the western wall of the offset channel just south of the northern fault zone has been eroded by flow in the modern channel, then the 32-33 m separation of the western wall of the channel may underestimate the actual offset of the channel across this fault zone. This is unlikely, however, because the portion of the western channel wall just north of the southern fault zone is clearly in a position where it can not have been eroded by flow in the modern channel, and the slope and trend of the portion of the western channel wall just south of the northern fault zone suggest that it has not been eroded any more recently than the portion of the channel wall farther south. (2) Perhaps only the northern fault strand was active between the time the shoreline formed and the channel incised, whereas both strands were active after the channel incised. (3) Although I expect the total slip rate across the entire fault zone to be uniform over distances of several tens to hundreds of meters along strike, the ratio of slip on the two fault strands may differ along strike. Thus, whereas the slip rate of the southern fault strand is roughly equal to that of the northern fault strand at the location of the offset channel, the slip rate of the northern fault strand may be greater than that of the southern fault strand at the location of the offset shoreline.

The alternative explanations given above do not require the part of the shoreline offset across the northern fault to be older than the most recent highstand. So, it is possible that the entire 42-46-m offset of the shoreline across the northern fault occurred after the most recent highstand. As an estimate of the maximum slip

rate, I thus divide the maximum offset of the shoreline across the entire fault zone (106 m) by the age of the end of the latest highstand.

Constraints on the ages of past highstands of Searles Lake come from radiocarbon dates on disseminated organic carbon and inorganic carbonate minerals from cores near the center of the basin (Stuiver and Smith, 1979), and on shells, oolites, tufa and marl from lacustrine sediments exposed at the surface (Benson and others, 1990). A minimum age for the abandonment of the most recent overflow shoreline is the age of the top of the Parting Mud unit in cores from the center of the basin. This unit is the uppermost unit in the cores associated with deep lakes. The age of the top of the Parting Mud is a minimum age for the abandonment of the latest overflow shoreline. If inflow into the lake stopped completely at the onset of desiccation, the lake could have dropped from the overflow level to the level at which evaporites began precipitating within a few hundred years (Stuiver, 1964). If some inflow continued during desiccation, then deposition of the Parting Mud may have continued for an unknown amount of time after the overflow shoreline was abandoned. The average of seven radiocarbon dates from the top of the parting mud unit is $10,500 \pm 165$ yr (Stuiver and Smith, 1979). The CO_2 in the lake water was probably not in equilibrium with the CO_2 in the atmosphere, however, making all dates on materials that derived their carbon from the lake water too old. The magnitude of this disequilibrium was probably such that radiocarbon dates from Searles Lake are between 500 and 2500 yr too old, depending on the depth, salinity and stratification of the lake (Stuiver and Smith, 1979). Stuiver and Smith (1979)

favor the smaller correction for the age of the top of the Parting Mud because the youngest lakes were probably stratified. Therefore, I use 10,000 ^{14}C -yr B.P. as a minimum age for the offset shoreline. Dividing the maximum offset (106 m) by the minimum age yields a maximum slip rate of 10.6 mm/ ^{14}C -yr.

Two radiocarbon dates on oolites and mollusks from surficial sediments of the C3 highstand are $11,730 \pm 350$ ^{14}C -yr B.P. and $11,700 \pm 160$ ^{14}C -yr B.P., respectively (Benson and others, 1990; G. I. Smith, oral communication, 1991). I use $11,700$ ^{14}C -yr B.P. as a best estimate for the age of the end of the most recent highstand of Searles Lake. Following Stuiver and Smith (1979), I assume that only a minimal (500 yr) correction for disequilibrium between the lake and the atmosphere need be made for the most recent highstand. Dividing the resulting date (11,200 ^{14}C -yr B.P.) into the best estimate for the offset of the shoreline (90 m) yields a slip rate of 8 mm/ ^{14}C -yr.

The two radiocarbon ages from lacustrine deposits of the C3 highstand do not provide a maximum age for the abandonment of that highstand because those samples were located at elevations of 619 m and 572 m and thus may represent the age of sediments deposited after the lake level dropped below the level of the offset shoreline. Radiocarbon dates on rock varnish on boulders at the overflow shoreline level are $13,610 \pm 110$ and $13,290 \pm 115$ ^{14}C -yr B.P., suggesting that the overflow level may have been abandoned that early (Dorn and others, 1990). As a maximum age for the C3 highstand of Searles Lake, I use 14,300 ^{14}C -yr B.P., the oldest radiocarbon date from deposits of the C1 highstand (Benson and others, 1990). This

may overestimate considerably the age of the end of the C3 highstand. Correcting this for disequilibrium between the CO₂ in the lake and the atmosphere yields a reservoir corrected age of 11,800 to 13,800 ¹⁴C-yr B.P. Dividing the minimum offset of the channel (67 m) by the maximum age yields a minimum slip rate of 4.9 mm/¹⁴C-yr.

I regard the upper and lower bounds on the slip rate reported above as conservative because it is unlikely that both the true offset is the maximum offset, and the true age is the minimum age and vice versa. Because the youngest shoreline may have paralleled the northern fault for some distance, I think the true slip rate is more likely to be less than the best estimate than greater than the best estimate. If the youngest shoreline did parallel the northern fault for some distance, the total offset since the end of the latest lakestand is likely to be close to the offset of the channel. Dividing the best estimate for the offset of the channel (69 m) by the best estimate for the age of the youngest shoreline (11,200 yr) yields a slip rate of 6.2 mm/yr. Thus, the slip rate of the Garlock fault near the outlet of Searles Lake is most likely between 6 and 8 mm/¹⁴C-yr, but could be as low as 5 mm/¹⁴C-yr or as high as 10.6 mm/¹⁴C-yr.

Current efforts to calibrate the radiocarbon timescale with the U-Th timescale suggest that the radiocarbon dates used in calculating the slip rate may underestimate the true ages by 2000-3000 yr (Bard and others, 1990). If this calibration is correct then the true slip rate of the Garlock fault is most likely between 5 and 7 mm/yr but may be as low as 4 mm/yr or as high as 9 mm/yr.

DISCUSSION

The slip rate determined from the offset shoreline of Searles Lake is consistent with (and much better documented than) the 7 ± 1 mm/ $^{14}\text{C-yr}$ rate determined at Koehn Lake (Clark and Lajoie, 1974; Clark and others, 1984). The 11-12 mm/yr rate reported by Carter (1980, 1982) is larger than the rate calculated in this paper, but Carter's rate is poorly constrained. That rate is based on the 16-20 km offset of alluvial fan gravels south of the fault from their bedrock source area in El Paso Mountains north of the Garlock fault. A fossil of genus *Equus* was collected from beneath gravels north of the fault that are thought to correlate with the offset gravels south of the fault. The genus *Equus* first appeared about 2.5 million years (m.y.) ago (David Whistler, Los Angeles County Museum of Natural History, oral communication, 1991). If the offset gravels south of the fault are indeed the same age as those overlying the *Equus* fossil, then the 16-20 km offset must have occurred within the past 2.5 m.y., yielding a minimum slip rate of 6.4 mm/yr, which falls within the range of slip rates reported in this paper and within the uncertainty in Clark and Lajoie's (1974) rate. Thus the slip rate since Plio-Pleistocene time, recorded by offset fans in El Paso Mountains, may be consistent with the latest Quaternary rates reported here and by Clark and Lajoie (1974).

If left-lateral slip on the Garlock fault accommodates east-west extension north of the Garlock fault, as proposed by Davis and Burchfiel (1973), then the slip rate of the Garlock fault would decrease eastward. The agreement between the best estimate of the slip rate in southeastern Searles Valley with the rate at Koehn Lake

suggests that extension north of the Garlock fault between these two locations may not contribute significantly to slip on the Garlock fault. If the slip rate in southeastern Searles Valley is the minimum allowed rate (5 mm/ $^{14}\text{C-yr}$) and the slip rate at Koehn Lake is the maximum allowed rate (8 mm/ $^{14}\text{C-yr}$), however, then up to 3 mm/yr of Holocene extension parallel to the Garlock fault may have occurred. Evidence consistent with extension in this area includes the many small, Quaternary faults in Indian Wells Valley and in the Coso Range (Figure 2-1; Jennings and others, 1962), aligned volcanic cones (Duffield and others, 1980; Roquemore, 1980), the orientation of the minimum compressive axes of earthquake focal mechanisms (Sanders and others, 1988; Walter and Weaver, 1980), and the presence of a magma body beneath Indian Wells Valley (Sanders and others, 1988; Ho-Liu and others, 1988).

The offset of the Searles Lake shoreline documented in this chapter probably occurred seismically (by repeated, discrete displacements associated with earthquakes) rather than by aseismic creep. An alignment array at Christmas Canyon, 10 km west of the offset shoreline discussed in this chapter, has not detected any aseismic creep since it was installed in 1971 (Louie and others, 1985). Similarly, U.S.G.S. quadrilaterals have not detected any aseismic creep along this or other parts of the fault (Malcolm Clark, written communication, 1990). Thus, there is no evidence that aseismic creep has occurred on this part of the Garlock fault, although the occurrence of aseismic slip prior to the establishment of these arrays and quadrilaterals can not be ruled out.

CONCLUSIONS

A latest-Pleistocene shoreline at the overflow level of Searles Lake has been offset about 90 m across the Garlock fault zone in southeastern Searles Valley. Although the lake has filled to its overflow level several times in the late Pleistocene, relations between the offset shoreline and an offset channel that has incised the shoreline indicate that the offset of the shoreline across the southern one of two main fault strands has occurred since the most recent highstand of Searles Lake. Wave action during the most recent highstand may not have completely eroded the offset of older shorelines across the northern fault, however. Therefore, the minimum offset of 82 m across the entire fault zone may not have all occurred since the most recent highstand. An offset channel indicates that at least 67 m of left-lateral slip has occurred across the Garlock fault zone since the end of latest highstand of Searles Lake (10,000 to 13,800 $^{14}\text{C-yr}$ B.P.), yielding a minimum slip rate of 4.9 mm/ $^{14}\text{C-yr}$. Dividing the maximum offset of the shoreline by the minimum age of the end of the latest highstand yields a maximum slip rate of 10.6 mm/ $^{14}\text{C-yr}$. Considering that the most recent highstand may not have completely destroyed the offset of older shorelines, the true offset of the shoreline of the most recent highstand is most likely between the best estimate of the offset of the channel (69 m) and the best estimate of the offset of the shoreline (90 m). Dividing these values by the best estimate of the age of the end of the latest highstands (11,200 $^{14}\text{C-yr}$) suggests that the slip rate of the Garlock fault in southeastern Searles Valley is most likely between 6 and 8 mm/ $^{14}\text{C-yr}$. If Bard and others' (1990) calibration of the

radiocarbon timescale is correct, then the slip rate is between 4 and 9 mm/yr and most likely between 5 and 7 mm/yr.

The slip rate in southeastern Searles Valley is compatible with the $7 \pm \frac{1}{2}$ mm/ ^{14}C -yr slip rate at Koehn Lake (Clark and Lajoie, 1974; Clark and others, 1984). No extension is required north of the Garlock fault between Koehn Lake and southeastern Searles Valley, but up to 3 mm/yr of extension parallel to the Garlock fault is allowed.

REFERENCES

Bard, E., B. Hamelin, R. G. Fairbanks, and A. Zindler, Calibration of the C-14 timescale over the past 30,000 years using mass-spectrometric U-Th ages from Barbados corals, *Nature*, 345, 405-410, 1990.

Benson, L. V., D. R. Currey, R. I. Dorn, K. R. Lajoie, C. G. Oviatt, S. W. Robinson, G. I. Smith, S. and Stine, Chronology of expansion and contraction of four Great Basin Lake systems during the past 35,000 years, *Palaeogeography, Palaeoclimatology, Palaeoecology*, 78, 241-286, 1990.

Carter, B. A., Quaternary displacement on the Garlock fault, California, in Fife D. L., and A. R. Brown, eds., *Geology and Mineral Wealth of the California Desert*, Santa Ana, California, South Coast Geological Society, pp. 457-466, 1980.

Carter, B., Neogene displacement on the Garlock fault, California, *EOS, Trans. Am. Geophys. Union*, 63, 1124, 1982.

Clark, M. M., K. K. Harms, J. J. Lienkaemper, D. S. Harwood, K. R. Lajoie, J. C. Matti, J. A. Perkins, M. J. Rymer, A. M. Sarna-Wojcicki, R. V. Sharp, J. Simms, J. C. Tinsley III, and J. I. Ziony, Preliminary slip-rate table and map of Late Quaternary faults of California, *U. S. Geol. Survey Open File Rept. 84-106*, 12 pp., 1984.

Clark, M. M. and K. R. Lajoie, Holocene behavior of the Garlock fault, *Geol. Soc. Am., Abstracts with Programs*, 6, 156-157, 1974.

Davis G. A., and B. C. Burchfiel, Garlock fault: an intracontinental transform

structure, southern California, *Geol. Soc. Am. Bull.*, 84, 1407-1422, 1973.

Dokka, R. K., and C. J. Travis, Late Cenozoic strike-slip faulting in the Mojave Desert, California, *Tectonics*, 9, 311-340, 1990.

Dorn, R. I., A. J. T. Jull, D. J. Donahue, T. W. Linick and L. J. Toolin, Latest Pleistocene lake shorelines and glacial chronology in the Western Basin and Range Province, U. S. A.: insights from AMS radiocarbon dating of rock varnish and paleoclimatic implications, *Palaeogeography, Palaeoclimatology, Palaeoecology*, 78, 315-331, 1990.

Duffield, W. A., C. R. Bacon, and G. B. Dalrymple, Late Cenozoic volcanism, geochronology, and structure of the Coso Range, Inyo County, California, *J. Geophys. Res.*, 85, 2381-2404, 1980.

Gale, H. S., Salines in the Owens, Searles and Panamint basins, southeastern California, *U. S. Geological Survey Bulletin 580-L*, 251-323, 1914.

Ho-Liu, P., H. Kanamori and R. W. Clayton, Applications of attenuation tomography to Imperial Valley and Coso-Indian Wells region, southern California, *J. Geophys. Res.*, 93, 10,501-10,520, 1988.

Jennings, C. W., J. L. Burnett, and B. W. Troxel, Geologic Map of California, Trona Sheet, California Division of Mines and Geology, 1962.

LaViolette, J. W., G. E. Christenson, and J. C. Stepp, Quaternary displacement on the western Garlock fault, southern California, in Fife, D. L. and A. R. Brown, eds., *Geology and Mineral Wealth of the California Desert*, Santa Ana, California, South Coast Geol. Soc., pp. 449-456, 1980.

Louie, J. N., C. R. Allen, D. C. Johnson, P. C. Haase, and S. N. Cohn, Fault slip in southern California, *Bull. Seism. Soc. Am.*, 75, 811-833, 1985.

McGill, S. F., and K. E. Sieh, Surficial offsets on the central and eastern Garlock fault associated with prehistoric earthquakes, *J. Geophys. Res.*, 96, 21,597-21,621, 1991.

Reheis, M. C., J. W. Harden, L. D. McFadden, and R. R. Shroba, Development rates of late Quaternary soils, Silver Lake playa, California, *Soil Sci. Soc. Am. J.*, 53, 1127-1140, 1989.

Roquemore, G., Structure, tectonics and stress field of the Coso Range, Inyo County, California, *J. Geophys. Res.*, 85, 2434-2440, 1980.

Sanders, C., P. Ho-Liu, D. Rinn, and H. Kanamori, Anomalous shear wave attenuation in the shallow crust beneath the Coso volcanic region, California, *J. Geophys. Res.*, 93, 3321-3338, 1988.

Smith, G. I., Holocene movement on the Garlock fault, *U. S. Geol. Surv. Profess. Pap.* 975, p. 202, 1975.

Smith, G. I., Subsurface stratigraphy and geochemistry of Late Quaternary evaporites, Searles Lake, California, *U. S. Geological Survey Professional Paper 1043*, 130 pp., 1979.

Smith, G. I., V. J. Barczak, G. F. Moulton, and J. C. Liddicoat, Core KM-3, a surface-to-bedrock record of Late Cenozoic sedimentation in Searles Valley, California, *U. S. Geological Survey Professional Paper 1256*, 24 pp., 1983.

Smith, G. I., and F. A. Street-Perrott, Pluvial lakes of the western United States, in

Wright, H. E., Jr., ed., *Late Quaternary Environments of the United States*, Minneapolis, University of Minnesota Press, pp.190-212, 1983.

Stuiver, M., Carbon isotopic distribution and correlated chronology of Searles Lake sediments, *Amer. J. of Sci.*, 262, 377-392, 1964.

Stuiver, M., and G. I. Smith, Radiocarbon ages of stratigraphic units, in Smith, G. I., Subsurface stratigraphy and geochemistry of Late Quaternary evaporites, Searles Lake, California, *U. S. Geological Survey Professional Paper 1043*, 130 pp., 1979.

U. S. Geological Survey, Pilot Knob Valley West Quadrangle California-- San Bernardino County, 7.5 minute series (topographic map), United States Geological Survey, Reston, VA, 1984.

Walter, A. W. and C. S. Weaver, Seismicity of the Coso Range, *J. Geophys. Res.*, 85, 2441-2458, 1980.

Weldon, R. and E. Humphreys, A kinematic model of southern California, *Tectonics*, 5, 33-48, 1986.

CHAPTER 3**DISPLACEMENT, MAGNITUDE AND FREQUENCY OF PAST EARTHQUAKES
ON THE CENTRAL AND EASTERN GARLOCK FAULT****ABSTRACT**

Geomorphic features offset along the central and eastern Garlock fault record the amount of surface slip associated with prehistoric earthquakes. Along the easternmost 90 km of the fault, the smallest offsets cluster around 2-3 m of left-lateral slip, apparently associated with the most recent earthquake on this portion of the fault. Larger offsets along this part of the fault, especially in Pilot Knob Valley, cluster around values consistent with 2 to 4 m of slip in each of the past several events. Farther west, south of El Paso Mountains, offset geomorphic features suggest that each of the past two earthquakes on this stretch of the Garlock fault was produced by about 7 m of slip, whereas the third event back was produced by about 4 m of slip.

Vertical displacements of geomorphic features range from 0% to 30% of the left-lateral offsets. Within Pilot Knob Valley (along the southern side of the Slate Range) vertical displacements are consistently up on the northern side, whereas within the Avawatz Mountains both north- and south-side-up vertical displacements are present.

On the basis of the geomorphic offsets, the geometry of the Garlock fault, and the precedents set by historical, strike-slip earthquakes elsewhere, a number of

different rupture patterns are plausible. These range from rupture of the entire Garlock fault in a single event with a maximum magnitude of about $M_w=7.8$, to separate rupture of the western segment and of the central and eastern segments combined, with approximate magnitudes $M_w\leq7.7$ and $M_w=7.5$, respectively, to separate rupture of even shorter segments, producing earthquakes of magnitudes $M_w=6.6$ to $M_w=7.5$.

In conjunction with available slip rates for the Garlock fault, the geomorphic offsets suggest that average recurrence intervals are probably within the range of 600-1200 yr south of El Paso Mountains, about 200-750 yr in Searles Valley, about 200-1300 yr in Pilot Knob Valley, and about 200-3000 yr near Leach Lake and in the Avawatz Mountains.

INTRODUCTION

Although the Garlock fault is not known to have produced large earthquakes during the period of historical record, abundant scarps and left-laterally offset geomorphic features of Holocene age indicate that the fault is active and that it has produced large earthquakes. Clark (1970, 1973) prepared a map of these features and suggested that 3 m of left-lateral slip had occurred in the most recent slip event along parts of the central and eastern Garlock fault. In this chapter, I present the measurements of about 200 geomorphic features offset along the central and eastern Garlock fault. These offsets record the amount of displacement in past earthquakes on the fault. I then use the resulting estimates of the slip in past earthquakes, the

geometry of the fault, and precedents set by historical, strike-slip earthquakes on other faults to address the likely rupture patterns and magnitudes of large earthquakes on the Garlock fault. Finally, by dividing the slip per earthquake into the slip rate of the fault, I estimate the average recurrence interval for large earthquakes on various parts of the central and eastern Garlock fault.

METHODOLOGY

Several previous authors have used offset geomorphic features to determine the amount of slip in past earthquakes (Clark, 1970; Sieh, 1978; Rockwell and Pinault, 1986; Zhang and others, 1987; Lindvall and others, 1989; and Zhang and others, 1990). In this study, I measured the offsets of many geomorphic features along the central and eastern Garlock fault. These features include channel walls, gullies, terrace risers, ridges, and debris flows. As will be shown, the offsets cluster around discrete values. I interpret each of these values to be the cumulative slip associated with some number of prehistoric earthquakes. For any particular portion of the fault, I interpret the smallest value around which offsets cluster to be the slip associated with the most recent earthquake, and I interpret each larger value to be the cumulative slip associated with the most recent and earlier earthquakes.

Potentially, every large earthquake on a strike-slip fault could be recorded by the lateral offset of geomorphic features, if new features form during every interseismic period, and if some of the features developed during each interseismic period are preserved up to the time of observation. Hundreds of new geomorphic features have

formed across the Garlock fault since the latest large earthquake, and at least one gully has formed across the fault since the aerial photographs I used were taken in 1976. Therefore, if recurrence intervals on the Garlock fault are fairly regular, it is reasonable to expect that many new geomorphic features have formed between each successive pair of earthquakes on the Garlock fault. If earthquakes on the Garlock fault are clustered in time, however, such that some earthquakes occur only a few decades apart, then in the geomorphic record these earthquakes may appear as a single event with a displacement equal to the combined displacement of the clustered events. In addition, as time passes, offset geomorphic features may be destroyed by erosion or buried by further deposition. Thus, the geomorphic record is usually not a complete record of past earthquakes for older events.

I assume that the displacement of the geomorphic features studied occurred seismically, rather than as a result of aseismic creep. This is a reasonable assumption, since creep has never been unambiguously documented on the central or eastern Garlock fault. Clark (1973) observed cracks with 3 to 6 mm of left-lateral displacement at a few places on the central Garlock fault, but two narrow-aperture alignment arrays and nine quadrilaterals distributed along the central and eastern Garlock fault have failed to detect any displacement across the fault zone for the past 19 years (Louie and others, 1985; Malcolm Clark, oral comm., Sept. 1990). A portion of the offset of the geomorphic features may have occurred as postseismic slip in the months following earthquakes. This does not discredit my use of the offset values as an indicator of the seismic slip in past events, however, because the

sum of the coseismic surface slip and the postseismic surface slip is probably a better estimate of the seismic slip at depth than is the coseismic surface slip alone.

DATA COLLECTION

After examining large-scale, vertical, aerial photographs of the Garlock fault zone¹, I selected for field study six areas of the fault where geomorphic features that are offset by small amounts are most abundant (Figure 3-1). From west to east the six areas are: (1) a half-km-length of the fault near the Garlock townsite, south of El Paso Mountains, (2) a 5-km-length of the fault located just west of U.S. Highway 395 and south of the eastern part of El Paso Mountains, (3) a 4-km-length located in eastern Searles Valley, (4) a 27-km-length in Pilot Knob Valley, south of the Slate Range and the western Quail Mountains, (5) a half-km-length located 4 km west of Leach Lake and just south of the eastern Quail Mountains, and (6) the easternmost 15 km of the fault, located within the Avawatz Mountains. This report is based on more than two months of field work in these areas.

In the field, each feature identified on the aerial photographs was examined to determine whether or not it was tectonically offset and whether the amount of separation was an accurate measure of the displacement associated with one or more past earthquakes. Each feature was given a quality rating that indicates the

¹ USGS GSGF and GDGF, 1976 and 1977, 1:5000-scale, low-sun, color; flown for studies of the active traces of the Garlock fault.

FIGURE 3-1: Reference map showing geological and geographical features discussed in text, as well as the six areas of the fault studied. Quaternary faults are simplified from Jennings (1985). Features mentioned in text are: AM, Avawatz Mountains; Bk, Bakersfield; BMF, Brown Mountain fault; BTC, Bear Trap Canyon, Bw, Barstow; C, Cantil; CC, Christmas Canyon; CL, Castac Lake; CR, Coso Range; DV, Death Valley; EPM, El Paso Mountains; IWV, Indian Wells Valley; KL, Koehn Lake; KW, Kingston Wash; LL, Leach Lake; M, Mojave; NBGF, North Branch Garlock fault; OL, Owens Lake; OLF, Owl Lake fault; PV, Panamint Valley; QM, Quail Mountains; SAF, San Andreas fault; SH, Spangler Hills; SR, Slate Range; SV, Searles Valley; T, Tehachapi; TM, Tehachapi Mountains; TR, Trona Road.

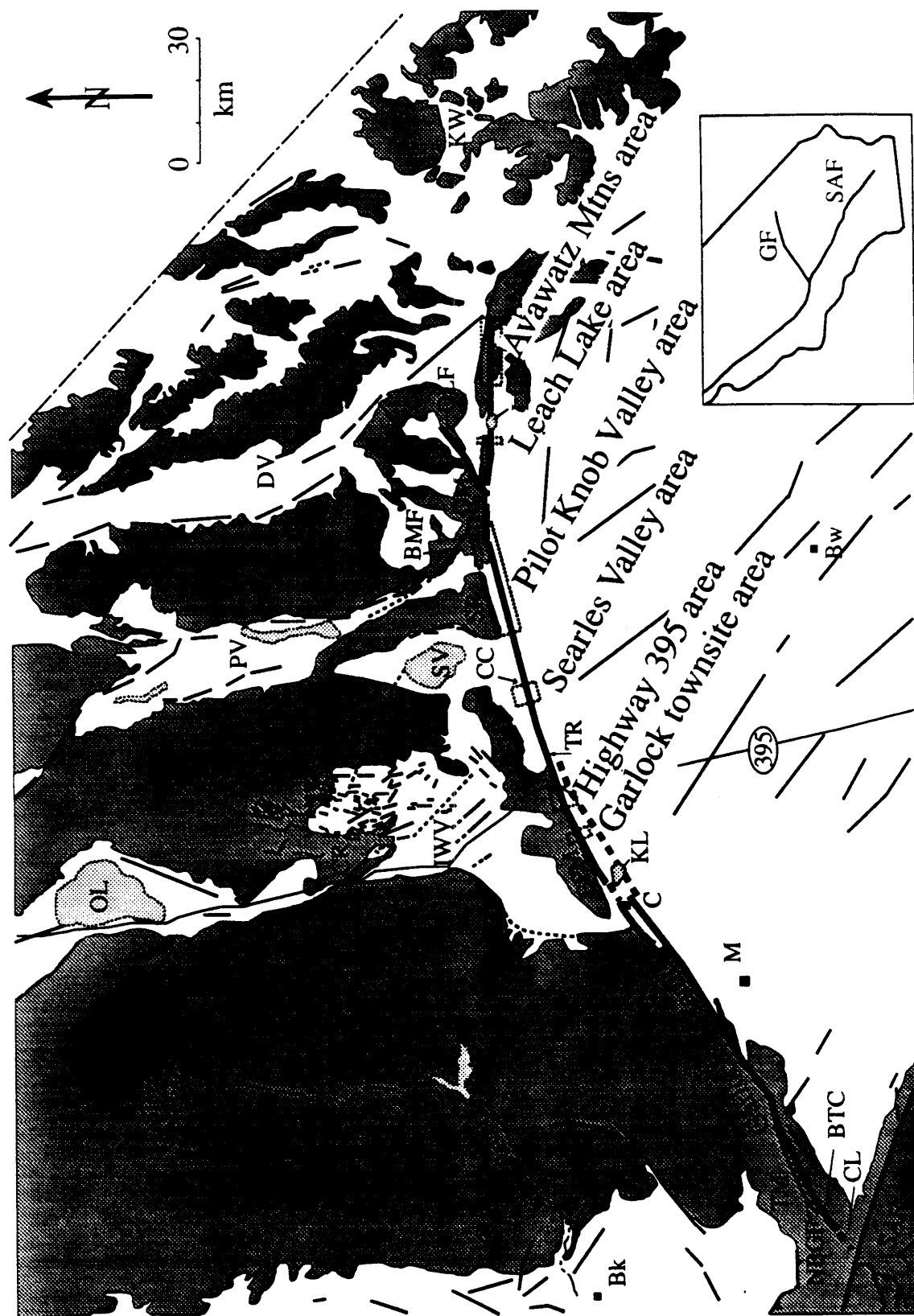


Figure 3-1

reliability and accuracy of the feature as an indicator of tectonic offset. For example, excellent and good ratings were given to geomorphic features that clearly have correlative features or deposits across the fault trace and that clearly have been separated by tectonic offset. Fair ratings were given to features that have less certain correlations across the fault. Poor ratings were given to features that could possibly be separated by non-tectonic means, or whose correlations across the fault are poor. Features that could easily have formed by non-tectonic means (such as deflection around an uphill-facing scarp, or stream capture), that have uncertain correlations across the fault, or that cross the fault zone in an area where the location of the fault trace(s) is uncertain, were not used. To assist in evaluating the reliability of each feature, and for later reference, a sketch was made of each offset feature.

The amount that each feature is offset was measured in the field with a tape measure. Error bars were given to each measurement to indicate the range of plausible offset amounts for that feature, assuming that the correlation of the two parts of the feature on opposite sides of the fault is correct. Sharp features that could be followed right up to the fault on both sides thus have small uncertainties in their offsets, whereas more subdued features and features that were projected a short distance to the fault have larger uncertainties. For most features a best-estimate value for the offset is also given. The offset for each feature is reported to the nearest 0.1 m, even though the uncertainty in the offset is usually much larger than this. I then round the average offset for each fault segment to the nearest 1 m before calculating earthquake magnitudes or recurrence intervals. A few features

were further documented by constructing topographic maps with a Wild TC-2000 total station (a theodolite with a built-in, electronic-distance measuring device).

Erosion of some of the geomorphic features may have enlarged or reduced the apparent offset. For example, the tips of most shutter ridges have probably been eroded, reducing the apparent offset. For this reason, all of the offset measurements on shutter ridges used in this study are reported as minimum values unless the amount of possible erosion can be constrained and included in the error bar. Terrace risers that separate the modern channel from a terrace are also subject to erosion. On the left-lateral Garlock fault, the western walls of southward-flowing channels are particularly vulnerable to erosion, because the downstream channel segment has been faulted into the active channel (Figure 3-2). On the other hand, the downstream segments of the eastern walls of such channels have been faulted away from the modern channel. There is still potential for erosion of the upstream segment of such eastern channel walls, however. Accordingly, if the upstream segment of such a channel shows evidence of recent erosion, the offset for that channel is reported as a minimum value. If, on the other hand, the eastern channel wall is protected from the modern channel by a low terrace (Figure 3-2), the offset is not reported as a minimum.

Another potential problem is that of multiple-fault strands. In this study each offset measurement reported is thought to represent the left-lateral slip across the entire recently active fault zone. Where multiple strands appear to have ruptured in the latest few earthquakes, only features that cross all of the recently active strands

FIGURE 3-2: Along left-lateral faults, the western walls of southward-flowing channels are especially prone to fluvial erosion because their downstream segments have been faulted into the active channel. The eastern walls of such channels are more likely to record the total offset of the channel, especially if they have been protected from recent erosion by a lower terrace.

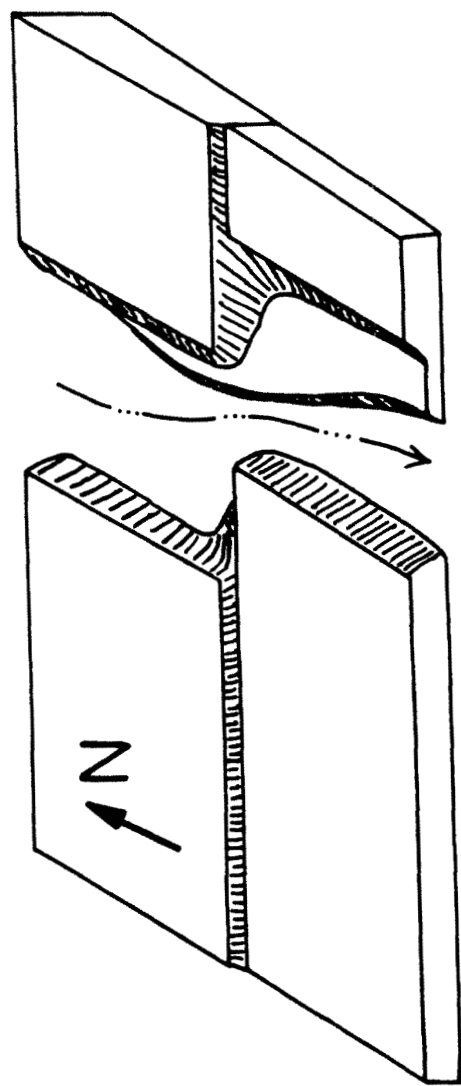


Figure 3-2

are used. In a few cases the offsets of different features of the same apparent age that span different fault traces within the fault zone were summed to obtain the offset across the whole recently active fault zone. Geomorphic features that cross the main fault trace(s) but do not cross fault traces that are clearly secondary in nature, were also used.

Where possible, the vertical displacement was also measured. Vertical displacement was measured only at sites where the horizontal offset could also be measured. The horizontal offset was then taken into account so that the true vertical displacement could be measured, rather than measuring vertical separation that could be due to lateral offset. Of the features where horizontal offset was measured, only those with planar surfaces of approximately the same slope on both sides of the fault were used for measuring vertical displacements. Thus, vertical displacements were measured on terraces adjacent to terrace risers, on debris flows, and on ridges with crests of similar slope on either side of the fault. Vertical displacement was not measured on gullies or channel walls.

DATA PRESENTATION AND ANALYSIS

Garlock Townsite and Highway 395 Areas

I studied 24 offset geomorphic features south of El Paso Mountains (Table 3-1). Five of these are located along a half-km-length of the fault west of the Garlock townsite, and the remaining 19 are along a 5-km-length of the fault just west of U.S. Highway 395. I made detailed topographic maps at the two sites discussed below,

TABLE 1. Geomorphic Offsets South of El Paso Mountains

Feature	Distance (km)	Quality	Horizontal Offset (m)	Description
1-39(1)	18.3	good	≥ 4.0	shutter ridge
1-41(1)	18.6	fair	6.5 ± 1.5	beheaded gully offset from source
1-41(2)	18.7	good	≥ 3.5	youngest part of shutter ridge
1-41(3)	18.8	poor	6.5 ± 2.0	beheaded gully offset from source
1-41(4)	18.9	good	6.5 ± 0.5	alluvial fan offset from channel
1-63(3)	28.22	fair	2.6 to 6.5	shutter ridge
1-63(5)	28.27	fair	2.2 to 7.9	west edge of gully offset
1-63(6)	28.30	good	7.3 ± 1.7	deeply incised gully offset
1-63(8)	28.32	fair	2.8 to 7.5	west edge of gully offset
1-65(1)	28.39	exc	13.7 ± 2.0	abandoned channel offset
1-65(2a)	28.73	fair	6.5 ± 1.7	terrace riser offset
1-65(2b)	28.74	exc	18.2 ± 3.5	alluvial fan offset from channel
1-65(3)	28.77	fair	≥ 2.0	shutter ridge
1-65(10)	28.97	good	8.8 ± 1.5	east wall of channel offset
1-67(2)	30.15	fair	7.0 ± 1.0	east wall of channel offset
1-67(1a)	30.18	good	≥ 5.2	shutter ridge
1-67(1b)	30.19	good	18.0 ± 2.0	east wall of channel offset
1-73(3)	32.40	poor	3.3 ± 1.6	gully offset at two fault traces
1-73(5a)	32.51	good	≥ 2.4	shutter ridge
1-73(5b)	32.51	fair	7.1 ± 1.0	east wall of channel offset
1-73(6a)	32.62	good	≥ 2.6	shutter ridge
1-73(6b)	32.62	poor	7.0 ± 1.0	east wall of channel offset
1-73(8b)	32.84	poor	6.8 ± 2.3	west edge of gully offset
1-73(8a)	32.85	fair	14.2 ± 2.0	center of gully offset

Distances measured eastward along Garlock fault from Cantil.

in order to document a few of these offset features.

Feature 1-65(1):

At this site an abandoned channel, Qt₄, has been left-laterally faulted (in at least two events) out of the path of the modern stream (Figure 3-3). The eastern wall of the abandoned channel is well defined and can be recognized to within a few meters of the fault. Adjacent to the fault it has been buried by colluvium derived from the fault scarp. The eastern wall of the abandoned channel south of the fault clearly correlates with the eastern wall of the modern channel north of the fault, because there is no other upstream channel segment that could be a match. The offset of this feature is 13.7 ± 2.0 m. I have given this offset an excellent quality rating because at the time of its formation, the eastern wall of the abandoned channel was clearly located directly opposite the eastern wall of the channel segment north of the fault.

Features 1-65(2a) and 1-65(2b):

At this site the apex of an alluvial fan (feature 1-65(2b), and Qa₃ on Figure 3-4) has been left-laterally faulted 18.2 ± 3.5 m from its source channel. Because there is no other possible source channel for this alluvial fan, the correlation is excellent. A younger terrace riser (feature 1-65(2a)) that cuts the Qa₃ fan has been offset 6.5 ± 1.7 m from the east edge of the Qt₂ terrace north of the fault (Figure 3-4). This feature has a fair quality rating because the correlation is less certain. Although there is a 1-m-high, south-facing scarp on the Qt₂ terrace, part or all of this scarp

FIGURE 3-3: Topographic map of an abandoned channel, Qt4, (feature 1-65(1) in Table 3-1 and Figure 3-5) faulted away from its source. The 13.7 ± 2.0 m offset was measured as follows. The top of the eastern wall of the abandoned channel was projected to the fault to obtain one piercing point. This piercing point is at an elevation of about 6.25 m (above an arbitrary point of zero elevation), and is buried by colluvium derived from the fault scarp. If the vertical displacement has been negligible, then the correlative piercing point on the north side of the fault should also be at an elevation of about 6.25 m. To find this piercing point, I projected the 6.25 m contour on the eastern wall of the upstream channel segment to the fault. Because the channel wall bends about 5 m north of the fault, there are two possible locations of the piercing point. The designation of alluvial deposits and surfaces in Figures 3-3, 3-4, 3-11, 3-12, and 3-16 is specific to each figure. Thus the Qt₄ surface in this figure is not the same age as the Qt₄ surface in Figure 3-4.

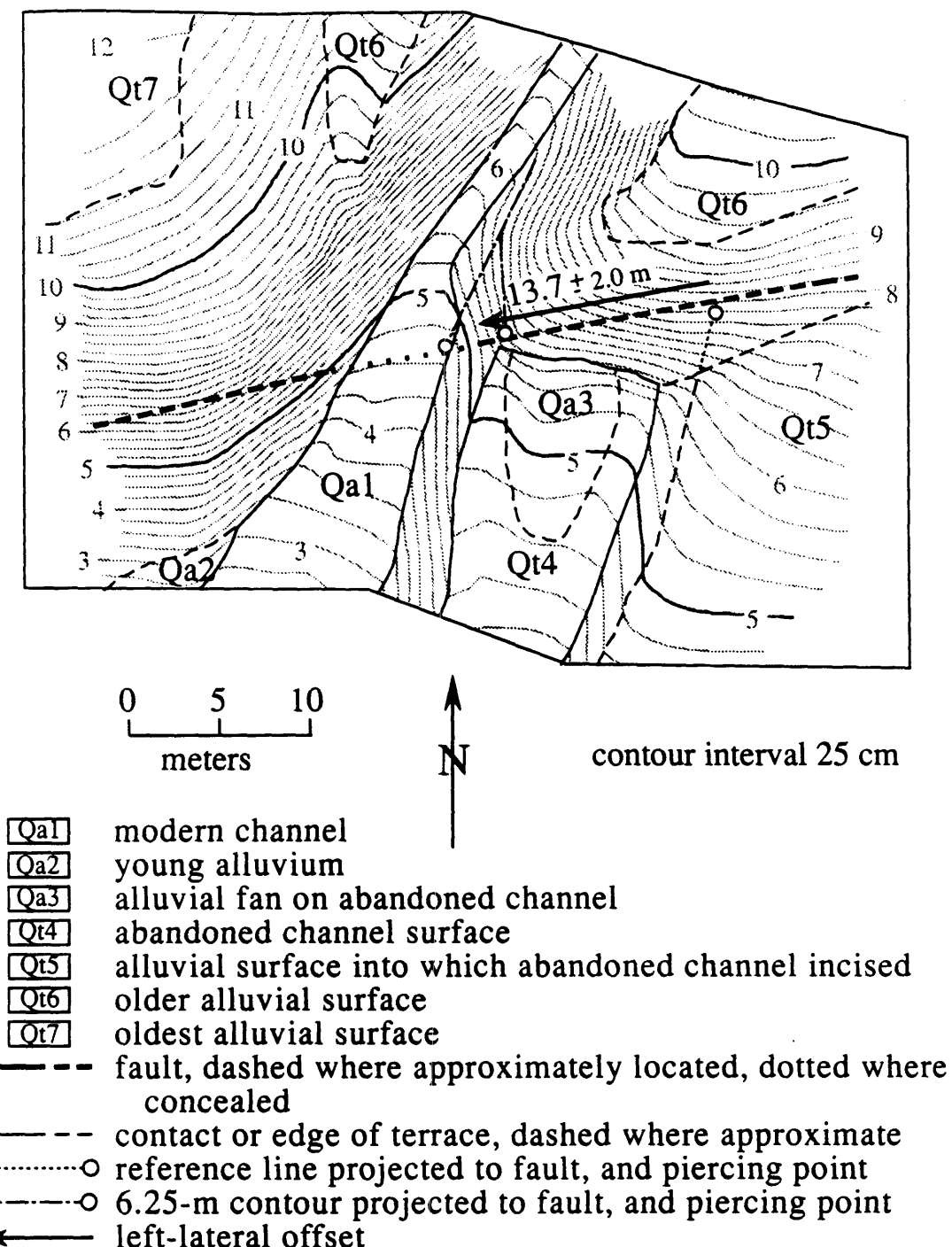


Figure 3-3

FIGURE 3-4: Topographic map of an alluvial fan, Qa_3 (feature 1-65(2b), in Table 3-1 and Figure 3-5) offset from its source channel and of an offset riser between the Qt_2 terrace and older deposits (feature 1-65(2a) in Table 3-1 and Figure 3-5). To measure the offset of the alluvial fan Qa_3 , the edges of the fan were projected beneath fault-scarp colluvium to the fault, to obtain two piercing points (solid circles south of the fault). The edges of the source channel, as defined by the outer edges of the Qt_2 terrace within the source channel, were then projected to the fault to obtain two other piercing points (solid circles north of the fault). The two piercing points south of the fault must restore to a position between the two piercing points north of the fault, yielding an offset of 18.2 ± 3.5 m. Piercing points from which the 6.5 ± 1.7 m offset of the terrace riser were measured are shown as open circles. The two open circles north of the fault reflect the westernmost and easternmost likely locations for the piercing point north of the fault, and are the source of the reported error.

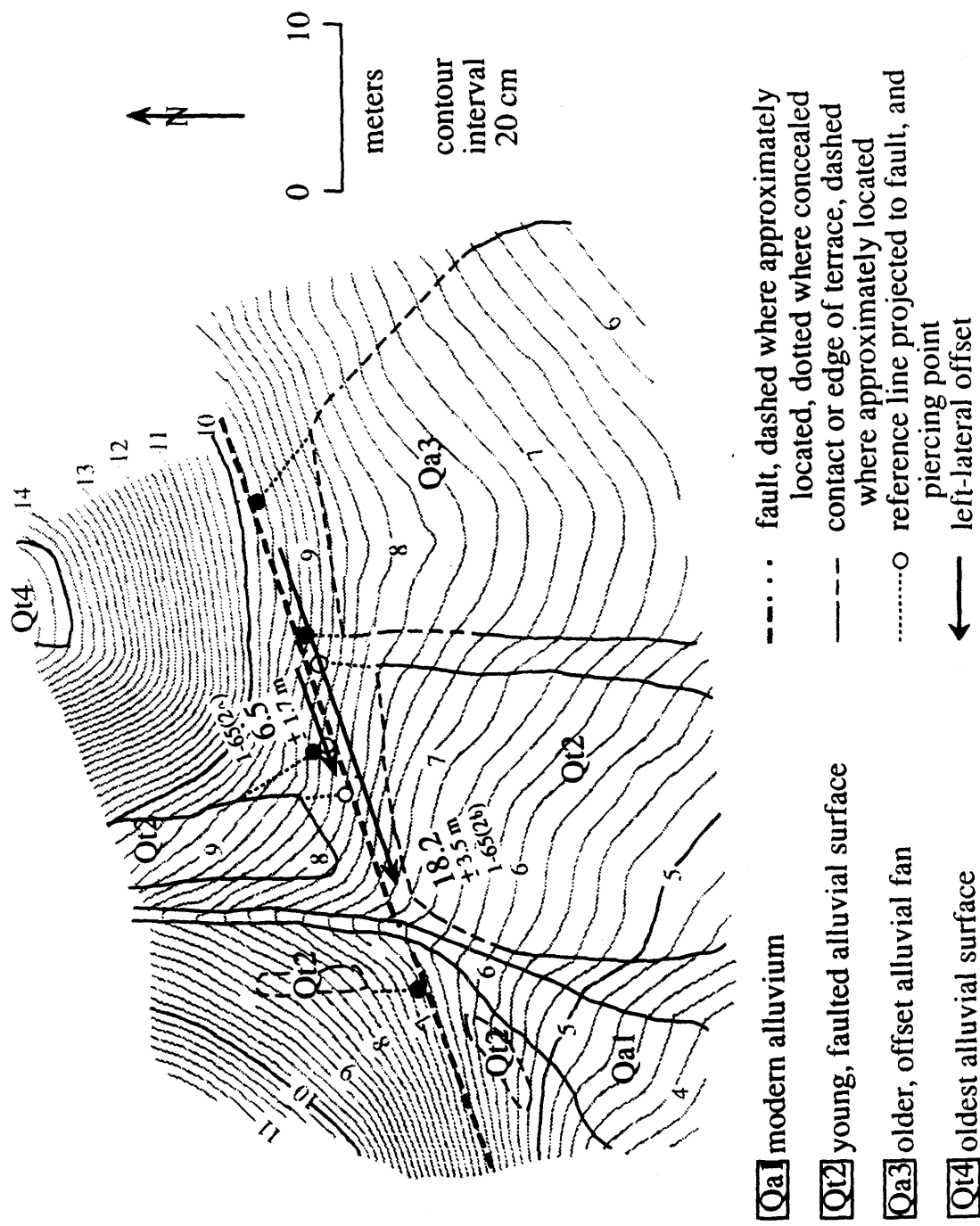


Figure 3-4

may be due to left-lateral offset of the terrace surface, which slopes obliquely to the fault. Three-dimensional projection of the east edge of the Qt₂ terrace to the fault suggests that there is probably no vertical displacement of the east edge of the terrace.

Other offset features:

In Figure 3-5 the left-lateral offset of each feature listed in Table 3-1 is plotted as a function of distance along the strike of the fault. Thin, horizontal lines pass through or near features that I believe have been offset by the same number of slip events. These lines are derived from Figure 3-6, which shows that the data cluster around the discrete offset values at these lines.

In Figure 3-6, the uncertainty in the offset of each geomorphic feature in Table 3-1 has been translated into a probability-density function and these probability-density functions have been summed. (See Figure 3-6 caption for a more complete discussion of the construction of this figure.) The presence of resolvable peaks in Figure 3-6 indicates that the offsets cluster around discrete values that probably represent the cumulative displacement associated with different numbers of past earthquakes. The area under the entire curve in Figure 3-6 is equal to the number of offset features represented (15), and the area under each peak is roughly equal to the number of offset features producing that peak. The width of the peaks reflects both the uncertainty in the measurements and the actual variability along strike of the offset during past earthquakes. The representation of the data in Figure

FIGURE 3-5: Offset of 24 geomorphic features south of El Paso Mountains (Table 3-1) plotted as a function of distance along strike, measured eastward from Cantil. The westernmost 5 features are from the Garlock townsite area, and the remaining 19 features are from the Highway 395 area. Horizontal lines are drawn at the offset values around which the offsets cluster (see Figure 3-6), and probably represent the cumulative slip in different numbers of past earthquakes. For shutter ridges, arrows are plotted with their bases at the minimum offset and have an arbitrary 2-m length.

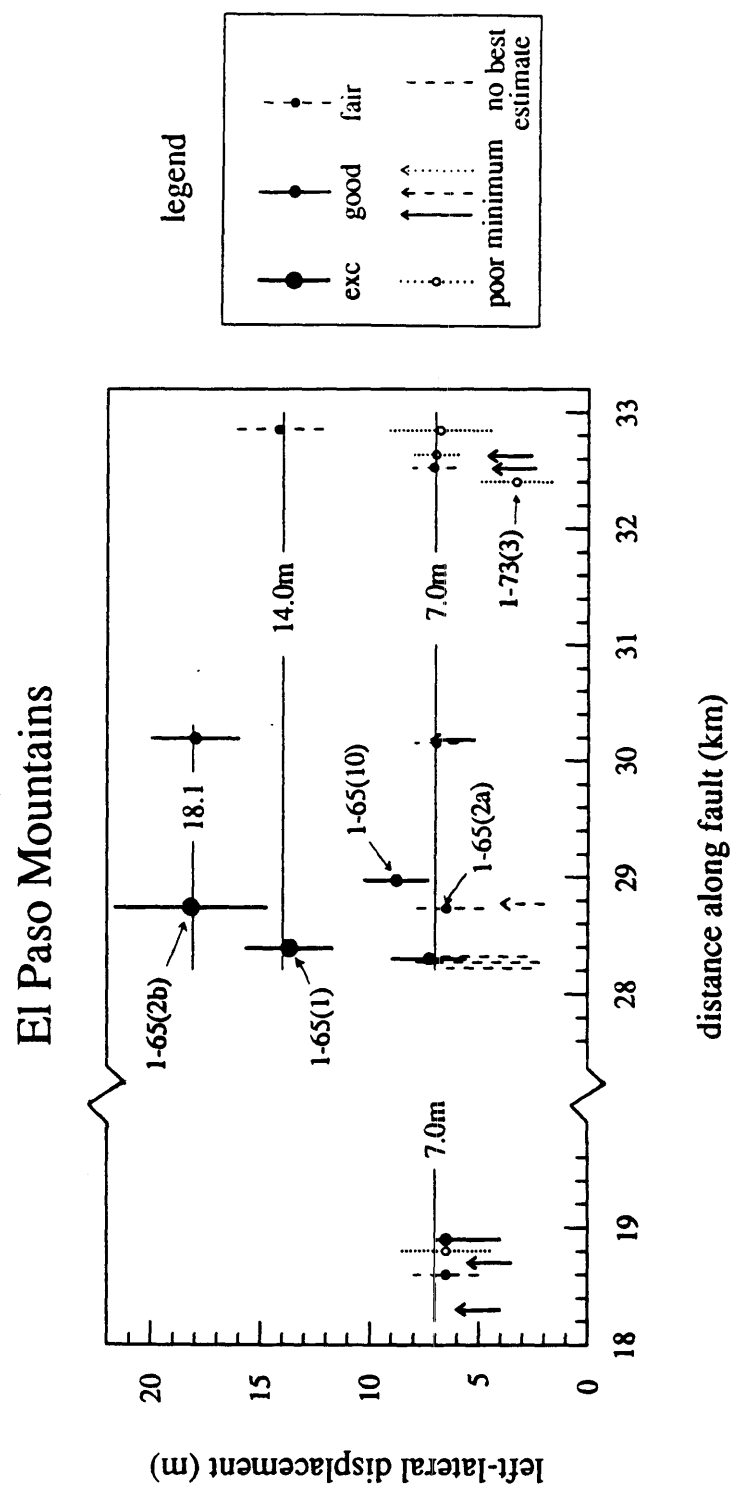


Figure 3-5

FIGURE 3-6: Summation of Gaussian probability-density functions for 15 offset features south of El Paso Mountains, from the Garlock townsit and Highway 395 areas (Table 3-1 and Figure 3-5, excluding measurements without a best estimate). Each offset is represented by a Gaussian probability-density function with a mean at the best estimate of the offset and with a standard deviation equal to one half of the uncertainty (*i.e.*, the uncertainties reported in Table 3-1 are assumed to be \pm 2-sigma uncertainties). For features with asymmetrical uncertainties, a standard deviation equal to one half of the larger of the two uncertainties is used. The probability-density functions for all of these offsets were then summed to produce this figure. Shading indicates the quality of the offset estimates used. Each peak probably represents the cumulative slip associated with a different number of past earthquakes. The peak at 3.3 m is dubious, however, because it represents only one, poor-quality offset.

El Paso Mountains

143

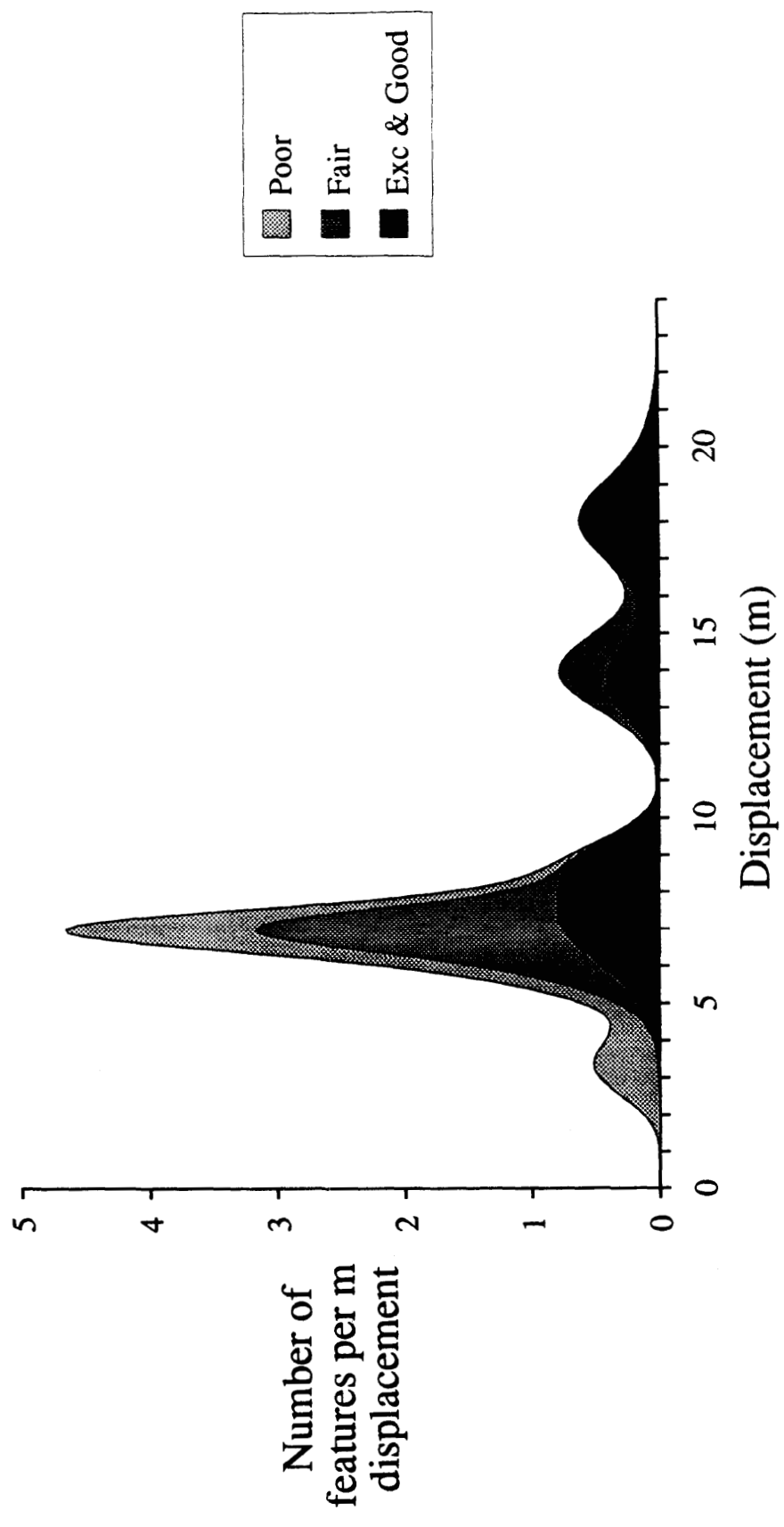


Figure 3-6

3-6 was chosen over a standard histogram because it allows the uncertainty of the measurements to be incorporated.

The data presented in Table 3-1, and in Figures 3-5 and 3-6, suggest that the most recent large earthquake on this part of the Garlock fault may have been produced by as much as about 7 m of left-lateral slip. Although a number of geomorphic features have apparent offsets of about 3 m, all but one of these are shutter ridges whose tips may have been eroded, so they provide only a lower bound on the true offset of these features. Feature 1-73(3) (Table 3-1 and Figure 3-5) is the only feature offset less than about 7 m that need not be regarded as a minimum estimate of the true offset. The correlation of this gully across the fault, however, is poor. Thus, there is no convincing evidence for less than about 7 m of slip in the latest slip event here. The features offset about 14 m and about 18 m also suggest slip of about 7 m (14 m - 7 m) in the penultimate event, and slip of about 4 m (18 m - 14 m) in the previous event. Because the geomorphic record may be incomplete, however, more frequent events with smaller slip amounts can not be ruled out, and may be weakly suggested by the apparent 3.3 m offset of the poor-quality feature 1-73(3).

The amount of slip in the latest earthquake probably varied somewhat along strike because none of the horizontal lines thought to represent the average cumulative slip in different numbers of past earthquakes pass through the error bar for feature 1-65(10) in Figure 3-5. The degree of variability required to interpret the 9-m offset of 1-65(10) as having formed during the most recent earthquake, along

with the 7-m offsets, is not unreasonable considering the variability of slip along strike documented after major, historical, strike-slip faulting events. For example, the slip associated with the 1968 Dasht-e Bayaz earthquake in Iran varied from 3.0 m to 1.5 m within about 100 m along the strike of the fault (Ambrasseys and Tchalenko, 1969). As another example, the surface displacement associated with the 1967 Mudurnu Valley earthquake in Turkey varied from 1.8 m to 0.7 m to 1.8 m to 0.8 m all within about 450 m along the strike of the fault (Ambrasseys and Zatopek, 1969). On the other hand, the 9-m offset of 1-65(10) could conceivably represent the cumulative slip in the past two events (about 7 m in the latest event and about 2 m in the previous event). I regard this as a less likely interpretation, however, because of the lack of other geomorphic features offset by about 9 m.

The amount of slip in past earthquakes suggested by the geomorphic offsets along the southern flank of El Paso Mountains (4 to 7 m) is consistent with a previous estimate of the slip per event in this area. At a site about 6 km west of the Garlock townsite area, Burke and Clark (1978) and Burke (1979) documented 9 to 17 slip events in the past 14,700 $^{14}\text{C-yr}$. On the basis of the 80-m left-lateral offset of a nearby lacustrine bar of similar age, they inferred that those 9 to 17 events each involved 5 to 9 m of left-lateral slip.

No features (other than feature 1-65(2a), discussed above) were found along this segment of the fault for which the vertical displacement could be unambiguously measured.

Searles Valley

Twenty-six offset geomorphic features were measured along a 4-km-length of the fault in Searles Valley (Table 3-2 and Figures 3-7 and 3-8). Each horizontal line on Figure 3-7 corresponds to a peak on Figure 3-8, and is thought to represent the cumulative slip in some number of past earthquakes. Two offset features with fair correlations and a number of features with poor correlations suggest that the latest earthquake on this part of the fault was produced by about 2.2 m of left-lateral slip. The larger offsets are separated by 1.7 to 3.5 m, suggesting that the previous several earthquakes have been generated by displacements within this range. The offset features on which this interpretation is based, however, are sparse, and most of them are of poor quality. The lack of features offset between 12 m and 21 m may reflect the incompleteness of the geomorphic record, rather than indicate the occurrence of a 9-m slip event.

Where the sense of vertical slip can be determined, it is uniformly south-side-up. One south-facing scarp exists along this portion of the fault, but it may be separation formed by lateral slip.

Pilot Knob Valley

The lateral displacements of 74 geomorphic features in Pilot Knob Valley also cluster around discrete values (Table 3-3, Figures 3-9 and 3-10). The six peaks in Figure 3-10 are spaced 1.9 to 4.1 meters apart, suggesting that the geomorphic offsets in Pilot Knob Valley record 6 large, prehistoric earthquakes with about 2 to 4 m of

TABLE 2. Geomorphic Offsets in Searles Valley

Feature	Distance (km)	Quality	Horizontal Offset (m)	Vertical Slip (m)	Description of offset feature
1-129(7)	57.52	poor	3.9 ± 0.8	S	gully
1-131(5)	58.27	fair	25.0 ± 3.0	S	east-facing terrace riser
1-131(1)	58.85	good	21.0 ± 1.2	0.35 S	east-facing terrace riser
1-131(2)	58.86	poor	7.0 ± 1.0	S	east-facing terrace riser
1-131(3)	59.23	good	≥ 8.4		west wall of channel
1-131(4)	59.26	poor	9.6 ± 2.0		east wall of channel
1-133(1)	59.34	fair	24.0 ± 3.0		beheaded channel
1-133(6)	59.80	poor	3.0 ± 0.5	S	gully
1-133(7)	59.80	poor	2.3 ± 0.5	S	gully
1-133(8)	59.83	poor	2.5 ± 0.7	S	gully
1-133(9)	59.86	poor	2.8 ± 0.5	S	beheaded gully
1-133(10)	59.86	poor	1.4 ± 0.5	S	gully
1-133(11)	59.90	poor	2.8 ± 0.4	S	gully
1-133(12)	59.94	poor	3.5 ± 1.3		west wall of channel
1-133(15)	60.03	poor	2.2 ± 0.2	S	gully
1-133(16)	60.03	poor	2.2 ± 0.2	S	gully
1-133(18)	60.05	poor	1.8 ± 0.2	S	gully
1-133(19)	60.07	poor	1.7 ± 0.5	S	gully
1-133(20)	60.07	poor	1.6 ± 0.5	S	gully
1-133(21)	60.19	good	≥ 12.5	S	shutter ridge
1-133(22)	60.20	fair	2.5 ± 0.5	S	gully
1-133(23)	60.20	fair	1.9 ± 0.5	S	gully
1-133(24)	20.26	good	≥ 4.4	S	shutter ridge
1-133(25)	60.35	good	≥ 4.6	S	shutter ridge
1-134(1a)	60.62	fair	12.0 ± 1.0		west wall of channel
1-134(1b)	60.63	fair	≥ 11.5		shutter ridge

Distances measured eastward along the fault from Cantil. S indicates south-up sense of vertical displacement.

FIGURE 3-7: Offset of 26 geomorphic features in Searles Valley (Table 3-2) plotted as a function of distance along strike, measured eastward from Cantil. Horizontal lines are drawn at the offset values around which the offsets cluster, as shown in Figure 3-8, and probably represent the cumulative slip in different numbers of past earthquakes. Horizontal lines through clusters (or single measurements) that are defined only by poor-quality offsets are dashed. For features that may have been modified by erosion, arrows are plotted with their bases at the minimum offset.

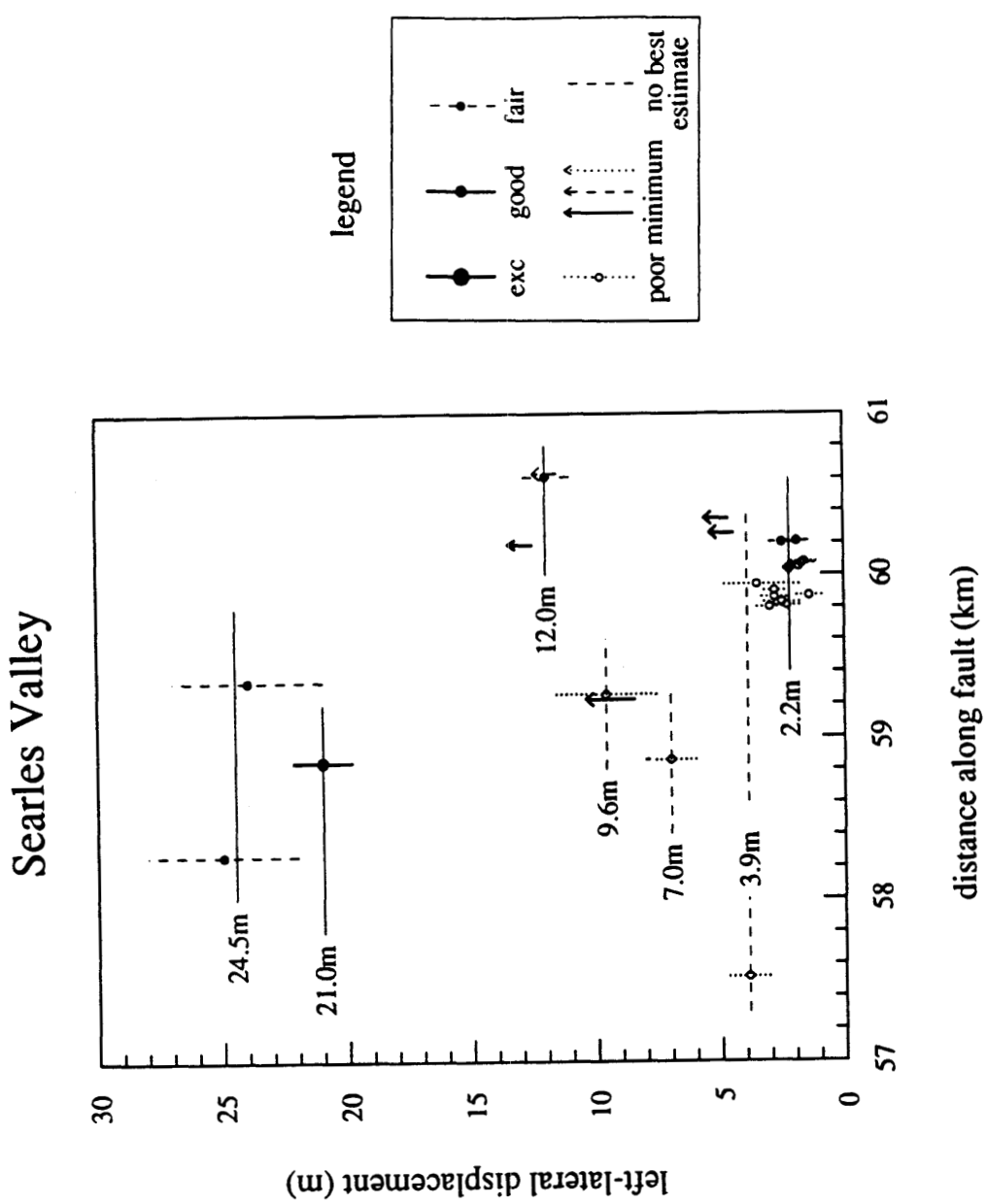


Figure 3-7

FIGURE 3-8: Summed Gaussian probability-density functions for 21 offset features in Searles Valley (Table 3-2 and Figure 3-7). Shading indicates the quality of the offset estimates used. See Figure 3-6 caption for a more complete explanation of the construction of this figure. The largest peak, at about 2.2 m, probably represents the slip in the most recent earthquake. Other peaks may represent the cumulative slip in greater numbers of past earthquakes, but their interpretation is less certain because of the small number of offset features represented.

Searles Valley

151

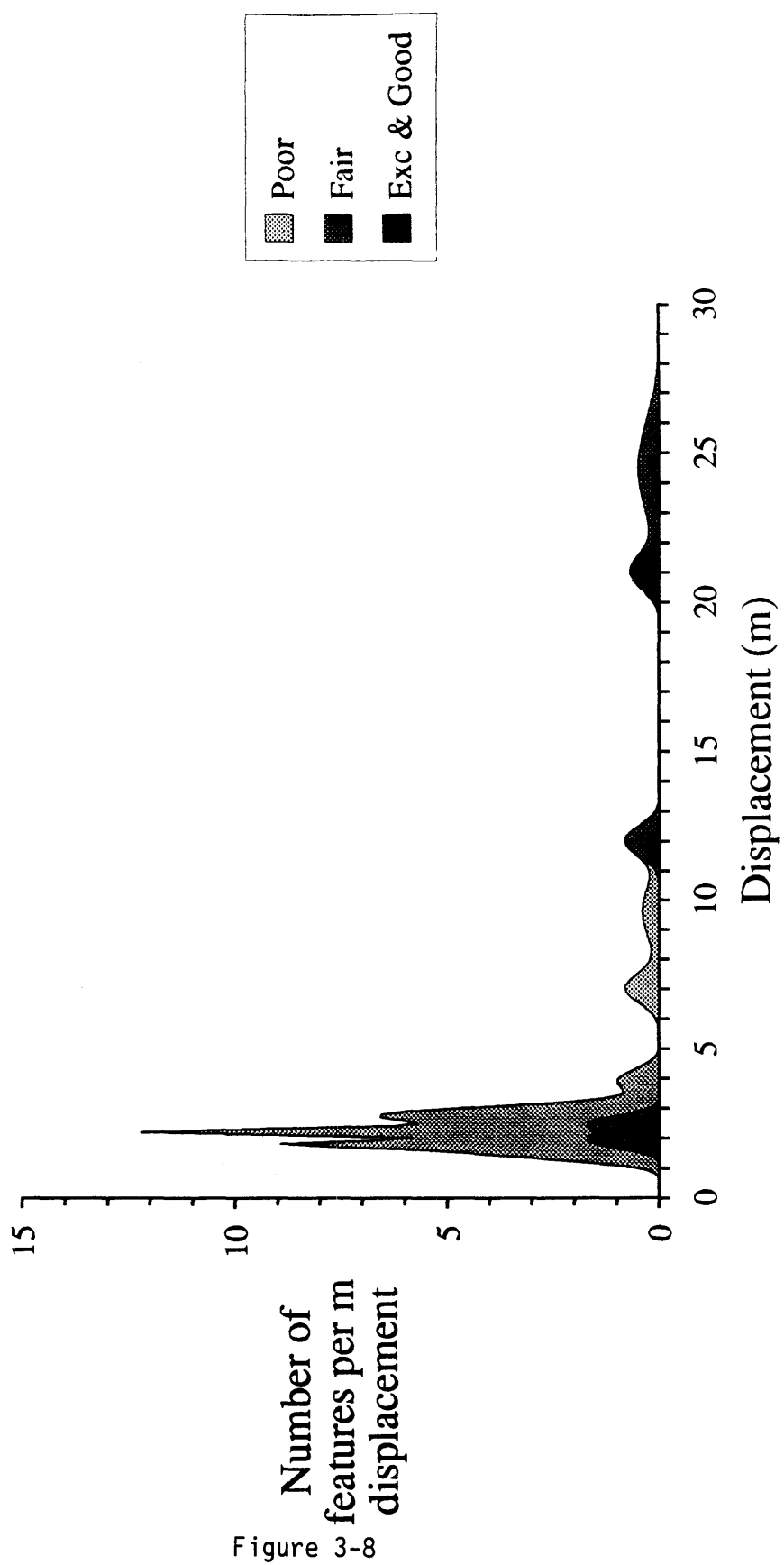


TABLE 3. Geomorphic Offsets in Pilot Knob Valley

Feature	Distance (km)	Quality	Horizontal Offset (m)	Vertical Slip (m)	Description of offset feature
2-9(3)	70.61	poor	6.0 \pm 1.0		east wall of channel
2-11(2a)	71.91	exc	\geq 9.9		shutter ridge
2-11(2b)	71.92	fair	12.4 \pm ^{1.0} _{1.5}		east wall of channel
2-21(1)	75.91	poor	2.1 \pm 0.5		terrace riser
2-21(8)	75.98	fair	3.1 \pm 0.5		debris flow
2-21(2)	76.07	exc	15.2 \pm 1.0		west wall of channel
2-21(3)	76.08	exc	14.0 \pm 1.5		east wall of channel
2-21(4)	76.22	poor	4.4 \pm 1.0		gully
2-21(7a)	76.53	poor	2.0 \pm 0.5		hillside
2-21(7b)	76.54	poor	2.5 \pm 0.5		hillside
2-23(1)	76.70	exc	5.6 \pm 1.0	0.50 N	terrace riser
2-23(2)	76.72	good	5.0 \pm 0.7	0.50 N	gully
2-23(12)	76.74	poor	4.9 \pm 0.8	0.55 N	debris flow
2-23(13)	76.76	poor	4.0 \pm 0.8		debris flow
2-23(3)	76.77	fair	5.3 \pm ^{1.0} _{0.5}		gully
2-23(6)	76.82	poor	4.8 \pm 1.0		gully and debris flow
2-23(8)	77.18	poor	6.2 \pm ^{0.3} _{1.5}		gully
2-23(10)	77.47	good	3.5 \pm ^{1.0} _{0.5}	0.40 N	debris flow
2-23(11)	77.64	poor	3.7 \pm 0.5		ridge and gully
2-25(2)	77.81	good	4.9 \pm 1.0		terrace riser
2-25(4)	77.98	good	5.4 \pm ^{1.5} _{0.5}		shutter ridge
2-25(5)	78.24	fair	11.7 \pm 1.0		east wall of channel
2-27(9)	78.69	poor	4.5 to 8.3		east wall of channel
2-27(1)	78.84	exc	\geq 8.2		terrace riser
2-27(3)	78.87	poor	2.6 \pm 1.0		gully
2-27(5)	78.89	good	4.6 \pm ^{2.0} _{1.0}	0.30 N	east wall of channel
2-27(6)	78.99	fair	\geq 3.5		shutter ridge
2-27(11)	79.07	good	\geq 7.3		shutter ridge
2-29(2)	79.29	poor	3.9 \pm 2.0		incised channel
2-29(4)	79.34	good	5.6 \pm ^{2.0} _{1.8}		east wall of channel
2-29(7)	79.71	exc	3.7 \pm ^{1.0} _{0.5}	0.60 N	terrace riser
2-29(8)	79.72	fair	3.5 \pm 0.4		gully
2-29(12)	79.75	fair	5.4 \pm ^{0.5} _{1.2}	0.58 N	gully
2-29(13)	79.78	poor	5.1 \pm 1.0	0.20 N	east wall of channel
2-29(9)	79.82	poor	5.3 \pm 1.0	0.50 N	east wall of channel
2-29(11)	79.95	good	7.3 \pm ^{4.7} _{1.5}		terrace riser
2-31(1b)	80.31	poor	15.0 \pm ^{2.0} _{5.0}		east wall of channel
2-31(2b)	80.79	poor	10.0 \pm 3.0		east wall of channel
2-33(5)	81.59	good	8.4 \pm 1.6		east wall of channel
2-33(6)	81.61	poor	2.4 \pm 0.5		gully
2-35(1)	81.70	good	3.0 \pm 0.5		gully

TABLE 3 (continued).

Feature	Distance (km)	Quality	Horizontal Offset (m)	Vertical Slip (m)	Description of offset feature
2-35(2)	81.83	good	6.1 \pm 1.0		east wall of channel
2-37(1)	83.16	exc	\geq 5.4		west wall of channel
2-45(1)	87.65	fair	15.3 \pm 1.0		gully and ridge
2-45(3)	87.70	fair	5.8 \pm 1.0		east edge of gully
2-53(1)	91.78	poor	3.5 \pm 0.5		east edge of mound
2-57(4a)	92.71	exc	\geq 2.5		west edge of terrace
2-57(4b)	92.71	good	2.1 \pm 0.8		east edge of terrace
2-59(1)	93.54	fair	4.0 \pm 0.7	0.55	west edge of terrace
2-59(14)	93.67	poor	2.3 \pm 0.7	0.25 N	debris flow
2-59(3)	93.73	good	2.8 \pm 0.7	0.80 N	debris flow
2-59(9)	93.77	fair	3.3 \pm ^{1.3} _{0.8}	0.60 N	gully
2-59(4)	93.85	poor	5.8 \pm 1.4		both edges of terrace
2-59(6)	93.88	good	\geq 2.5		east wall of channel
2-59(11)	94.04	good	3.1 \pm ^{1.4} _{1.0}	0.40 N	west edge of debris flow
2-59(12)	94.10	good	3.4 \pm 1.2	0.35 N	west edge of debris flow
2-59(13)	94.12	good	\geq 2.5	0.65 N	west edge of debris flow
2-61(4)	95.44	fair	2.7 \pm 0.7		east wall of channel
2-61(5)	95.45	fair	5.6 \pm 0.7		east edge of terrace
2-61(6)	95.45	good	5.3 \pm 0.3		west wall of channel
2-61(7)	95.46	fair	3.4 \pm 0.5		east wall of channel
2-61(8)	95.47	fair	3.5 \pm 0.7		terrace riser
2-61(11)	95.74	good	8.3 \pm 1.0		west wall of channel
2-61(12)	95.75	good	7.6 \pm 1.0		east wall of channel
2-61(13)	95.81	good	16.0 \pm 0.5		west wall of channel
2-61(14)	95.82	good	16.5 \pm ^{7.0} _{1.0}		east wall of channel
2-61(15)	95.84	good	15.5 \pm ^{2.5} _{1.5}		west wall of channel
2-61(16)	95.87	good	18.0 \pm 1.5		east wall of channel
2-63(2)	95.99	fair	2.5 \pm ^{1.7} _{0.7}		east wall of channel
2-63(3)	96.00	fair	8.8 \pm 0.7		old east wall of channel
2-63(5a)	96.04	fair	2.3 \pm ^{2.0} _{0.5}		west edge of seive deposit
2-63(8)	96.59	good	7.0 \pm 1.5		channel
2-63(4a)	96.77	good	4.2 \pm ^{1.8} _{1.2}		west wall of channel
2-63(4b)	96.78	good	3.4 \pm 1.1		east wall of channel

Distances measured eastward along fault from Cantil. N indicates north-up senses of vertical displacement.

FIGURE 3-9: Offset of 74 geomorphic features in Pilot Knob Valley (Table 3-3), plotted as a function of distance along strike eastward from Cantil. Horizontal lines correspond to peaks in Figure 3-10, and probably represent the average cumulative offset associated with different numbers of past slip events. Dotted curve illustrates an alternate interpretation, in which slip is more variable along strike (see text). For features that may have been modified by erosion, arrows are plotted with their bases at the minimum offset.

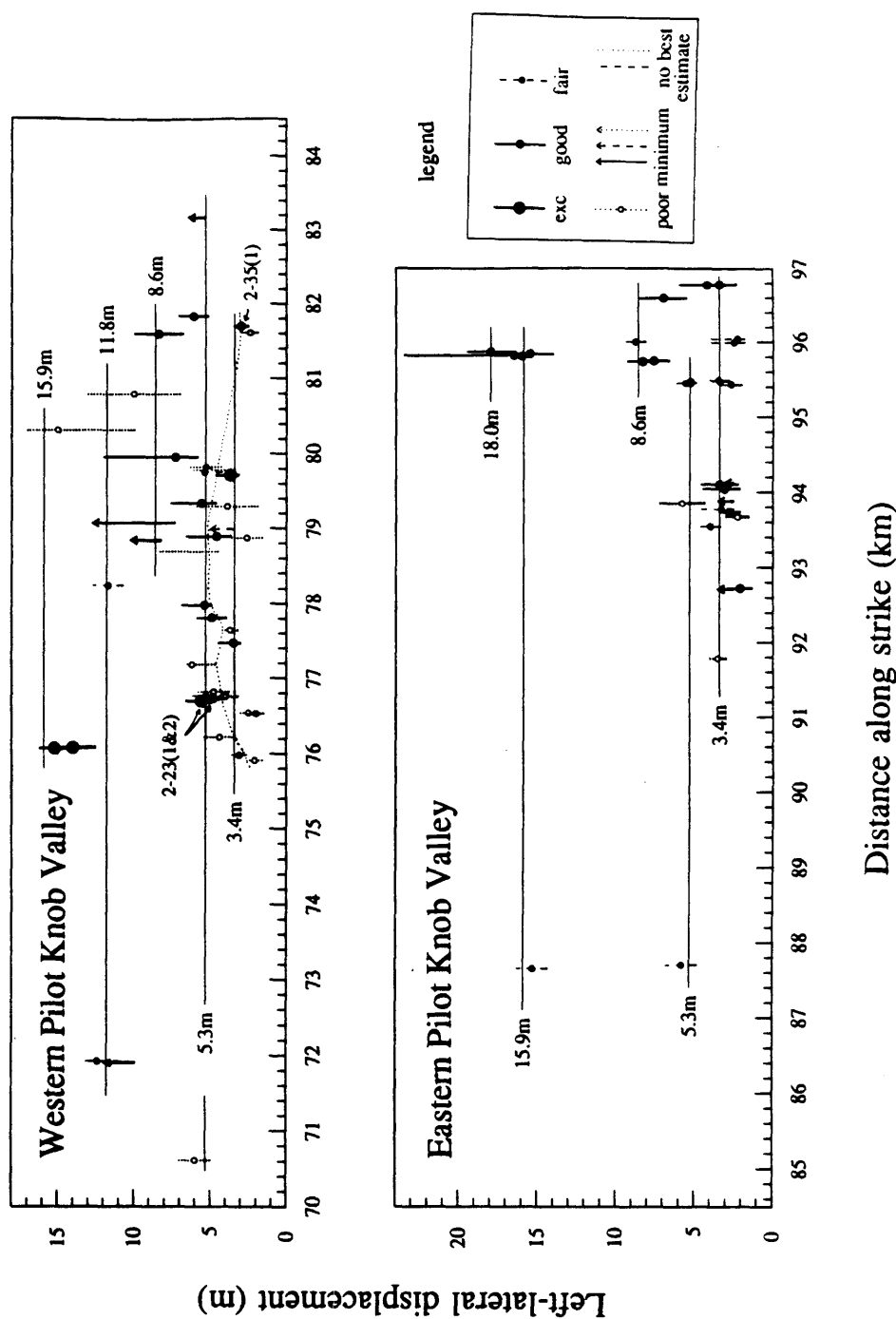


Figure 3-9

FIGURE 3-10: Summed Gaussian probability-density functions for 62 geomorphic offsets in Pilot Knob Valley (Table 3-3 and Figure 3-9). Shading indicates the quality of offset estimates used. See caption of Figure 3-6 for explanation of the construction of this figure. Each peak probably represents the cumulative slip associated with a different number of past earthquakes.

Pilot Knob Valley

157

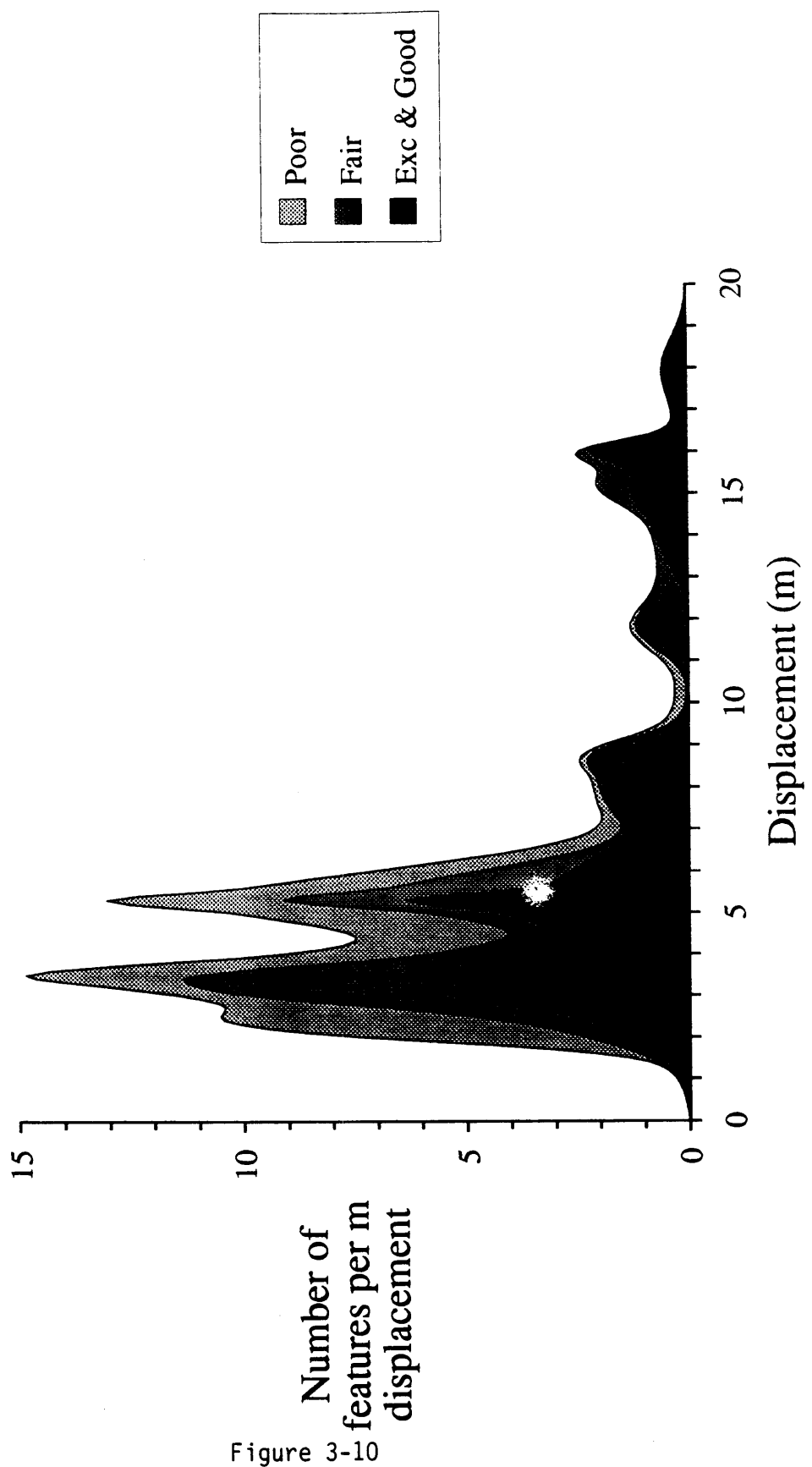


Figure 3-10

left-lateral slip each.

Other interpretations of the data are possible, however. For example, consider the geomorphic features in western Pilot Knob Valley that are offset about 6 m or less. An alternate interpretation is that all of the features offset about 6 m or less in western Pilot Knob Valley were offset in the latest event, and that the amount of slip in that event varied along strike from about 2 m to about 6 m. This degree of variability of slip along strike has been exhibited by several historical, strike-slip earthquakes, namely, the 1940 Imperial Valley (California) earthquake (Sharp, 1982), the 1968 Dasht-e Bayaz (Iran) earthquake (Ambrasseys and Tchalenko, 1969), and the 1976 Motagua (Guatemala) earthquake (Bucknam and others, 1978).

In spite of the existence of historical precedents for the type of slip distribution along strike required by the alternate interpretation of the data in Figure 3-9, I prefer the interpretation stated initially-- that the features offset about 2 to 4 m record the slip in the latest earthquake, while those offset about 4-1/2 to 6 m record the slip in the latest two earthquakes combined-- for the following reasons. First, the alternate interpretation can not be easily extended to eastern Pilot Knob Valley. A terrace riser offset 2.7 ± 0.7 m (feature 2-61(4)) is located less than 10 m west of two terrace risers offset 5.6 ± 0.7 m and 5.3 ± 0.3 m (features 2-61(5) and 2-61(6), Table 3-3). Less than 20 m east of features 2-61(5) and 2-61(6) are two terrace risers offset 3.4 ± 0.5 m and 3.5 ± 0.7 m (features 2-61(7) and 2-61(8), Table 3-3). Changes in slip along strike that are this large, that occur in such a short distance, and that occur where the fault has only one strand (as opposed to areas where there is a step-over

in the fault), have no documented historical precedent.

Second, the fact that there are two separate peaks in Figure 3-10, at 3.4 m and at 5.3 m, supports the interpretation that features offset 2 to 4 m record slip in the latest event, while features offset 4-1/2 to 6 m record the slip associated with the two latest events combined. If all features offset about 6 m or less are attributed to a single event with variable slip, then one would expect to see more features offset between 4 and 5 m. That is, one would expect to see a single, broad peak between about 2 and 6 meters, rather than two separate peaks. The lack of features offset between about 4 and 5 m is particularly true of the good and fair quality offsets.

The vertical component of each displacement in Pilot Knob Valley averages about 12% of the horizontal component (Table 3-3). Along the section of the fault lying south of the Slate Range, the vertical slip is uniformly up to the north. The few north-facing scarps along this part of the fault are either part of grabens within step-overs of the fault or may be explained by lateral offset. Although the only measured vertical displacements south of the Quail Mountains are up to the north (both in eastern Pilot Knob Valley and west of Leach Lake, see Table 3-4), there are north-facing scarps along other parts of the fault south of Panamint Valley and the Quail Mountains that are difficult to explain by lateral movement and that probably indicate south-side-up displacement at some places.

Topographic maps of a few of the offset features in Pilot Knob Valley are discussed below.

Feature 2-35(1):

At this site, a gully is offset 3.0 ± 0.5 m left-laterally (Figure 3-11). The gully is well defined and is offset sharply at the fault. The upstream and downstream gully segments have the same width, and there are no other channels nearby and northwest of the fault of suitable size to be sources for the downstream segment. For these reasons I have given this feature a good quality rating. As discussed above, I believe that the 3 m of slip recorded by this gully represent the left-lateral slip in the latest earthquake along this part of the fault.

Features 2-23(1) and 2-23(2):

At this site, both a terrace riser and a small gully on top of the terrace are offset left-laterally (Figure 3-12). The top of the riser between the Qt_2 and Qt_3 terraces (feature 2-23(1)) is left-laterally displaced 5.6 ± 1.0 m. The terrace riser is sharp and extends nearly up to the fault on both sides of the fault. It is very unlikely that the terrace-riser segment south of the fault could have been cut in its present position. It is much more likely that the riser south of the fault was originally aligned with the riser north of the fault and was subsequently offset. The riser segment north of the fault can not have been eroded recently, because it is protected from the modern channel by the Qt_2 terrace. Any reduction of the apparent offset by erosion of the northern riser segment had to occur before deposition of the Qt_2 terrace. I thus regard this terrace riser as an accurate indicator of the amount of slip in the past one or more earthquakes at this site, and I have given it an excellent quality rating.

FIGURE 3-11: Topographic map of a gully (feature 2-35(1) in Table 3-3 and Figure 3-9) offset 3 m in Pilot Knob Valley.

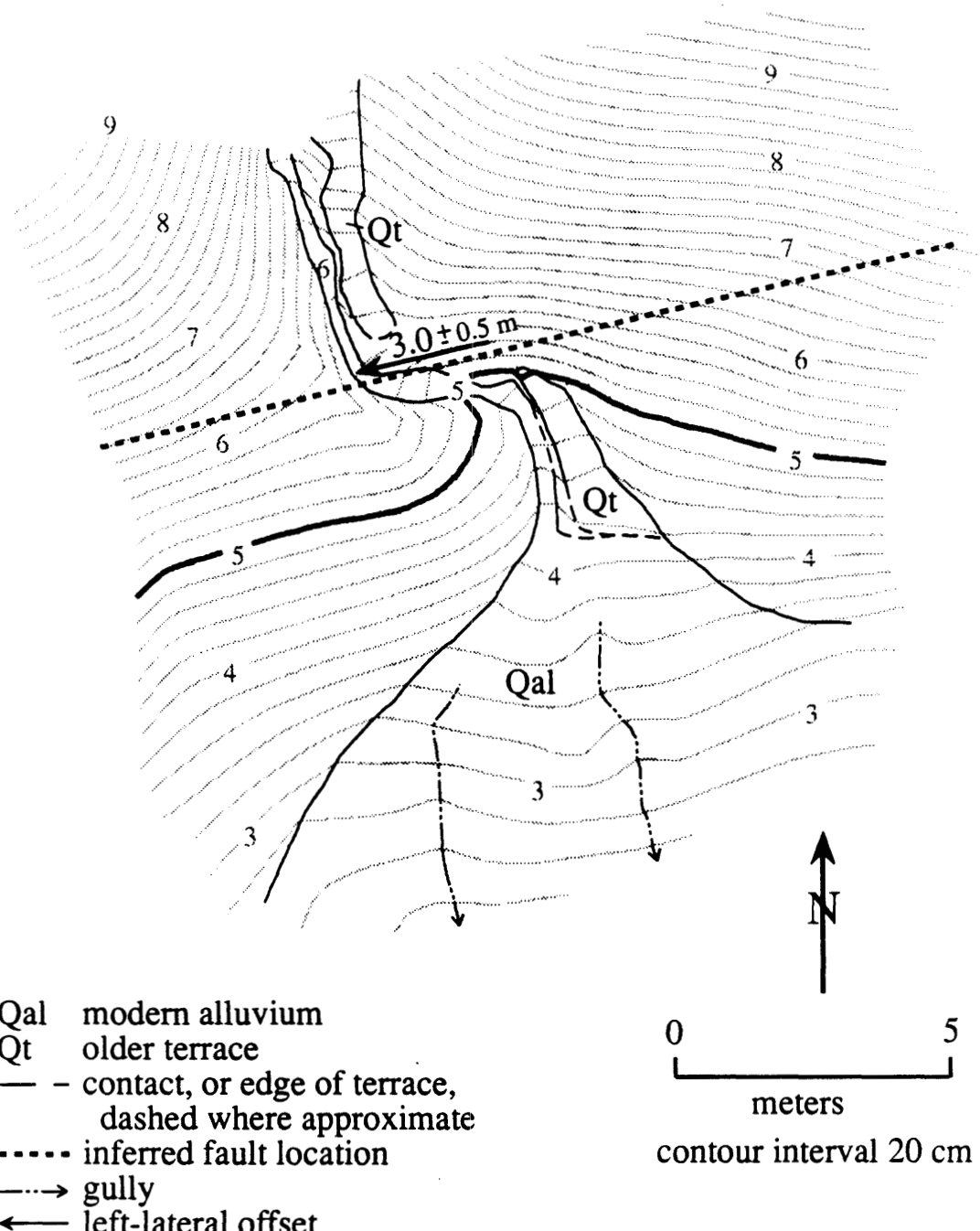


Figure 3-11

FIGURE 3-12: Topographic map of a terrace riser (feature 2-23(1) in Table 3-3 and Figure 3-9) offset 5.6 ± 1.0 m and a gully (feature 2-23(2) in Table 3-3 and Figure 3-9) offset 5.0 ± 0.7 m in Pilot Knob Valley.

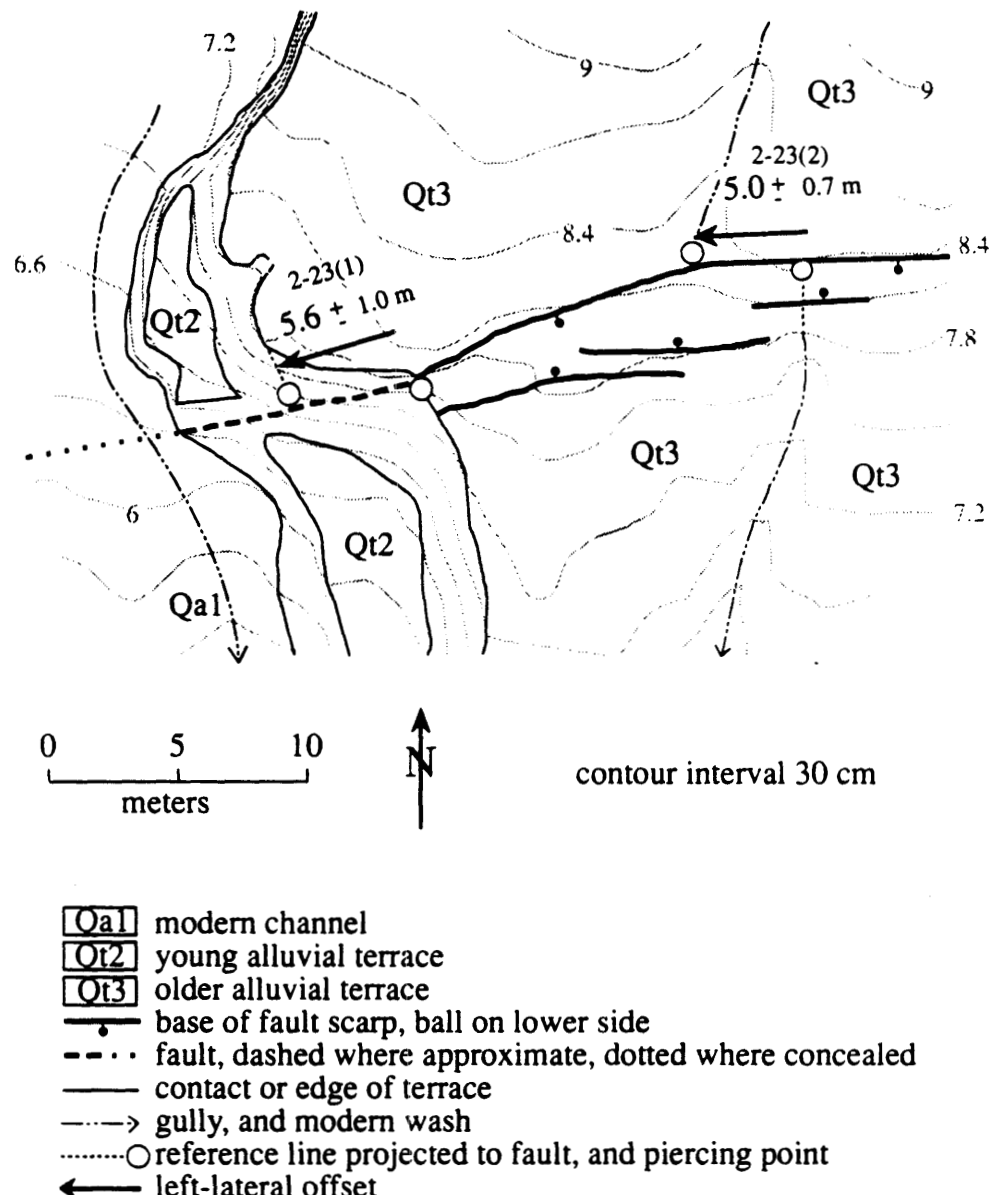


Figure 3-12

A small gully (feature 2-23(2)) incised into the Qt₃ terrace has also been offset left-laterally by about 5.0 ± 0.7 m. The correlation of this offset feature is good because there is no other possible source for the beheaded gully south of the fault. This feature and feature 2-23(1) probably were offset in the past two earthquakes, because features offset only about 3 m are located within a kilometer along strike of the fault.

The vertical separation of the Qt₃ terrace is 45-50 cm, north-side-up. Because the lateral offset of features cut into this terrace is only about 5 m here, and because the gradient of the Qt₃ surface is roughly perpendicular to the fault within 5 m from the places where vertical separation was measured, the vertical separation can be interpreted as true vertical displacement, rather than as vertical separation caused by lateral slip. Because the terrace riser and channel cut into this terrace have been offset in two past events, the 50 cm vertical displacement of this terrace probably also occurred in two events. Although the terrace is older than the terrace riser and channel that have been cut into it, no features on this terrace are offset more than 5.6 m left-laterally, so the terrace itself has probably experienced only two faulting events.

Leach Lake Area

Along a 0.5-km-long stretch of the fault located 4 km west of Leach Lake, south of the eastern Quail Mountains, four geomorphic features are offset 2.2 to 3.3 m and one feature is offset 5.8 m (Table 3-4 and Figures 3-13 and 3-14). I interpret the

TABLE 4. Geomorphic Offsets near Leach Lake and in the Avawatz Mountains

Feature	Distance (km)	Quality	Horizontal Offset (m)	Vertical Slip (m)	Description of offset feature
2-156(5)	118.24	fair	2.2 ± 0.5		west edge of debris flow
2-156(4)	118.40	poor	3.3 ± 0.5	0.30 N	west edge of debris flow
2-156(1)	118.44	good	2.3 ± 0.7	0.35 N	gully
2-156(2)	118.51	good	3.2 ± 0.7	0.40 N	gully
2-156(3)	118.57	poor	5.8 ± 1.2	0.60 N	west-facing terrace riser
E3-39(1)	133.81	poor	≥ 1.4		west-facing terrace riser
E3-39(2a)	134.10	good	≥ 1.9		west-facing terrace riser
E3-39(2b)	134.11	poor	2.3 ± 0.7		east edge of debris flow
E3-39(2c)	134.12	poor	2.5 ± 1.0	0.80 N	east-facing terrace riser
E3-41(1)	134.27	poor	5.3 ± 1.5		ridge
E3-41(2)	134.36	poor	4.8 ± 1.5		ridge
E3-43(1)	135.25	good	≥ 8.1		west wall of channel
E3-43(13)	135.61	poor	6.0 ± 1.0		west-facing terrace riser
E3-43(2)	135.80	good	3.5 ± 1.0	0.50 N	west-facing terrace riser
E3-43(3)	135.81	poor	2.5 ± 0.7	0.60 N	east edge of debris flow
E3-43(4b)	135.82	fair	2.6 ± 0.5	0.0	west edge of ridge
E3-43(4a)	135.83	fair	2.4 ± 0.5	0.0	east edge of ridge
E3-43(6)	135.84	fair	2.5 ± 0.6	0.30 S	east edge of debris flow
E3-43(7)	135.85	fair	2.4 ± 0.8	0.40 S	west wall of channel
E3-43(8)	135.86	fair	3.0 ± 0.5	0.40 S	east wall of channel
E3-43(9)	135.87	fair	2.3 ± 0.5		west edge of debris flow
E3-43(10)	135.89	poor	2.9 ± 0.5	0.20 S	west edge of gully
E3-43(11)	136.14	good	2.5 ± 0.5		gully
E3-45(9)	136.43	poor	3.2 ± 1.0		ridge
E3-45(8)	136.44	poor	2.4 ± 1.0		ridge
E3-45(7)	136.45	poor	4.0 ± 1.5		ridge
E3-45(6)	136.96	fair	2.6 ± 1.0		ridge
E3-45(1)	137.06	fair	2.9 ± 0.8	0.50 N	east wall of channel
E3-45(2)	137.09	good	3.2 ± 0.7	0.50 N	west wall of channel
E3-45(4)	137.11	fair	2.4 ± 0.8	0.40 N	gully
E3-45(5)	137.15	good	0.8 ± 0.5	0.10 N	east edge of debris flow
E3-47(1)	137.30	good	≥ 3.4	0.40 S	west wall of channel
E3-47(2)	137.32	good	3.2 ± 2.0		east wall of channel
E3-47(10)	137.52	fair	3.6 ± 1.0	0.40 S	east-facing terrace riser
E3-47(3)	137.61	poor	2.1 ± 1.0		ridge
E3-47(4)	137.81	fair	3.6 ± 1.0		west edge of ridge
E3-47(5)	137.88	poor	2.7 ± 1.5		east wall of channel
E3-47(6)	137.96	fair	2.7 ± 1.5	0.75 S	ridge
E3-47(8)	138.09	fair	2.6 ± 0.5		west wall of channel
E3-47(9)	138.11	poor	2.3 ± 1.0		ridge
E3-49(15)	138.22	fair	3.4 ± 1.0	0.50 S	gully

TABLE 4. (continued)

Feature	Distance (km)	Quality	Horizontal Offset (m)	Vertical Slip (m)	Description of offset feature
E3-49(14)	138.29	good	2.4 \pm 0.5 0.8	0.30 S	west-facing terrace riser
E3-49(13)	138.39	poor	3.0 \pm 1.0 1.3	S	west wall of channel
E3-49(12)	138.60	fair	\geq 1.9	S	west wall of channel
E3-49(11)	138.67	poor	7.3 \pm 1.0	S	debris flow
E3-49(10)	138.69	poor	6.2 \pm 1.0	S	debris flow
E3-49(9)	138.71	poor	3.5 \pm 1.0	S	east-facing terrace riser
E3-49(8)	138.72	poor	3.6 \pm 0.7	S	east-facing terrace riser
E3-49(1)	138.75	fair	\geq 1.5	>0.15 S	ridge
E3-49(2)	138.77	fair	3.8 \pm 0.7	0.25 N	east wall of channel
E3-49(3)	138.78	fair	5.2 \pm 1.0		ridge
E3-49(4)	138.80	fair	5.0 \pm 1.0		ridge
E3-49(5)	138.82	poor	5.0 \pm 1.0		ridge
E3-49(6)	138.84	poor	5.3 \pm 1.0		ridge
E3-49(7)	138.94	good	3.3 \pm 0.5	0.50 S	east-facing terrace riser
E3-51(1)	139.29	poor	4.6 \pm 0.5		west edge of ridge
E3-51(3)	139.31	good	3.6 \pm 1.0	0.0	old west wall of channel
E3-51(6)	139.41	good	3.6 \pm 0.7	0.60 S	east wall of channel
E3-51(7)	139.44	fair	3.1 \pm 0.8	0.60 S	east-facing terrace riser
E3-51(8)	139.51	fair	5.6 \pm 1.3		west edge of ridge
E3-51(9)	139.53	exc	\geq 1.9	0.0	east wall of channel
E3-51(10)	139.60	fair	5.4 \pm 0.5 2.8		west wall of channel
E3-51(11)	139.61	fair	4.6 \pm 1.8	0.0	east wall of channel
E3-51(13)	139.63	poor	2.2 \pm 1.0		east wall of channel
E3-51(14)	139.65	fair	3.0 \pm 0.5	0.50 S	gully
E3-51(14b)	139.66	poor	2.5 \pm 0.5	0.40 S	debris flow
E3-51(14c)	139.67	poor	3.5 \pm 0.5	0.40 S	debris flow
E3-51(15)	139.68	poor	2.8 \pm 1.0 1.5	0.50 S	west wall of channel
E3-51(16)	139.70	poor	2.2 \pm 0.5	0.40 S	west side of ridge
E3-51(17)	139.71	fair	3.6 \pm 0.6	0.40 S	east side of ridge
E3-51(18)	139.76	poor	5.3 \pm 0.8 2.3	S	west wall of channel
E3-51(19)	139.80	good	\geq 1.1		east wall of channel
E3-51(20)	140.02	fair	3.0 \pm 1.0		east side of ridge
E3-51(21)	140.05	poor	11.0 \pm 1.5		west wall of channel
E3-51(22)	140.06	fair	\geq 2.3		east wall of channel
E3-51(24)	140.08	poor	7.0 \pm 1.0		west wall of channel
E3-51(25)	140.12	fair	\geq 1.5	0.35 S	east wall of channel
E3-51(26)	140.14	fair	3.5 \pm 0.7	0.35 S	west wall of channel
E3-53(1)	140.19	fair	3.8 \pm 1.0	<0.20 N	east-facing terrace riser
E3-53(2)	140.31	fair	3.4 \pm 1.0	<0.10 N	west wall of channel
E3-53(3)	140.22	fair	2.5 \pm 0.5	0.35 S	east wall of channel
E3-53(5)	140.29	fair	4.7 \pm 1.6 0.7	0.50 N	east-facing terrace riser

TABLE 4. (continued)

Feature	Distance (km)	Quality	Horizontal Offset (m)	Vertical Slip (m)	Description of offset feature
E3-53(6)	140.31	fair	2.4 ± 1.3 0.5	0.35 N	west wall of channel
E3-53(7)	140.33	good	≥ 2.8	0.30 S	east wall of channel
E3-53(9)	140.84	poor	12.7 ± 1.0 4.0		ridge
E3-53(10)	140.87	fair	4.1 ± 1.5		ridge
E3-55(2)	141.46	fair	1.7 to 7.2		west wall of channel
E3-55(3)	141.69	poor	1.5 ± 1.0	S?	hillside
E3-67(1)	145.47	good	2.3 ± 0.5	0.20 N	east edge of gully
E3-67(2)	145.48	good	2.4 ± 1.0 0.5	0.20 N	east edge of gully
E3-67(5)	146.07	good	3.3 ± 2.8 0.8		gully
E3-69(6)	146.46	fair	6.0 ± 3.5		west wall of channel
E3-69(7)	146.52	fair	≥ 3.2		west wall of channel
E3-69(1)	146.84	good	2.8 ± 0.8		ridge
E3-71(4)	147.57	good	2.0 ± 1.0	0.13 S	east edge of debris flow
E3-71(1)	147.58	exc	2.7 ± 0.6	0.20 S	east-facing terrace riser
E3-71(2)	147.63	poor	1.8 ± 1.0		east-facing terrace riser
E3-71(5)	147.64	poor	3.0 ± 1.0		east wall of channel
E3-71(6)	147.66	fair	2.8 ± 2.0 1.0		west wall of channel
E3-71(3b)	147.73	good	4.6 ± 1.0 2.0	N?	east edge of alluvial fan
E3-71(7)	147.93	fair	3.0 ± 2.0		east wall of channel

Distances measured eastward along fault from Cantil. N, S indicate relative uplift of the north and south sides of the fault, respectively.

FIGURE 3-13: Displacement of 5 geomorphic features near Leach Lake and 96 features within the Avawatz Mountains (Table 3-4). Distance is measured along the fault, eastward from Cantil. The solid horizontal lines correspond to the center of the broad peak between 2 and 4 meters in Figure 3-14, and to the shoulder on the side of that peak, at about 5 m. These may represent the cumulative slip in the past one and two events, respectively. The dashed horizontal lines are drawn through smaller clusters of offsets of poorer quality. These may represent the cumulative slip in past 3 events (7.0 m) and the past 4 or 5 events (11.0 m). For features that may have been modified by erosion, arrows are plotted with their bases at the minimum offset.

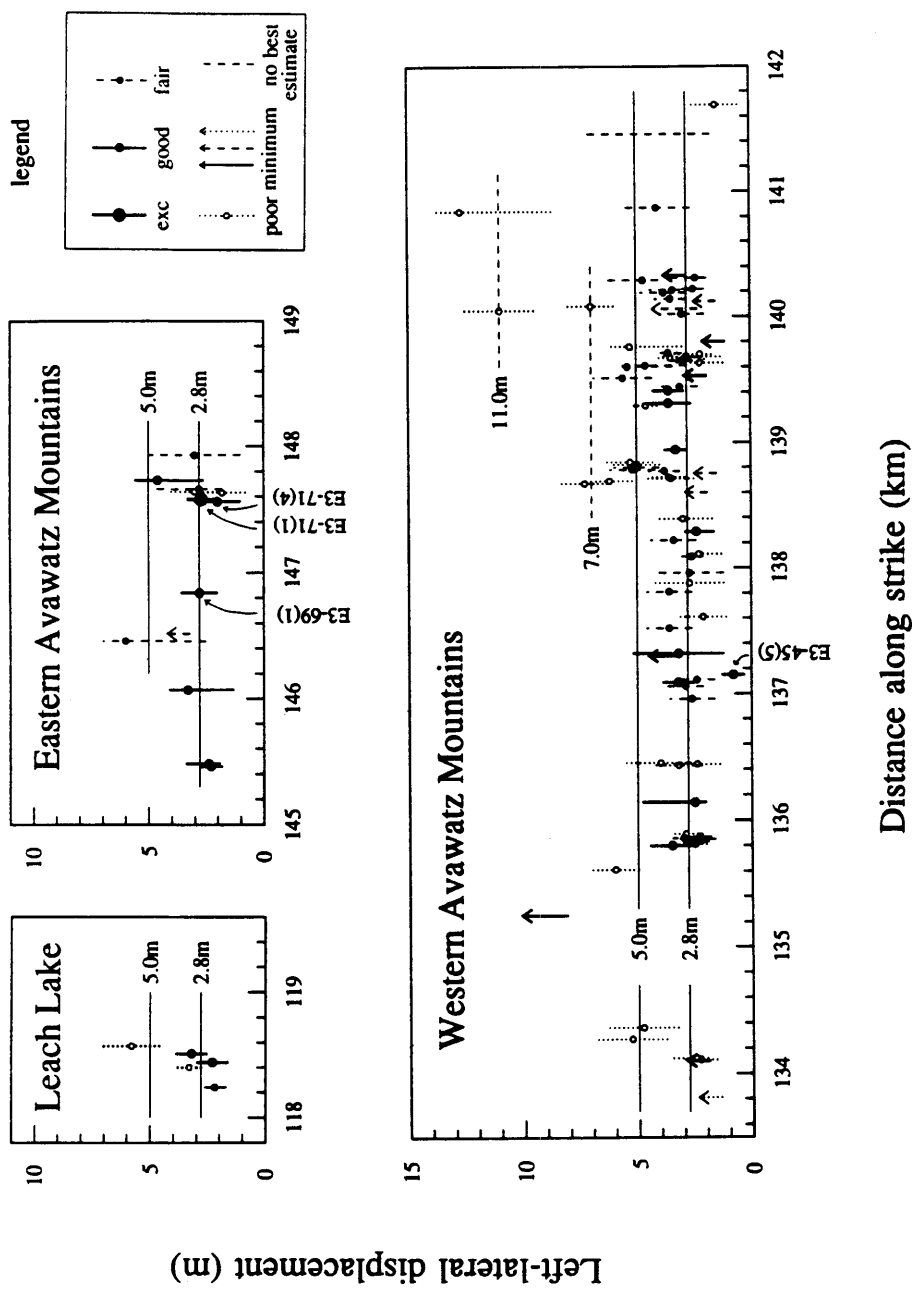


Figure 3-13

FIGURE 3-14: Summed Gaussian probability-density functions for 74 geomorphic offsets near Leach Lake and within the Avawatz Mountains (Table 3-4 and Figure 3-13). Shading indicates the quality of the offset estimates used. See caption of Figure 3-6 for explanation of the construction of this figure. The broad peak between 2 and 4 m probably represents the slip in the most recent event, while the shoulder on the side of this peak, at about 5.0 m, may represent the cumulative slip in the past two events.

Leach Lake and Avawatz Mountains

172

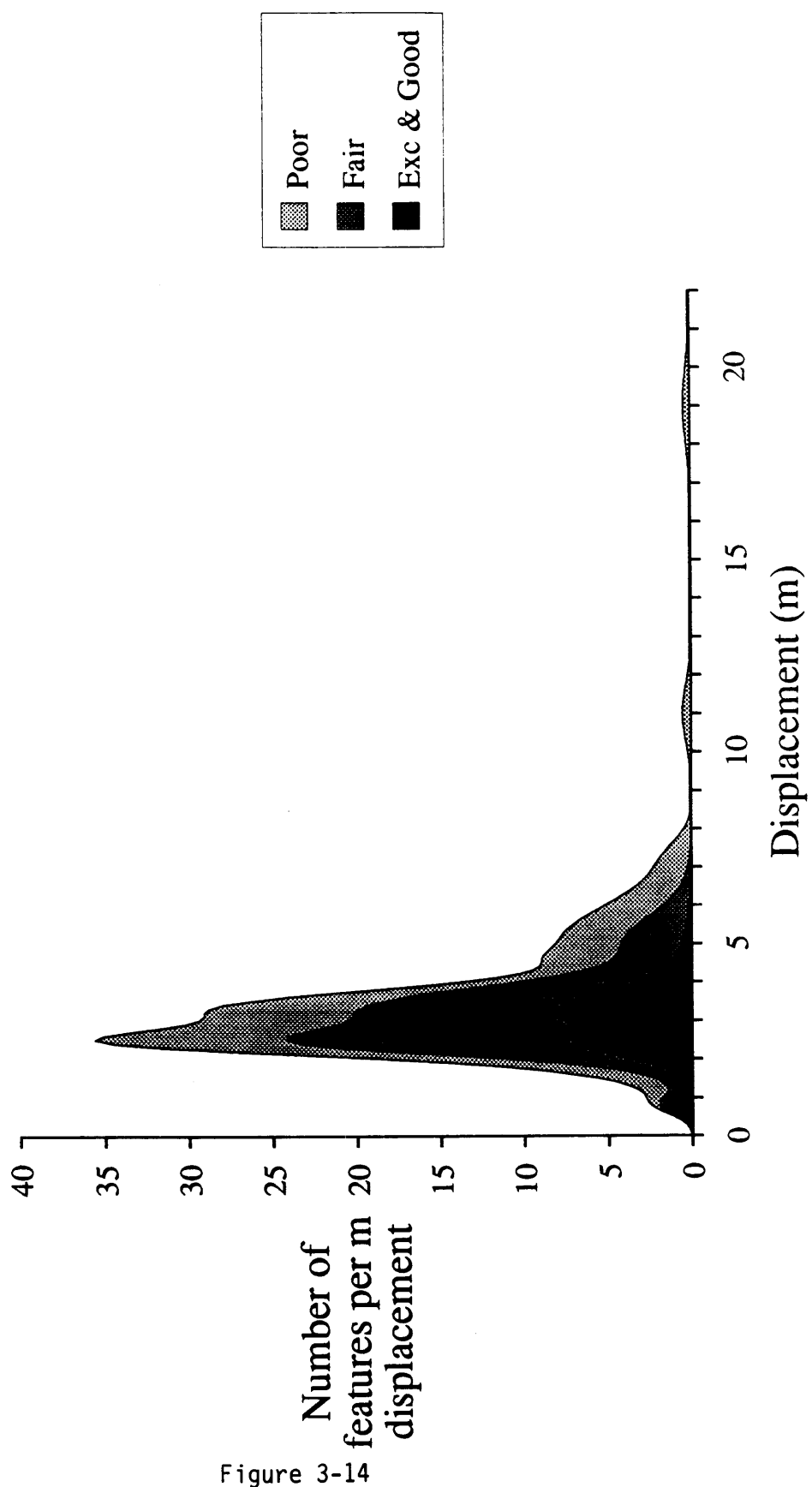


Figure 3-14

features offset 2.2 to 3.3 m to be from the most recent event only, while the feature offset 5.8 m was probably offset in the past two events. The vertical component of slip, where available, is consistently north-side-up and averages about 12% of the left-lateral component.

Avawatz Mountains

In this area, offsets were measured only along the Holocene trace of the fault, as mapped by Clark (1973). Other fault scarps in Quaternary deposits are present within a zone up to 5-km wide spanning the Holocene fault trace (Brady, 1986), but none of these faults displaces alluvium as young-looking as that displaced by the Holocene fault trace.

Within the Avawatz Mountains, 64 geomorphic features are offset 0.8 to 4.1 m across the Garlock fault (Table 3-4, and Figures 3-13 and 3-14). I interpret these features to have been offset in the most recent event. I interpret the average amount of slip associated with this event to be 2.8 m, the value at the center of the broad peak in Figure 3-14. Eighteen features, of generally poorer quality, are offset 4.6 to 7.3 m, and may represent the cumulative slip of the past two large earthquakes. The average cumulative slip for the past two events is probably about 5.0 m, the value at the center of the shoulder on the side of the large, broad peak on Figure 3-14. A few features of poor quality are offset larger amounts (about 7 m, and 11 m), presumably recording the slip associated with a greater number of past earthquakes.

This interpretation requires substantial variability along strike of the amount

of slip in the latest earthquake. Except for feature E3-45(5) (discussed below), however, the degree of variability required is nowhere greater than that exhibited by some historical, strike-slip earthquakes (e.g., the 1968 Dasht-e Bayaz earthquake in Iran, Ambrasseys and Tchalenko, 1969). An alternate interpretation is that the most recent event averaged about 2 m slip and that the past two events combined averaged about 3.5 m of left-lateral slip. The uncertainties in the offset measurements could have caused the peaks from these two hypothetical events to merge into the single, broad peak between about 2 and 4 m in Figure 3-14.

Along the northern flank of the Avawatz Mountains, the vertical displacement of geomorphic features on the Garlock fault is about 13% of the left-lateral offset, but the sense of vertical slip varies along strike (Table 3-4).

Features E3-69(1), E3-71(1) and E3-71(4):

A ridge offset 2.8 ± 0.8 m (feature E3-69(1)) is pictured in Figure 3-15. Feature E3-71(1) (Figure 3-16) is a terrace riser between a faulted terrace (Qt_6) and two lower, unfaulted terraces (Qt_5 and Qt_4). The riser is offset 2.7 ± 0.6 m left-laterally. The terrace riser is well defined and extends close to the fault, where it is offset across a well-defined fault trace. Several lower, unfaulted terraces have protected the offset terrace riser from erosion by the modern channel. For these reasons this offset feature has an excellent rating. The terrace just west of the offset terrace riser is vertically displaced with the south side raised about 20 cm above the north side.

FIGURE 3-15: Ridge (feature E3-69(1) in Table 3-4 and Figure 3-13) offset 2.8 ± 0.8 m from the person to the backpack, across the eastern Garlock fault in the Avawatz Mountains. White arrows indicate location of fault.

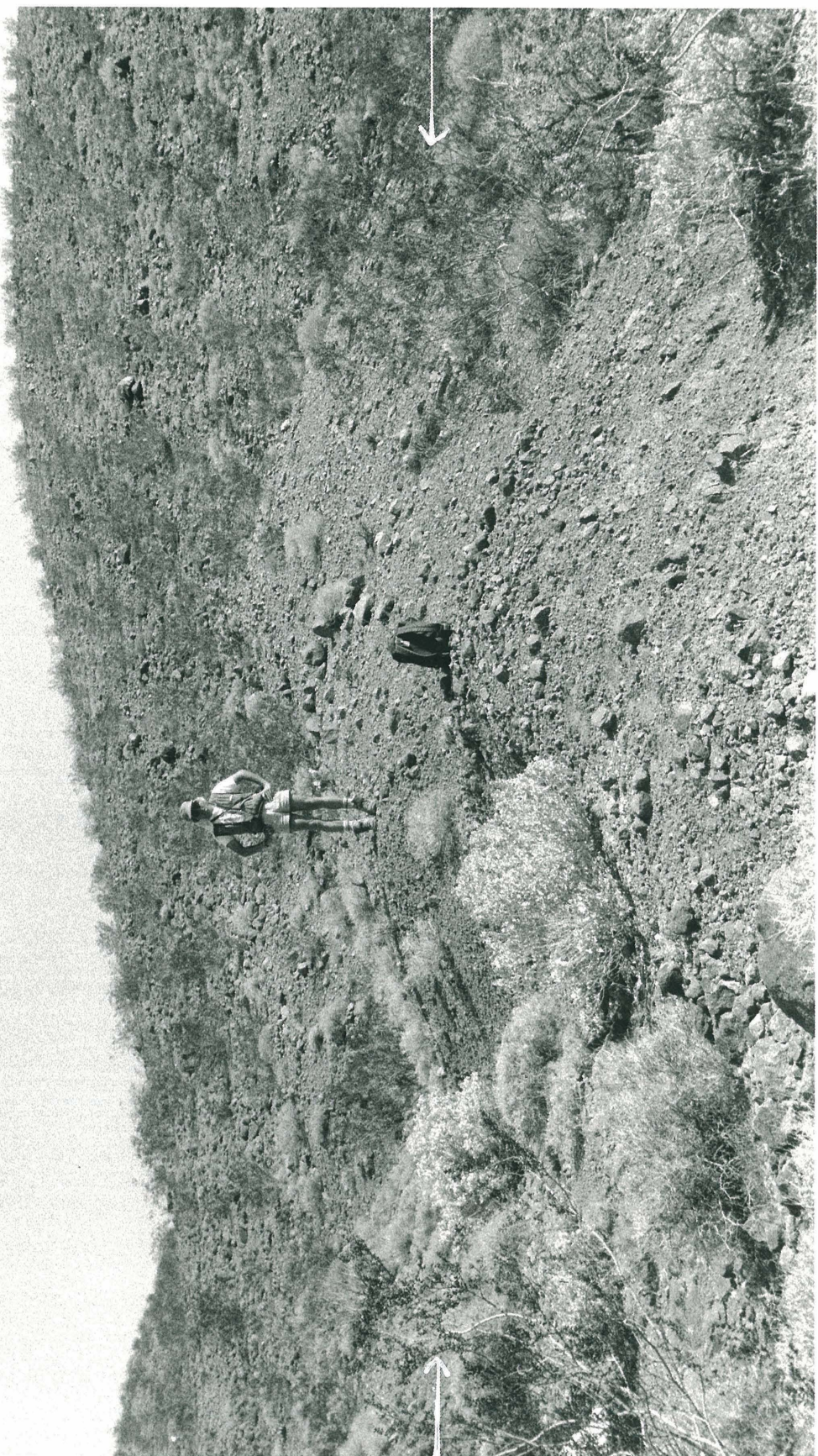
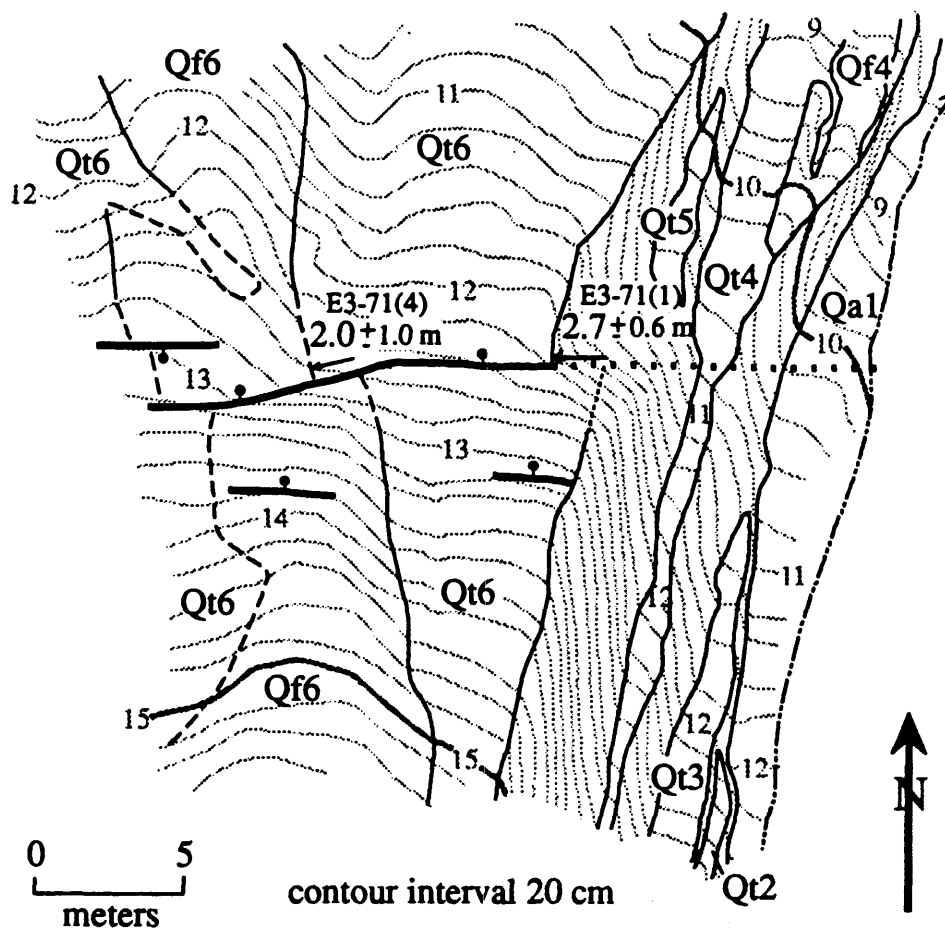


Figure 3-15

FIGURE 3-16: Topographic map of an offset terrace riser (feature E3-71(1) in Table 3-4 and Figure 3-13) and an offset debris flow (feature E3-71(4) in Table 3-4 and Figure 3-13). The terrace riser between terrace Qt_6 and terraces Qt_4 and Qt_5 is offset 2.7 ± 0.6 m. The debris flow labelled Qf_6 has been offset 2.0 ± 1.0 m.



Qa1	modern wash	— — contact, or edge of terrace,
Qt2,Qt3	unfaulted alluvial terraces	dashed where approximate
Qf4	unfaulted debris flow	—·— fault, dotted where concealed
Qt4,Qt5	unfaulted alluvial terraces	—·—> modern wash
Qf6	offset debris flow	······ edge of terrace projected to fault
Qt6	faulted alluvial terrace	← left-lateral offset

Figure 3-16

A debris flow (feature E3-71(4) and Qf₆ in Figure 3-16) on the surface of the Qt₆ terrace is also faulted. The debris flow is evident as a north-south-trending bulge in the contour lines. In the field, the debris flow can also be identified by the abundance of cobbles on it, relative to the remainder of the terrace. The east edge of the debris flow is offset 2.0 ± 1.0 m left-laterally. Displacement of the west edge of the debris flow is consistent with this amount of offset, but it is not as well defined. The crest of the debris flow is displaced about 15 cm vertically, with the south side up.

Feature E3-45(5):

Feature E3-45(5) (Figure 3-13) is problematic. This feature is a cobbly debris flow that is offset only 0.8 ± 0.5 m, much less than the other offset features within the Avawatz Mountains that I have attributed to the latest slip event. To interpret both the 0.8 m offset and the 2 to 4 m offsets as having formed in the latest event requires a large degree of variability in slip along strike, because features offset about 3 m are located only about 60 m west of and 150 m east of feature E3-45(5). Slip gradients during the 1968 Dasht-e Bayaz earthquake were almost this extreme (Ambrasseys and Tchalenko, 1969), suggesting that this amount of variability may not be impossible.

I offer below three alternate explanations for the anomalously small offset of feature E3-45(5), but I find these less satisfactory than the explanation offered above.

- (1) The debris flow may not span the entire width of the rupture zone of the latest

earthquake and thus may record only a part of the slip associated with that event. In the vicinity of feature E3-45(5), there is a secondary fault strand that the debris flow does not cross. However, this fault strand offsets only alluvium that is much older than the debris flow; there is no evidence that slip occurred on this secondary fault strand in the most recent event. (2) The latest earthquake on the Garlock fault within the Avawatz Mountains may have been produced by only about 0.8 m of left-lateral slip, and the features offset 2 to 4 m may record the slip associated with more than one event. It would be extremely unusual, however, for only one geomorphic feature to record the slip in the most recent event and for 64 features to record the slip in the past two events. Considering the large number of channels that have incised since the latest slip event, it is nearly inconceivable that only a few channels would have incised between the penultimate event and the most recent event, unless those two events were very closely spaced in time (e.g., separated by only a few decades or less). (3) The debris flow may have been deposited within days or weeks after the latest earthquake and may then have been offset 0.8 m by post-seismic slip. Post-seismic slip exceeding 50% of the total slip has been recorded on faults in the Imperial Valley (Sharp and others, 1982), but the large amounts of post-seismic slip may be a result of an extremely thick layer of sediments above the basement. The presence of bedrock outcrops on either side of the fault near E3-45(5) indicates that the sediment thickness on the north flank of the Avawatz Mountains is not nearly as thick as it is in the Imperial Valley, making large amounts of post-seismic slip less likely.

DISCUSSION

The geomorphic offsets presented in the previous section suggest that the most recent large earthquake along the easternmost 90 km of the Garlock fault (from Searles Valley to the eastern end of the fault) was produced by an average of about 2-3 m of left-lateral slip. The offsets in Pilot Knob Valley also suggest that each of the past six slip events along this part of the fault has involved 2-4 m of left-lateral slip. Along the southern flank of El Paso Mountains, on the other hand, there is no clear evidence for slip events as small as 3 m. Rather, it appears that slip on this part of the fault may have been about 7 m in the two most recent events and may have been about 4 m in the third event back. However, smaller amounts of slip per event along this part of the fault can not be ruled out. In the following sections I use these estimates of the amount of left-lateral displacement in past events to address the likely rupture lengths, magnitudes and frequency of large earthquakes produced by the Garlock fault.

Segmentation of the Garlock fault

For the purpose of seismic-hazard analysis it would be helpful to know if large earthquakes on the Garlock fault rupture the entire fault in a single event, or if shorter segments of the fault fail separately. Few dates for individual faulting events on the Garlock fault are available, so indirect methods must be used to address this question. I show below that whereas it is apparently more likely that shorter

segments of the Garlock fault will fail separately, rupture of the entire fault in a single event is nevertheless quite plausible.

Using Bonilla and others' (1984) ordinary least-squares regression of rupture length on displacement for 22 strike-slip events, the most likely rupture length for an event with a maximum of 7 m displacement (the estimated displacement in the latest event south of El Paso Mountains) is 110 km. This regression suggests that the earthquake associated with the 7-m offsets south of El Paso Mountains did not rupture the entire 245-km length of the fault. The variance in rupture lengths of historical earthquakes for a given displacement is large, however. Using the *t* distribution, the one-sided, 95% confidence limit on the maximum rupture length associated with a 7 m displacement is 490 km (Mark, 1977). Thus, it is quite possible that a slip event with a maximum displacement of 7 m could involve rupture of a 245-km fault length. In fact, there are several examples of historical, strike-slip earthquakes with maximum displacements of 7 m or less and rupture lengths of 245 km or greater. For example, the 1906 earthquake on the northern San Andreas fault has a rupture length of 435 km and a maximum displacement of 6.4 m (Lawson, 1908), and the 1976 Motagua earthquake in Guatemala had a rupture length of 230 km and a maximum displacement of only 3.3 m (Bucknam and others, 1978). Other examples are the 1939 Erzincan earthquake and the 1943 Tosya earthquake, both on the North Anatolian fault in Turkey. The former event had a rupture length of 360 km and a maximum left-lateral displacement of about 7 m, and the latter event had a rupture length of 260 km and a maximum displacement of about 4 m (Aykut

Barka, written comm., 1990).

The following observations also suggest that both rupture of the entire Garlock fault and separate rupture of segments of the fault are plausible. Previous studies indicate that earthquake epicenters and rupture endpoints for strike-slip earthquakes frequently coincide with bends or jogs in the surface trace of the fault (Aki, 1987; Barka and Kadinsky-Cade, 1988; King and Nabalek, 1985; Knuepfer and others, 1987; Sibson, 1985). Thus, one might expect the 3.5-km-wide dilational step-over in the Garlock fault at Koehn Lake to arrest ruptures, causing the segments west and east of this step-over to fail separately. Some surface ruptures associated with historical strike-slip earthquakes have apparently been arrested by such fault jogs. For example, the rupture associated with the 1943 Tosya earthquake ($M_s = 7.3$, rupture length = 260 km) on the North Anatolian fault in Turkey terminated to the east and west at a series of 1.5- to 2-km-wide and smaller dilational fault jogs (Barka and Kadinsky-Cade, 1988). On the other hand, the rupture associated with the 1939 Erzincan earthquake ($M_s = 8$; rupture length = 360 km), also on the North Anatolian fault, propagated through a 4-km-wide releasing double bend at Susehri (Barka and Kadinsky-Cade, 1988). Thus, on the basis of historical earthquake rupture patterns, both termination of a rupture at the Koehn Lake dilational fault jog and propagation of ruptures through that jog must be regarded as plausible. The resolution of this question awaits direct, precise dating of recent offsets both east and west of the Koehn Lake step-over, or the occurrence of the next large event on the Garlock fault.

In addition to the two plausible rupture patterns outlined above (rupture of the entire fault in a single event [Figure 3-17a], and separate rupture of the segments east and west of the Koehn Lake step-over [Figure 3-17b and 3-17c]), I now investigate the possibility of further segmentation of the part of the fault east of Koehn Lake. (Evaluating the possibility of further segmentation of the western Garlock fault is beyond the scope of this paper, because I have no measurements of geomorphic offsets from that part of the fault.) Another prominent discontinuity in the Garlock fault that may be capable of arresting seismic ruptures lies in the Quail Mountains. In this region, there is a 0.7-km-wide convergent fault jog and a 3-km-long area (parallel to fault strike) in which there are no recent fault scarps (Clark, 1973). A 15-degree bend in the fault is also present nearby. Furthermore, two Quaternary faults, the right-lateral Brown Mountain fault and the left-lateral-oblique-slip Owl Lake fault, intersect the Garlock fault here (Figure 3-1). Each of these features may impede rupture propagation (Aki, 1987; King and Nabalek, 1985; Knuepfer and others, 1987).

In addition, for 13 km east of this area, the most recent fault breaks on the Garlock fault appear substantially older than the most recent fault breaks elsewhere along the central and eastern Garlock fault, on the basis of aerial photo observations of scarp preservation and on the degree of incision of and rock varnish formation on the youngest faulted surfaces. This suggests that the most recent ruptures east and west of this 13-km-long stretch may have occurred separately rather than were part of a single rupture extending for the entire length of the central and eastern Garlock

FIGURE 3-17: Some possible rupture patterns for the Garlock fault and the associated earthquake magnitudes. Letters correspond to rupture patterns in Table 3-5. Portions of the fault assumed to rupture in each case are shown in bold. Magnitudes are probably uncertain by \pm 0.1 to 0.2.

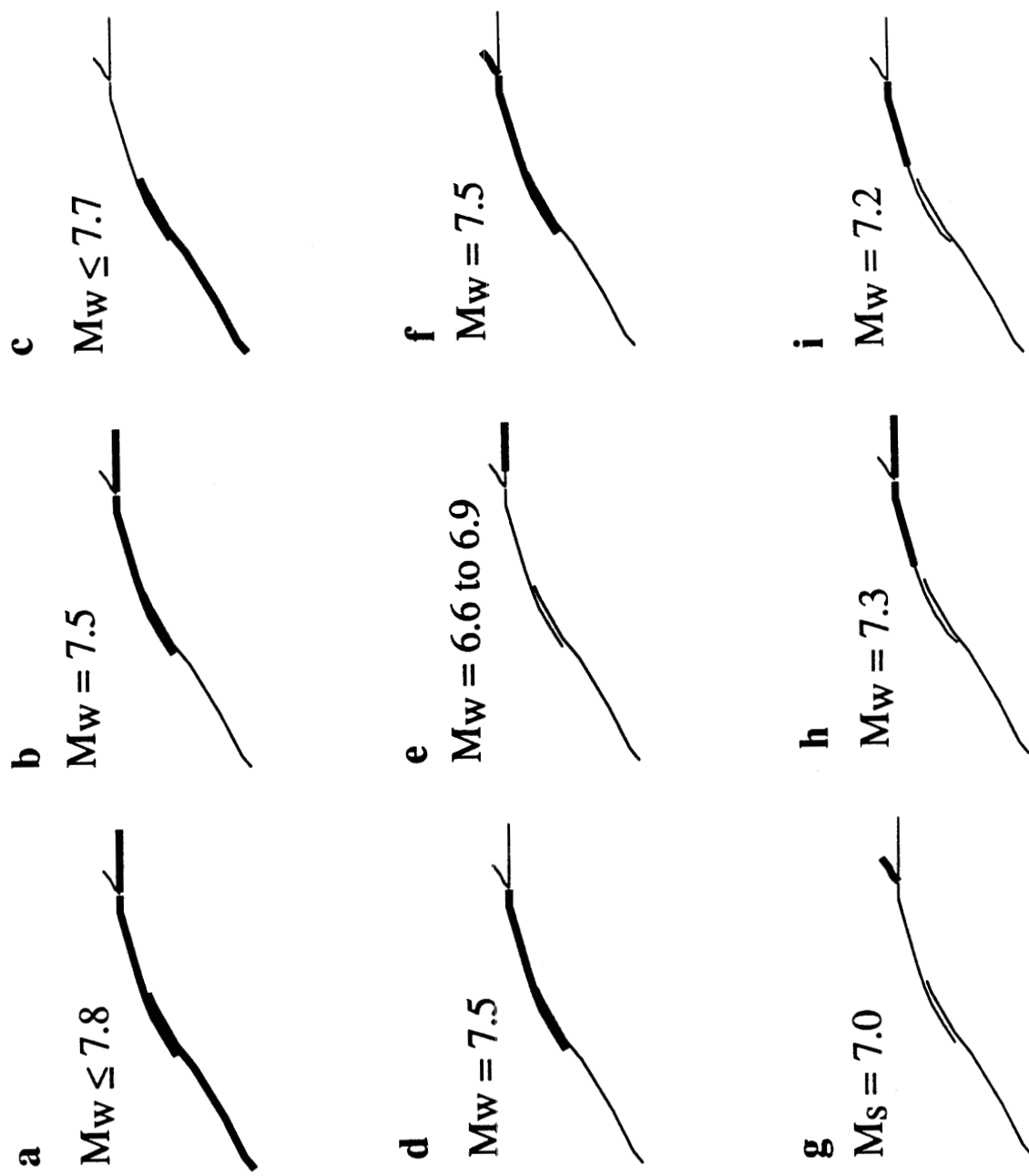


Figure 3-17

fault. Also consistent with this hypothesis are the presence of two, east-facing fault scarps (identified on aerial photos) extending at least 0.6 km north from the easternmost recent breaks along the Pilot Knob Valley segment of the Garlock fault. These may be secondary faults related to rupture termination in this vicinity. For example, they may be normal faults associated with westward movement of the block north of the Garlock fault and west of the Quail Mountains discontinuity. The observations mentioned above are suggestive of separate rupture of the segments east and west of the Quail Mountains discontinuity (Figure 3-17d and 3-17e), but this hypothesis must be tested by further field studies.

The rupture lengths implied by the proposed segmentation of the fault at the Quail Mountains discontinuity are comparable to the rupture lengths of historical strike-slip earthquakes with similar displacements. The 105-km length from Cantil (within the Koehn Lake basin, at the western end of the central Garlock fault) to the intersection of the Garlock fault with the Owl Lake fault is close to the most likely rupture length (110 km) for an earthquake with a maximum displacement of 7 m (the inferred slip during the most recent event south of El Paso Mountains). The 30-km length from a point 5 km west of Leach Lake (the eastern end of the 13-km-long segment lacking evidence for very recent offset) to the eastern end of the fault is less than the most likely rupture length (67 km) for earthquakes with 2.8 m of slip (the inferred slip in the most recent event at Leach Lake and in the Avawatz Mountains), but is still within the range of plausible rupture lengths for a 3 m displacement. For example, the 1930 Izu earthquake in Japan was associated with 3.5 m of lateral slip

and had a rupture length of 24 km (Bonilla and others, 1984). In addition, the 1970 Tonghai (China) earthquake was produced by 2.7 m of lateral slip on a 47-km-long rupture (Bonilla and others, 1984).

Another intriguing observation is that the most recent fault breaks along the Owl Lake fault appear to be younger than the most recent breaks along the 13-km-long stretch of the Garlock fault that is just east of the proposed segmentation point in the Quail Mountains (based on aerial photo observation, as above). Field observations by Malcolm Clark (written communication, 1990) also confirm this observation. This raises the possibility that the most recent rupture along the Garlock fault in Pilot Knob Valley may also have extended along the Owl Lake fault rather than continued along the Garlock fault east of the discontinuity in the Quail Mountains (Figure 3-17f). The southwesternmost recent fault breaks on the Owl Lake fault actually lie closer to the easternmost recent fault breaks on the Garlock fault in Pilot Knob Valley than do the westernmost recent fault breaks on the Garlock fault west of Leach Lake (Clark, 1973). This suggests that the Owl Lake fault may be part of the Garlock fault system. It is interesting to note that all evidence for Holocene left-lateral slip on the Owl Lake fault lies directly north of the 13-km-long stretch of the Garlock fault that appears to have ruptured less recently than other segments of the central and eastern Garlock fault. Farther northeast, the Owl Lake fault has only a dip-slip component of Holocene movement (Clark, 1973). These observations suggest the hypothesis (which has yet to be tested) that the 13-km-long stretch of the Garlock fault just east of the Quail Mountains discontinuity

has been inactive during the past few earthquake cycles, and that left-lateral shear has been accommodated on the Owl Lake fault rather than on this portion of the Garlock fault.

The apparent decrease in slip per earthquake between Highway 395 and Searles Valley also suggests the possibility that some ruptures on the Garlock fault may terminate between these two localities. If the slip rate on the Garlock fault is constant along strike, then earthquakes on the easternmost 90 km of the fault would have to occur roughly twice as frequently as along the southern flank of El Paso Mountains. For example, earthquakes rupturing the entire length of both the central and eastern segments with about 7 m slip south of El Paso Mountains and with about 3 m slip from Searles Valley to the eastern end of the fault, might alternate with earthquakes rupturing only from Searles Valley eastward with about 3 m of slip (Figure 3-17h,i). Alternatively, the decrease in slip per event between Highway 395 and Searles Valley may be due (at least in part) to a decrease in the slip rate between these two areas.

Several plausible rupture patterns for the Garlock fault have been delineated above, ranging from rupture of the entire fault in a single event to separate rupture of segments as short as 30 km. It is important to note that the Garlock fault need not always rupture in the same manner. Some events may rupture the entire Garlock fault, whereas other events may rupture individual segments separately. Furthermore, the segments that rupture separately may not always have the same endpoints (Rundle, 1988, his Figure 6).

Probable sizes of earthquakes produced by the Garlock fault

Using the various rupture patterns discussed in the preceding section, the probable moment-magnitudes of earthquakes generated by the Garlock fault may be estimated from the relations $M_o = \mu As$ (Brune, 1968) and $M_w = 0.667 \log M_o - 10.7$ (Hanks and Kanamori, 1979), where M_o is the seismic moment, $\mu = 3 \times 10^{11}$ dyne-cm⁻² is the rigidity, A is the area of the fault rupture and s is the average fault displacement for a given earthquake (Table 3-5). These magnitudes range from $M_w = 6.6$ to $M_w = 7.8$. Given the uncertainties in displacement, rupture length and depth of faulting, the magnitudes are probably uncertain by ± 0.1 to 0.2. Some of the uncertainties are discussed in the following paragraphs.

In calculating the magnitudes, I assume that large earthquakes on the Garlock fault rupture to a depth comparable to the maximum depth of current microseismicity on and near the fault (Sibson, 1984). This depth is about 13 km for the part of the fault from the El Paso Mountains southwestward and about 10 km for the part of the fault east of El Paso Mountains (U.S.G.S./Caltech southern California network catalog). Both earthquakes and seismic stations are sparse east of El Paso Mountains, however, so the maximum depth of faulting is very poorly constrained in this area.

The magnitudes given in Table 3-5 use 7 m of displacement for each event on the portion of the central Garlock fault between Cantil and Trona Road. Some events on this part of the fault may only involve about 4 m of slip, but this reduces the moment generated by this portion of the fault by less than a factor of two, and

Table 5. Possible rupture patterns
and associated earthquake magnitudes

rupture pattern	fault segments ruptured simultaneously	rupture length (km)	depth (km)	slip (m)	M_{o25} (10^{25} dyne-cm)	M_w
A. Entire Garlock fault	Castac Lake to Cantil	100	13	≤ 10	≤ 390	
	Cantil to Trona Rd	39	13	7	106	
	Trona Rd to E end of flt	109	10	3	98	
					≤ 594	≤ 7.8
B. Central and Eastern Garlock Garlock fault	Cantil to Trona Rd	39	13	7	106	
	Trona Rd to E end of flt	109	10	3	98	
					$\overline{204}$	7.5
C. Western Garlock fault	Castac Lake to Cantil	100	13	≤ 10	≤ 390	≤ 7.7
D. Central Garlock fault	Cantil to Trona Rd	39	13	7	106	
	Trona Rd to Quail Mtns	66	10	3	59	
					$\overline{165}$	7.5
E1. Easternmost 30 km of fault	5 km W of Leach L to E end of Garlock flt	30	10	3	27	6.9
E2. Easternmost 30 km of fault	5 km W of Leach L to E end of Garlock flt	30	10	1	9	6.6
F. Central Garlock fault and Owl Lake fault	Cantil to Trona Rd	39	13	7	106	
	Trona Rd to Quail Mtns	66	10	3	59	
	SW half of Owl Lake flt	11	10	3	10	
	NE half of Owl Lake flt	8	10	1	2	
					$\overline{177}$	7.5
G. Owl Lake fault only	Owl Lake fault	19	--	--	--	7.0*

Table 5. (continued)

rupture pattern	fault segments ruptured simultaneously	rupture length (km)	depth (km)	slip (m)	M_s^{25} (10^{25} dyne-cm)	M_w
H. Trona Rd to E end of Garlock	Trona Rd to E end of flt	109	10	3	98	7.3
I. Trona Rd to	Trona Rd to Quail Mtns	66	10	3	59	7.2

* Magnitude (M_s) calculated from an empirical relation between rupture length and magnitude (Bonilla and others, 1984).

the resulting magnitudes are reduced by only 0.1 or less. The choice of Trona Road as the point at which slip for each event changes from 7 m to 3 m is arbitrary, but is based on the presence of a 5° bend in the fault several km east of Trona Road.

I have no data regarding the amount of slip for each event on the western Garlock fault. Guptill and others (1979) report a few gullies offset in increments of about 10 m in Bear Trap Canyon, but a significant fraction of these displacements may be due to aseismic creep. Left-lateral creep at rates of 1.7 ± 0.5 mm/yr (Snay and Cline, 1980) and 6 to 8 mm/yr (Rodgers, 1979, p.62) has been measured along the Garlock fault in Bear Trap Canyon, and a similar creep rate has been measured a few tens of km northeast along the fault (Louie and others, 1985). On the other hand, four U.S.G.S. quadrilaterals have not recorded any aseismic creep along this part of the fault. Estimates of the long-term slip rate of the western Garlock fault range from 1.6 to 3.3 mm/yr (LaViolette and others, 1980) to 11 ± 2 mm/yr (Eberhart-Phillips and others, 1990). Thus, anywhere from 0% to 100% of the 10-m offsets in Bear Trap Canyon may be due to aseismic creep. To estimate the maximum magnitude earthquake likely to be generated by the Garlock fault, I assume that the 10-m displacements measured by Guptill and others (1979) were generated by seismic slip during a single earthquake. I emphasize, however, that this is the maximum amount of slip per event that is plausible for this part of the fault. The average slip per event may be substantially lower.

I also have no data on the amount of slip per event on the Owl Lake fault. For preparation of Table 3-5, I assume that if the Owl Lake fault ruptures simultaneously

with the Garlock fault segment from Cantil to the Quail Mountains, the slip per event on the southwestern Owl Lake fault will be 3 m, consistent with the documented slip per event in Pilot Knob Valley. Because there is no evidence of lateral offset on the northeastern Owl Lake fault (Clark, 1973), I assume 1 m of dip slip per event for the northeastern Owl Lake fault, for lack of a better estimate. For the case in which the Owl Lake fault ruptures alone, I use the length of the fault and an empirical relation between fault length and earthquake magnitude for strike-slip faults (Bonilla and others, 1984) to calculate the magnitude shown in Table 3-5. This may slightly overestimate the magnitude of future events on the Owl Lake fault, however, if the rupture lengths for several of the early historic earthquakes used in the empirical relation were underestimated.

It is interesting to note that the $M \approx 6$ earthquake that occurred near the eastern end of the Garlock fault in 1916 (Slemmons and others, 1965; Toppozada and others, 1978; see also Chapter 1 of this dissertation) was probably not large enough to be related to the geomorphic offsets near Leach Lake and in the Avawatz Mountains. Even if the most recent offset along this part of the fault was only about 1 m (as one interpretation of feature E3-45(5) might suggest), the resulting earthquake would probably have been around $M_w = 6.6$ (see Table 3-5, rupture pattern E2), larger than the 1916 event. The 1916 earthquake was also smaller than the most probable size for the length of the Owl Lake fault (Table 3-5, rupture pattern G).

Recurrence Interval

In conjunction with the slip rate, the mean amount of slip in past earthquakes may be used to estimate the average recurrence interval for large earthquakes on the Garlock fault. For the El Paso Mountains section of the fault, I use Clark and Lajoie's (1974) 7 ± 1 mm/ ^{14}C -yr slip rate. This rate is based on the 80 ± 5 -m offset of a bar of Koehn Lake with a ^{14}C -age of 11-15 ka (Clark and others, 1984). Although Carter (1980, 1982) reports an 11-12 mm/yr minimum slip rate for the portion of the fault near El Paso Mountains, that rate is poorly constrained (Clark and others, 1984), and could be consistent with Clark and Lajoie's (1974) rate. Carter's (1980, 1982) rate is based on the 16-20 km offset of alluvial fan gravels south of the fault from their source in El Paso Mountains, north of the fault. An *Equus* fossil was collected from beneath gravels in the source area north of the fault (David Whistler, oral communication, 1991). If the offset gravels are the same age as those overlying the fossil, then a minimum of 16 km of left-lateral slip has occurred since about 2.5 m.y., the age of the first appearance of the genus *Equus* (David Whistler, oral communication, 1991). This yields a minimum slip rate of about 6.4 mm/yr, which is consistent with Clark and Lajoie's rate.

Recent comparison of the ^{14}C timescale with the U-Th timescale, however, suggests that ^{14}C dates in the range of 10,000 to 15,000 ^{14}C -yr may be 2000-3000 yr too young (Bard and others, 1990). This suggests that the Garlock-fault slip rate in the vicinity of El Paso Mountains may be 4-7 mm/yr, slightly lower than the 5-8 mm/ ^{14}C -yr rate reported by Clark and others, 1984). Using the preliminary,

calibrated slip rate, the average recurrence interval for large earthquakes on the Garlock fault near El Paso Mountains is 600-1200 yr (Table 3-6). The calibration of the late Pleistocene portion of the radiocarbon timescale is preliminary, however, and the recurrence intervals reported in Table 3-6 may change slightly as the calibration is refined.

For the portion of the fault in Searles Valley, I use the 4.9-10.6 mm/ $^{14}\text{C-yr}$ slip rate determined from an offset shoreline of Searles Lake (Chapter 2 of this dissertation). If the calibration of Bard and others is correct, this corresponds to a preliminary, calibrated slip rate of 4-9 mm/yr. Smith (1975, and an unpublished field guide) estimates a slip rate of about 1 mm/yr for the Garlock fault in Searles Valley on the basis of the 8-m offset of a channel cut into ~10,000-yr old lake gravels near Christmas Canyon. I regard this rate as a minimum, however, because the channel may have incised long after deposition of the lake gravels. Using the 4-9 mm/yr slip rate, the average recurrence interval for large earthquakes in Searles Valley is 200-750 yr (Table 3-6).

Unfortunately, no slip-rate estimates are available for the Garlock fault east of Searles Valley. As an upper bound, I assume that the 9 mm/yr (calibrated) maximum rate in Searles Valley is valid for the length of the fault east of Searles Valley. As a lower bound, I consider the slip rates of faults north of the Garlock fault and the implications these might have for an eastward-decreasing slip rate along the Garlock fault. If left-lateral slip on the Garlock fault accommodates extension north of the fault, as proposed by Davis and Burchfiel (1973), then the slip rate

TABLE 6. Estimated Recurrence Intervals for Portions
of the Central and Eastern Garlock fault

fault section	displacement per event (m)	preliminary, calibrated slip rate (mm/yr)	Recurrence Interval (yr)
El Paso Mountains	4-7	4-7	600-1200
Searles Valley	2-3	4-9	200-750
Pilot Knob Valley	2-4	3-9	200-1300
Leach Lake and Avawatz Mountains	2-3	1-9	200-3000

would increase westward from a point of zero slip at the eastern termination of the fault, with each normal fault north of the Garlock fault adding an additional increment of left-lateral slip. This would lead to lower slip rates and longer recurrence intervals eastward along the fault.

The current knowledge of slip rates for faults north of the Garlock fault indicates that a westward-increasing slip rate for the Garlock fault is plausible but precludes precise determinations of the Garlock-fault slip rate at any point. In the following paragraphs I estimate the minimum slip rate for the Garlock fault in Pilot Knob Valley, near Leach Lake and in the Avawatz Mountains.

The Tank Canyon fault, a normal fault at the base of the west side of the Slate Range probably slips at 0.5-1.6 mm/yr in a westerly direction (Smith and others, 1968; Clark and others, 1984). Triangular facets on the southwest corner of the Slate Range that may be related to the Tank Canyon fault project to the Garlock fault a few km *east* of the offset shoreline from which the 4-9 mm/yr slip rate was determined. This suggests that the slip rate of the Garlock fault in Pilot Knob Valley may be about 1 mm/yr less than the 4-9 mm/yr rate in Searles Valley. I use 3 mm/yr as a minimum slip rate for the Garlock fault in Pilot Knob Valley. The 3-9 mm/yr slip rate in Pilot Knob Valley suggests that the average recurrence interval for large earthquakes on this part of the fault is 200-1300 yr (Table 3-6).

A Holocene, right-lateral slip rate of 2.4 ± 0.8 mm/yr on the N20W trending Panamint Valley fault was determined by Zhang and others (1990). Farther north along the fault, Burchfiel and others (1987) estimated a 2-3.2 mm/yr, N60W

displacement rate for the block west of the Panamint Valley fault relative to the block east of the fault, since Plio-Pleistocene time. Resolved onto the N75E-striking Garlock fault, these motions would produce an additional 0.2 to 2 mm/yr of left-lateral slip on that fault. This suggests that the slip rate of the Garlock fault east of Panamint Valley may be up to 2 mm/yr less than the rate in Pilot Knob Valley. The minimum slip rate near Leach Lake and in the Avawatz Mountains is thus probably 1 mm/yr. The 1-9 mm/yr slip rate of the eastern Garlock fault suggests an average recurrence interval of 200-3000 yr for large events on this part of the fault.

The 1 mm/yr value is a very conservative estimate of the minimum slip rate for this part of the fault. Relationships presented by Butler and others (1988) suggest that the slip rate along the western subzone of the southern Death Valley fault zone has been 3 mm/yr for the past 12 m.y. If this rate is valid for the Holocene (a condition that may not be true), it would result in a 2 mm/yr component of left-lateral slip on the Garlock fault, which trends roughly east-west in this area. If thrust faults along the eastern front of the Avawatz Mountains have been active in the Quaternary, as suggested by Brady and Troxel (1981) and by Brady (1986, pp.136-137), this would also contribute to the left-lateral slip rate of the eastern Garlock fault. The 3000-yr maximum recurrence interval for the eastern Garlock fault may thus overestimate considerably the true recurrence interval for this part of the fault.

The large range of plausible recurrence intervals (Table 3-6) underscores the importance of determining the slip rate at other points along the central and eastern

Garlock fault and of directly dating prehistoric earthquakes.

The recurrence intervals reported in Table 3-6 are consistent with previous estimates of the recurrence interval on the central Garlock fault. The 600- to 1200-yr average recurrence interval for the segment of the fault south of El Paso Mountains overlaps the 900- to 1700-yr average recurrence interval determined by Burke and Clark (1978) at Koehn Lake. Farther east, Roquemore and others (1982) found evidence for a minimum of 6 Holocene faulting events in a trench across the fault near Christmas Canyon (in Searles Valley), suggesting a *maximum* recurrence interval of about 1700 yr for this part of the fault. The results presented in this chapter suggest that this maximum value substantially overestimates the actual recurrence interval for the Garlock fault in Searles Valley.

Eastern termination of the Garlock fault

The lateral offsets measured in the Avawatz Mountains do not decrease gradually towards the eastern end of the fault, as typically occurs at the end of historical ruptures. Left-lateral offsets of about 3 m are found within about 250 m of the easternmost recognizable feature attributable to Holocene faulting on the Garlock fault, and within about 1.3 km of the eastern end of the Garlock fault as mapped in bedrock by Brady (1986; his Leach Lake branch of the Garlock fault zone). This suggests that the slip in the latest earthquake tapered from about 3 m to 0 m within no more than 1.3 km and possibly within as little as a few hundred meters along strike.

Displacements in the vicinity of the rupture endpoints of most historical, strike-slip fault ruptures with displacements larger than 1 m have not been well documented. However, the large displacement gradient indicated at the east end of the Garlock fault appears to be atypical of historical, strike-slip earthquakes. Displacement along the North Anatolian fault (Turkey) associated with the 1967 Mudurnu Valley earthquake tapered from a maximum of 1.9 m to 0 m at one end of the rupture over a distance of 13.5 km (Ambrasseys and Zatopek, 1969). Even along ruptures with smaller displacements, the offset near the ends of the rupture typically decreases gradually over a distance of a few km along strike (Clark, 1972; Williams and Magistrale, 1989). One exception is the surface rupture associated with the 1979 Imperial Valley (California) earthquake. At the south end of this rupture, surface slip decreased from 55 cm to 4 cm within about 400 m along strike (Sharp and others, 1982), although subsurface slip continued farther south (Hartzell and Helmberger, 1982).

In a more general sense, the eastern termination of the Garlock fault in the Avawatz Mountains is not surprising. The eastern limit of Holocene faulting along the Garlock fault zone (Clark, 1973) is not far from the eastern limit of recent basin and range extension north of the fault (Davis and Burchfiel, 1973; Zhang and others, 1990), and is near an east-vergent, reverse fault system south of the fault, along the eastern front of the Avawatz Mountains (Brady and Troxel, 1981; Brady, 1986, pp.136-137). Davis and Burchfiel (1973) proposed that the pre-Quaternary eastern limit of the Garlock fault lay beneath Kingston Wash (several tens of km east of the

eastern limit of Holocene faulting on the Garlock fault) because they viewed as unlikely the 300% extension that would otherwise be required between the Spangler Hills and the Death Valley fault zone. Recent work suggesting the presence of low-angle normal faults in Panamint and Death Valleys indicates that such extreme values of extension may have occurred in this region (Wernicke and others, 1988; Burchfiel and others, 1987; MIT 1985 Field Geophysics Course and Biehler, 1987; Hodges and others, 1989; Stewart, 1983). If the Avawatz Mountains were thrust over the terrain to the east by a significant amount, this would also reduce the amount of extension required north of the Garlock fault. Thus, termination of the Garlock fault in the Avawatz Mountains may not be as unreasonable as it once seemed. Brady (1986, Chapter 6) also presents several arguments for termination of the Garlock fault in the Avawatz Mountains.

CONCLUSIONS

Geomorphic features offset by small amounts across the Garlock fault suggest that the most recent earthquake along the easternmost 90 km of the Garlock fault was produced by about 2-3 m of left-lateral slip, and that several previous events probably involved a similar amount of slip. Farther west, south of El Paso Mountains, the latest 2 earthquakes probably involved about 7 m of left-lateral slip each, whereas the third event back was probably produced by about 4 m of slip.

A number of rupture patterns for the Garlock fault are plausible, ranging from rupture of the entire fault in a single $M_w \leq 7.8$ event to separate rupture of shorter

fault segments, resulting in $M_w=6.6$ to $M_w=7.5$ earthquakes. Consideration of the slip rates for various parts of the Garlock fault suggests average recurrence intervals of 600-1200 yr south of El Paso Mountains, of 200-750 yr in Searles Valley, of 200-1300 yr in Pilot Knob Valley and of 200-3000 yr near Leach Lake and in the Avawatz Mountains. The large range of plausible recurrence intervals, the possibility of recurrence intervals as short as a few hundred years, and the uncertainty in the age of the youngest rupture along different portions of fault warrant further slip-rate and paleoseismic investigations of the central and eastern Garlock fault.

REFERENCES

Aki, K., How to find the nucleation point of an earthquake faulting? *Seism. Res. Lett.*, 58, 31, 1987.

Ambrasseys N. N. and J. S. Tchalenko, The Dasht-e Bayaz (Iran) earthquake of August 31, 1968: a field report, *Seism. Soc. Am. Bull.*, 59, 1751-1792, 1969.

Ambrasseys, N. N. and A. Zatopek, The Mudurnu Valley, West Anatolia, Turkey, earthquake of 22 July 1967, *Seism. Soc. Am. Bull.*, 59, 521-589, 1969.

Bard, E., B. Hamelin, R. G. Fairbanks, and A. Zindler, Calibration of the C-14 timescale over the past 30,000 years using mass-spectrometric U-Th ages from Barbados corals, *Nature*, 345, 405-410, 1990.

Barka, A. A., and K. Kadinsky-Cade, Strike-slip fault geometry in Turkey and its influence on earthquake activity, *Tectonics*, 7, 663-684, 1988.

Bonilla, M. G., R. K. Mark, and J. J. Lienkaemper, Statistical relations among earthquake magnitude, surface rupture length, and surface fault displacement, *Bull. Seismol. Soc. Am.*, 74, 2379-2411, 1984.

Brady, R. H., Cenozoic geology of the northern Avawatz Mountains in relation to the intersection of the Garlock and Death Valley fault zones, San Bernardino County, California, *Ph. D. Dissertation, Univ. of Calif., Davis, Calif.*, 292 pp., 1986.

Brady, R. H., and B. W. Troxel, Eastern termination of the Garlock fault in the Avawatz Mountains, San Bernardino County, California (abstract), *Geol. Soc. Am. Abstracts with Programs*, 13, 46-47, 1981.

Brune, J. N., Seismic moment, seismicity and rate of slip along major fault zones, *J. Geophys. Res.*, 73, 777-784, 1968.

Bucknam, R. C., G. Plafker, and R. V. Sharp, Fault movement (afterslip) following the Guatemala earthquake of February 4, 1976, *Geology*, 6, 170-173, 1978.

Burchfiel, B. C., K. V. Hodges, and L. H. Royden, Geology of Panamint Valley-Saline Valley pull-apart system, California: palinspastic evidence for low-angle geometry of a Neogene range-bounding fault, *J. Geophys. Res.*, 92, 10422-10426, 1987.

Burke, D. B., Log of a trench in the Garlock fault zone, Fremont Valley, California, *U. S. Geol. Surv. Map MF-1028*, 1979.

Burke, D. B., and M. M. Clark, Late Quaternary activity along the Garlock fault at Koehn Lake, Fremont Valley, California (abstract), *EOS, Trans. Am. Geophys. Union*, 59, 1126, 1978.

Butler, P. R., B. W. Troxel, and K. L. Verosub, Late Cenozoic history and styles of deformation along the southern Death Valley fault zone, California, *Geol. Soc. Am. Bull.*, 100, 402-410, 1988.

Carter, B. A., Quaternary displacement on the Garlock fault, California, in Fife D. L., and A. R. Brown, eds., *Geology and Mineral Wealth of the California Desert*, Santa Ana, California, South Coast Geological Society, pp. 457-466, 1980.

Carter, B., Neogene displacement on the Garlock fault, California, *EOS, Trans. Am. Geophys. Union*, 63, 1124, 1982.

Clark, M. M., Some characteristics of the most recently active traces of the Garlock

fault, *Geol. Soc. Am., Abstracts with Programs*, 2, 82, 1970.

Clark, M. M., Surface rupture along the Coyote Creek fault, in *The Borrego Mountain earthquake of April 9, 1968, U. S. Geol. Survey Prof. Paper 787*, 55-87, 1972.

Clark, M. M., Map showing recently active breaks along the Garlock and associated faults, California, *U.S. Geol. Surv. Misc. Geol. Inv. Map, I-741*, 1973.

Clark, M. M., K. K. Harms, J. J. Lienkaemper, D. S. Harwood, K. R. Lajoie, J. C. Matti, J. A. Perkins, M. J. Rymer, A. M. Sarna-Wojcicki, R. V. Sharp, J. Simms, J. C. Tinsley III, and J. I. Ziony, Preliminary slip-rate table and map of Late Quaternary faults of California, *U. S. Geol. Survey Open File Rept. 84-106*, 12 pp., 1984.

Clark, M. M. and K. R. Lajoie, Holocene behavior of the Garlock fault, *Geol. Soc. Am., Abstracts with Programs*, 6, 156-157, 1974.

Davis G. A., and B. C. Burchfiel, Garlock fault: an intracontinental transform structure, southern California, *Geol. Soc. Am. Bull.*, 84, 1407-1422, 1973.

Eberhart-Phillips, D., M. Lisowski, and M. D. Zoback, Crustal strain near the big bend of the San Andreas fault: analysis of the Los Padres-Tehachapi trilateration networks, California, *J. of Geophys. Res.*, 95, 1139-1153, 1990.

Guptill, P., D. Collins, and E. Heath, Quaternary displacements on the south branch of the Garlock fault, Tehachapi Mountains, California, *Geol. Soc. Am., Abstracts with Programs*, 11, 81, 1979.

Hanks, T. C., and H. Kanamori, A moment-magnitude scale, *J. Geophys. Res.* 84, 2348-2350, 1979.

Hartzell, S. and D. V. Helmberger, Strong-motion modeling of the Imperial Valley earthquake of 1979, *Seismol. Soc. Am. Bull.*, 72, 572-596, 1982.

Hodges, K. V., L. W. McKenna, J. Stock, J. Knapp, L. Page, K. Sternlof, D. Silverberg, G. Wust, and J. D. Walker, Evolution of extensional basins and basin and range topography west of Death Valley, California, *Tectonics*, 8, 453-467, 1989.

Jennings, C. W., Fault map of California, Calif. Div. of Mines and Geol., *Calif. Data Map Series 1*, 1985.

King, G. C. P. and Nabalek, J., The role of bends in faults in the initiation and termination of earthquake rupture, *Science*, 228, 984-987, 1985.

Knuepfer, P. L. K., M. J. Bamberger, J. M. Turko, and K. J. Coppersmith, Characteristics of the boundaries of historical surface fault ruptures, *Seism. Res. Lett.*, 58, 31, 1987.

LaViolette, J. W., G. E. Christenson, and J. C. Stepp, Quaternary displacement on the western Garlock fault, southern California, in Fife, D. L. and A. R. Brown, eds., *Geology and Mineral Wealth of the California Desert*, Santa Ana, California, South Coast Geol. Soc., pp. 449-456, 1980.

Lawson, A. C., ed. *The California earthquake of April 18, 1906, Report of the State Earthquake Investigation Commission*, Carnegie Inst. Washington Publ. 87, 451 pp., 1908.

Lindvall, S. C., T. K. Rockwell, and K. W. Hudnut, Evidence for prehistoric earthquakes on the Superstition Hills fault from offset geomorphic features,

Bull. Seism. Soc. Am., 79, 342-361, 1989.

Louie, J. N., C. R. Allen, D. C. Johnson, P. C. Haase, and S. N. Cohn, Fault slip in southern California, *Bull. Seism. Soc. Am.*, 75, 811-833, 1985.

Mark, R. K., Application of linear statistical models of earthquake magnitude versus fault length in estimating maximum expectable earthquakes, *Geology*, 5, 464-466, 1977.

MIT 1985 Field Geophysics Course and S. Biehler, A geophysical investigation of the northern Panamint Valley, Inyo County, California: evidence for possible low-angle normal faulting at shallow depth in the crust, *J. Geophys. Res.*, 92, 10,427-10,441, 1987.

Rockwell, T. K., and C. T. Pinault, Holocene slip events of the southern Elsinore fault, Coyote Mountains, southern California, in *Neotectonics and Faulting in Southern California: Geol. Soc. Am. Guidebook for the Cord. Sect. Meeting in Los Angeles*, pp. 193-196, 1986.

Rodgers, D. A., Vertical deformation, stress accumulation and secondary faulting in the vicinity of the Transverse Ranges of southern California, *Calif. Div. of Mines and Geol. Bull.* 203, 74 pp, 1979.

Roquemore, G. R., P. E. Smith, and E. W. Banks, Holocene earthquake activity of the eastern Garlock fault in Christmas Canyon, San Bernardino County, California, *Abstracts with Programs, Cordilleran Section, Geol. Soc. Am.*, 14, 228, 1982.

Rundle, J. B., A physical model for earthquakes, 2. Application to southern

California, *J. Geophys. Res.*, 93, 6255-6274, 1988.

Sharp, R. V., Comparison of 1979 surface faulting with earlier displacements in the Imperial Valley, in *The Imperial Valley, California, Earthquake of October 15, 1979, U. S. Geol. Surv. Profess. Paper 1254*, 213-221, 1982.

Sharp, R. V., J. J. Lienkaemper, M. G. Bonilla, D. B. Burke, B. F. Cox, D. G. Heard, D. M. Miller, D. M. Morton, D. J. Ponti, M. J. Rymer, J. C. Tinsley, J. C. Yount, J. E. Kahle, E. W. Hart, and K. E. Sieh, Surface faulting in Central Imperial Valley, in *The Imperial Valley, California, Earthquake of October 15, 1979, U. S. Geol. Surv. Profess. Paper 1254*, 119-143, 1982.

Sibson, R. H., Roughness at the base of the seismogenic zone: contributing factors, *J. Geophys. Res.*, 89, 5791-5799, 1984.

Sibson, R. H., Stopping of earthquake ruptures at dilational fault jogs, *Nature*, 316, 248-251, 1985.

Sieh, K. E., Slip along the San Andreas fault associated with the great 1857 earthquake, *Bull. Seism. Soc. Am.*, 68, 1421-1448, 1978.

Slemmons, D. B., A. E. Jones, and J. I. Gimlett, Catalog of Nevada earthquakes, 1852-1960, *Bull. Seism. Soc. Am.*, 55, 537-583, 1965.

Smith, G. I. , Holocene movement on the Garlock fault, *U. S. Geol. Surv. Profess. Pap. 975*, p. 202, 1975.

Smith, G. I., B. W. Troxel, C. H. Gray, Jr., and R. von Huene, Geologic Reconnaissance of the Slate Range, San Bernardino and Inyo Counties, California, *Calif. Div. of Mines and Geol. Special Report 96*, 1968.

Snay, R. A., and M. W. Cline, Crustal movement investigations at Tejon Ranch California, *Natl. Oceanic and Atmosph. Adm. Technical Rept. 87*, 1980.

Stewart, J. H., Extensional tectonics in the Death Valley area, California: Transport of the Panamint Range structural block 80 km northwestward, *Geology*, 11, 153-157, 1983.

Toppozada, T. R., D. L. Parke, and C. T. Higgins, Seismicity of California, 1900-1931. *Calif. Div. of Mines and Geol. Special Report 135*, 1978.

Wernicke, B., G. J. Axen, and J. K. Snow, Basin and Range extensional tectonics at the latitude of Las Vegas, Nevada, *Geol. Soc. Am. Bull.*, 100, p.1738-1757, 1988.

Williams, P. L., and H. W. Magistrale, Slip along the Superstition Hills fault associated with the 24 November 1987 Superstition Hills, California, earthquake, *Seism. Soc. Am. Bull.*, 79, 390-410, 1989.

Zhang, W., D. Jiao, P. Zhang, P. Molnar, B. C. Burchfiel, Q. Deng, and Y. Wang, Displacement along the Haiyuan fault associated with the great 1920 Haiyuan, China, earthquake, *Bull. Seism. Soc. Am.*, 77, 117-131, 1987.

Zhang, P., M. Ellis, D. B. Slemmons, and F. Mao, Right-lateral displacements and the Holocene slip rate associated with prehistoric earthquakes along the southern Panamint Valley fault zone: implications for southern basin and range tectonics, *J. Geophys. Res.*, 95, 4857-4872, 1990.

CHAPTER 4**AGE OF THE MOST RECENT SLIP EVENT
ALONG THE GARLOCK FAULT IN SEARLES VALLEY****ABSTRACT**

Stratigraphic relations exposed in two trenches across the Garlock fault in Searles Valley provide clear evidence for several late Holocene, prehistoric faulting events. A radiocarbon date on detrital charcoal from one of the trenches indicates that the most recent surface-faulting event on this portion of the Garlock fault occurred no more than 530 years ago. This earthquake probably had a magnitude in the range of $M_w = 7.2$ to $M_w \leq 7.8$. Historical evidence suggests that this event occurred more than about 90 years ago. These constraints and previous estimates of the recurrence interval for this portion of the fault suggest that the next large earthquake on the Garlock fault in Searles Valley will occur within the next 660 yr and could, in fact, be overdue.

INTRODUCTION

The Garlock fault is an active, left-lateral, strike-slip fault that abuts the San Andreas fault near Gorman and extends northeastward about 250 km to the southern end of Death Valley (Figure 4-1). The fault is not known to have produced large earthquakes during the period of historical record, but the presence of small fault scarps and offset geomorphic features along much of the fault attests to the

FIGURE 4-1: Reference map shows location of paleoseismic site and other places mentioned in text. In this paper, the portion of the Garlock fault extending from the San Andreas fault to Koehn Lake is termed the western Garlock fault; that portion extending from Koehn Lake to the Quail Mountains is termed the central Garlock fault, and that portion extending eastward from the Quail Mountains is termed the eastern Garlock fault.

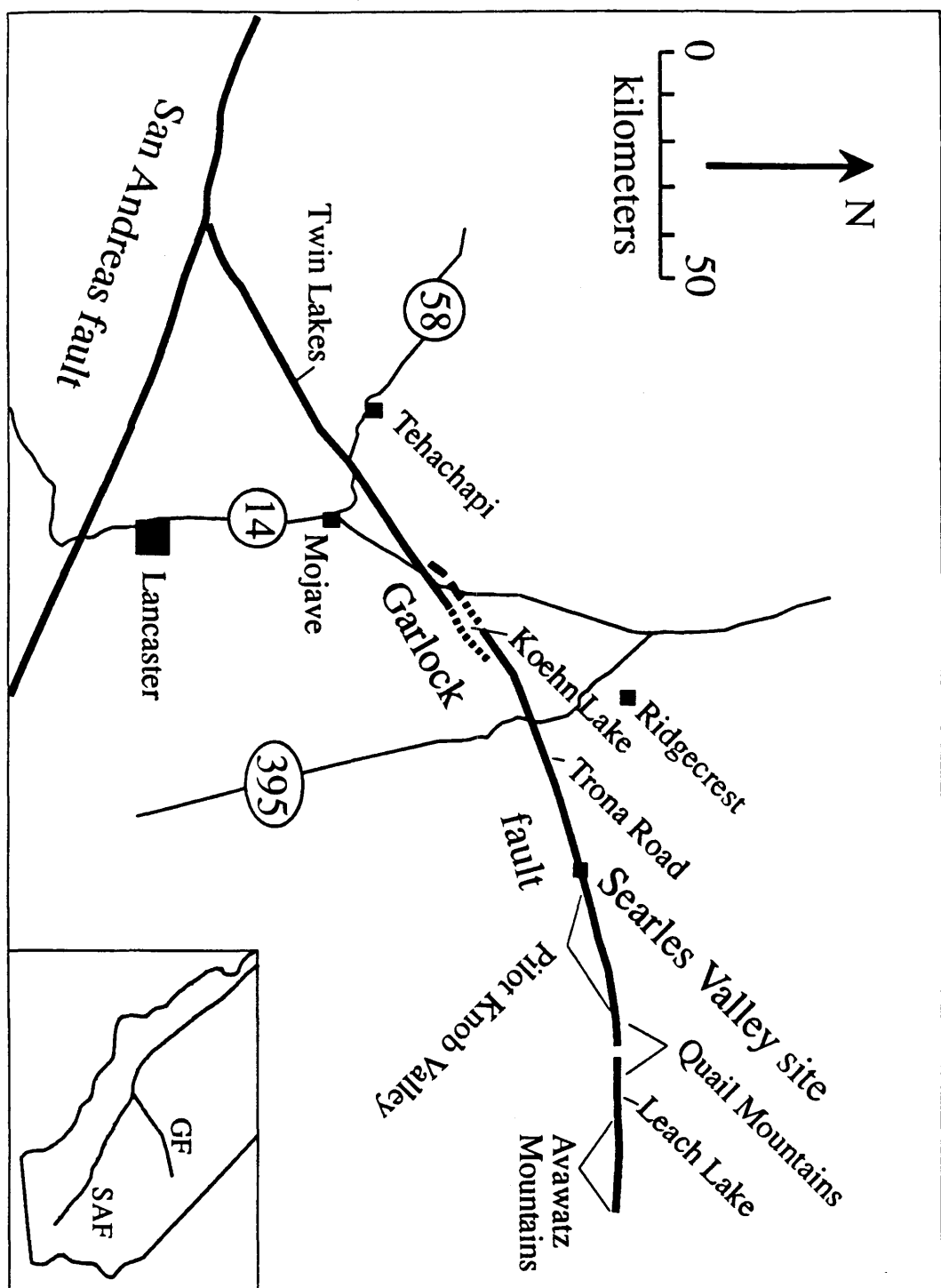


Figure 4-1

occurrence of recent prehistoric earthquakes on the fault (Clark, 1970, 1973; McGill and Sieh, 1991, and Chapter 3 of this dissertation). Left-lateral offsets of 2-3 m appear to have accompanied the most recent event in Searles Valley (McGill and Sieh, 1991, and Chapter 3 of this dissertation). Smith (1975), Burke and Clark (1978), LaViolette and others (1980), Roquemore and others (1982), and McGill and Sieh (1991, and Chapter 3 of this dissertation) have estimated recurrence intervals for large earthquakes at various localities along the fault. Prior to the work described herein, however, the date of the most recent event had not been constrained by radiocarbon dating anywhere along the central or eastern part of the fault. In this paper I present evidence that the latest earthquake on the Garlock fault in Searles Valley occurred no more than 530 years ago.

DESCRIPTION OF SITE

Two trenches across the Garlock fault in Searles Valley, 1.9 km west-southwest of the mouth of Christmas Canyon, reveal evidence for several prehistoric faulting events. The trenches, about 30 m apart, expose alluvial fan sediments derived from low hills composed predominantly of sandstone, siltstone and conglomerate of the Pleistocene Christmas Canyon Formation (Smith, 1964). At the trench site, the fault is buried by modern alluvium, but fault scarps are present in older alluvium about 150 m to the west and east of the site (Figure 4-2).

The trenches expose alluvial-fan sediments, including poorly sorted, pebble- and small-cobble-rich gravel layers, moderately sorted, coarse sand and granule

FIGURE 4-2: Photo-geologic map of the trench site. Channels drain northward.

Scale is approximate.

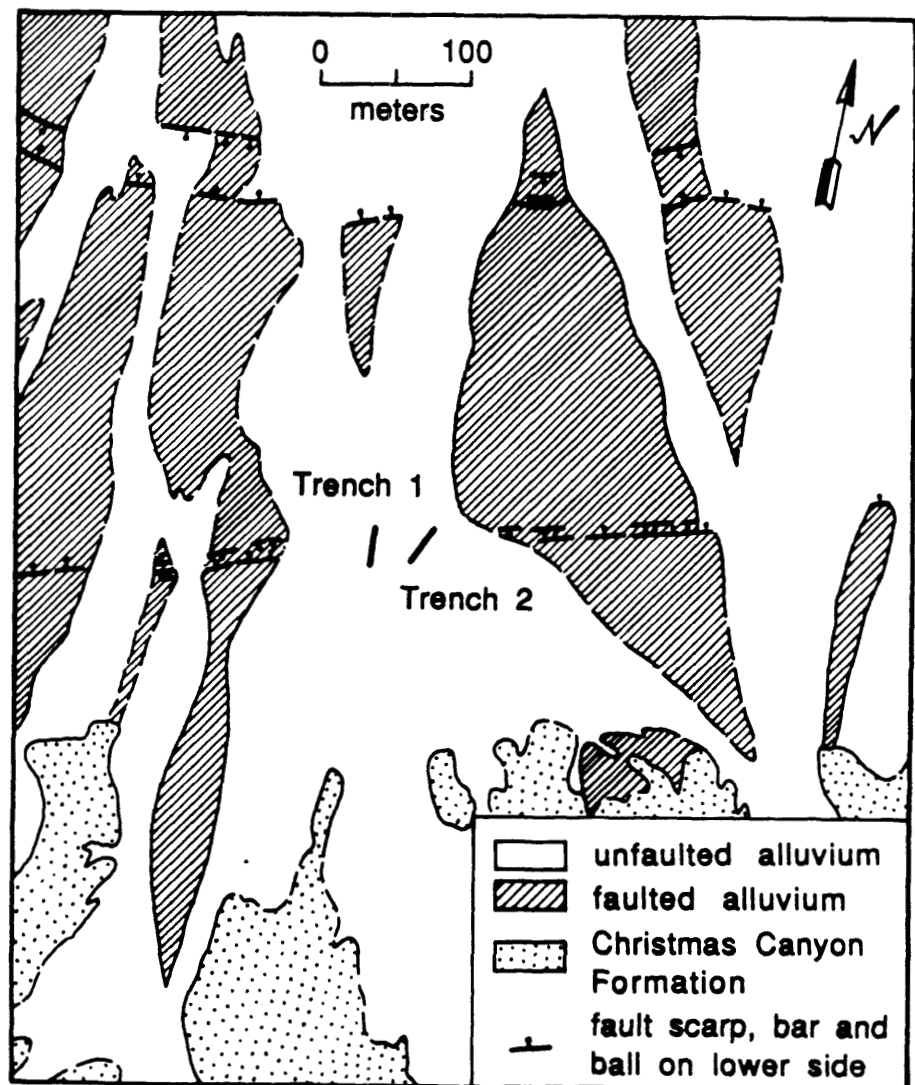


Figure 4-2

layers, a few silt lenses, and massive, unsorted units thought to be bioturbated regions below former ground surfaces. In addition, well-cemented, laminated silt and silty sand, which may be lacustrine deposits of Pleistocene Searles Lake, occur in the lower part of one trench. The sediments are faulted across a 13-m-wide zone, which includes fault strands with major strike-slip displacements, as evidenced by dramatic facies changes across the strands, as well as other strands with minor, apparently normal and reverse displacements (Figure 4-3). Only portions of some of the cross sections along the trench walls are presented here. Copies of the undrafted, field cross sections constitute plates 3-5.

In the southern portion of Trench 1 is evidence for at least 3 and probably 4 faulting events (Figure 4-4). The most recent event involved unit 3 and lower units. Any scarps formed during this event were scoured by fluvial erosion prior to deposition of unit 2, which is unfaulted and extends for the entire length of Trench 1. The penultimate event occurred after unit 4 was deposited. Several small scarps of fault zone D associated with this event were buried by unit 3. Evidence for the third event back consists of a pebble layer (unit 7) and underlying units that were tilted and faulted, especially along fault zones A and B (Figure 4-4), prior to deposition of unit 5. In addition, several fissures in units 7-10 were filled prior to deposition of unit 5 (faults B, D and south of fault A, Figure 4-4). A fourth event is indicated by tilted unit 15 overlain by flat-lying units 14 and 10 and by upward termination of two strands of fault C. The dramatic facies change across faults A and B in the lower part of the trench, where thickly bedded gravels (units 11-13) are

FIGURE 4-3: Cross section along the eastern wall of Trench 1 illustrates the width and character of the fault zone. Some of the alluvial units that can be correlated across various fault strands are shaded.

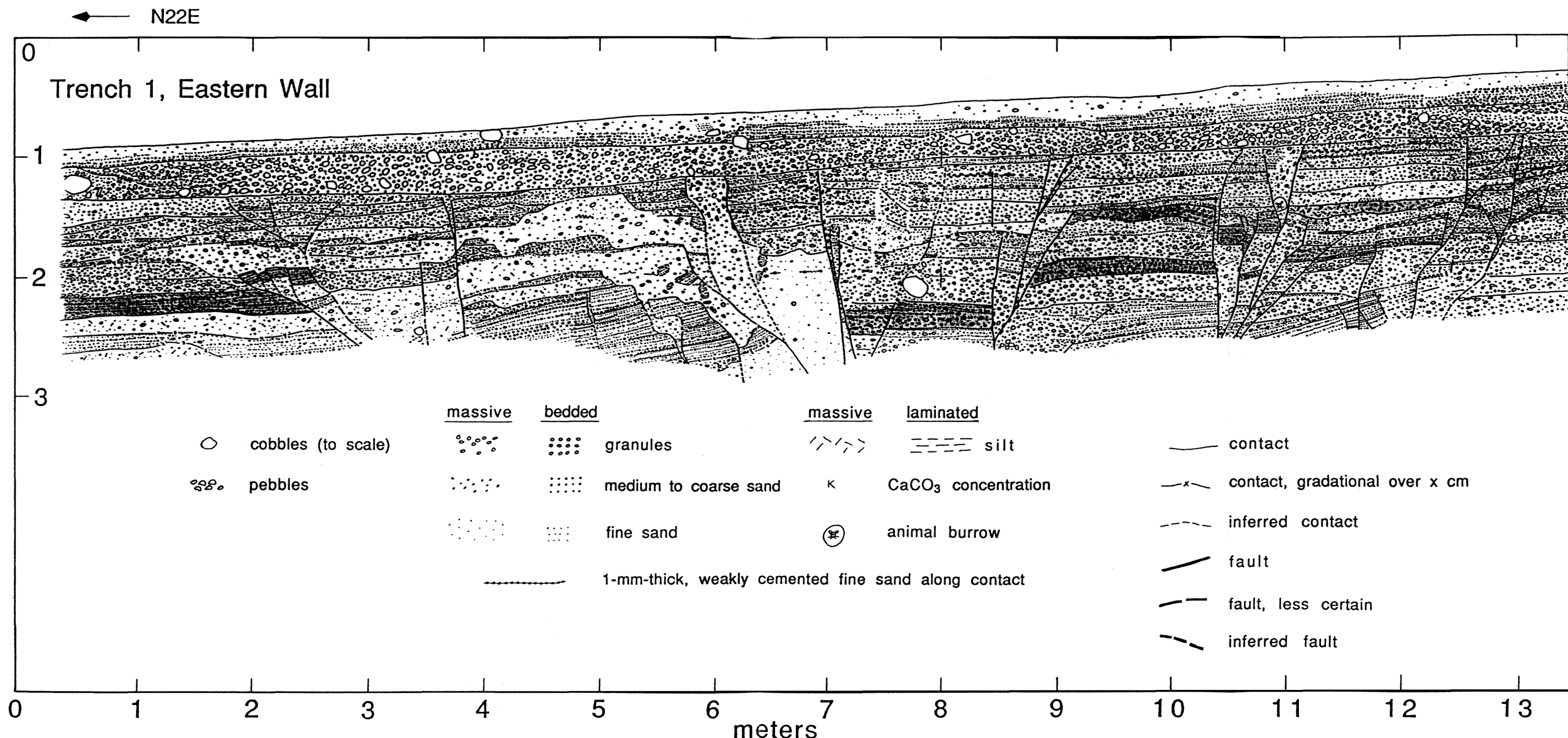


Figure 4-3

FIGURE 4-4: Cross section along the southern portion of the eastern wall of Trench 1. Stratigraphic units are numbered; faults are lettered. Units 4 and 10 have been shaded to aid in correlation of units. Events 1, 2, 3 and 4 indicate stratigraphic horizons that represent the ground surface at the time of ancient faulting events. Event 1 is well expressed along faults A, B and D. Event 2 is expressed as small, buried fault scarps within fault zone D. Event 3 is best expressed by tilted beds, filled fissures and upward fault termination along faults A, B and south of fault A, but it is also expressed by upward fault termination along fault C and along the southernmost strand of fault D. A fourth event is indicated by tilted unit 15 overlain by flat-lying unit 10 and by termination of two strands of fault C at the top of unit 15. The facies change across faults A and B beneath unit 10 also suggests an event at this horizon.

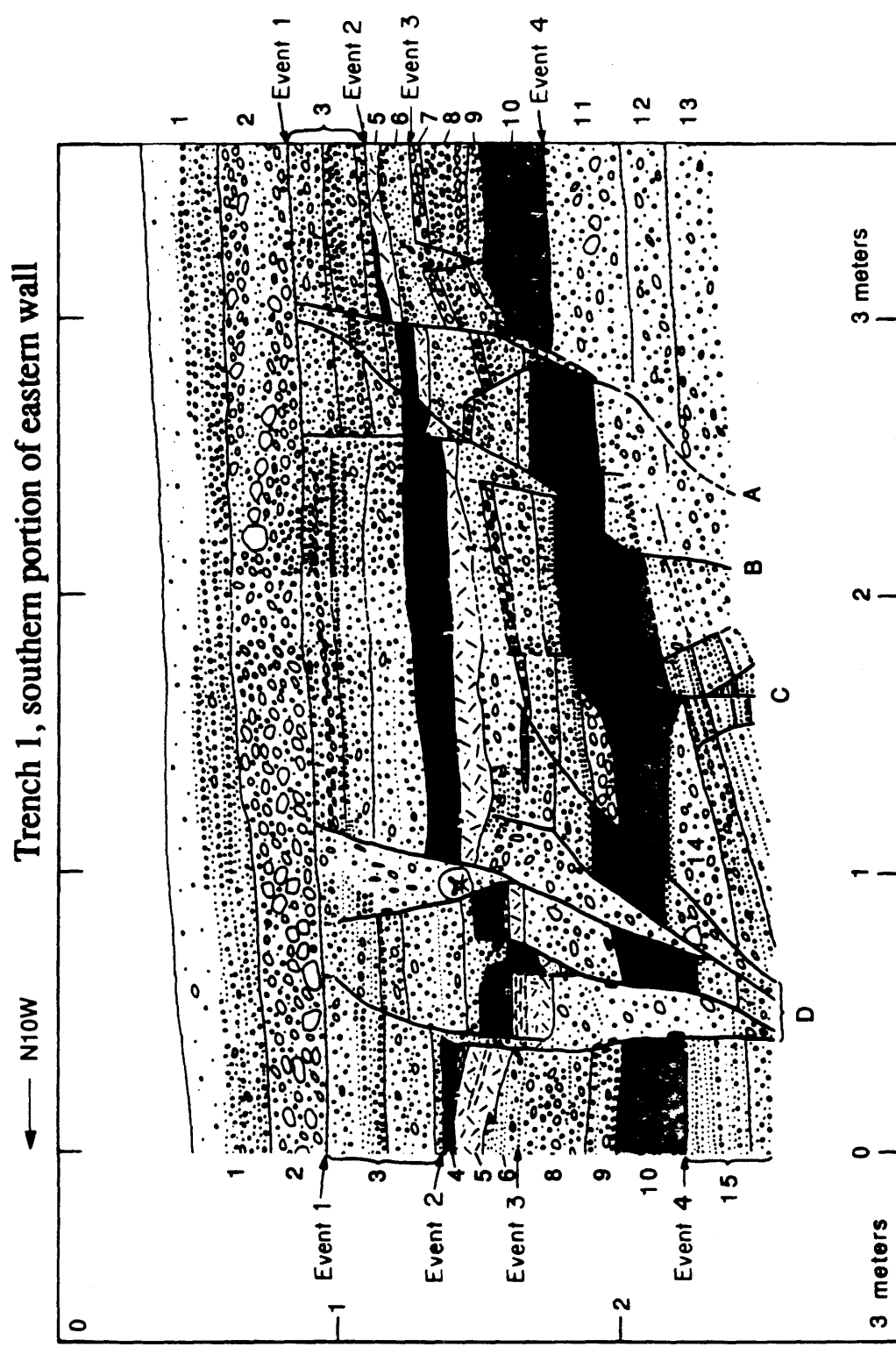


Figure 4-4

Trench 1, East Wall

22lb

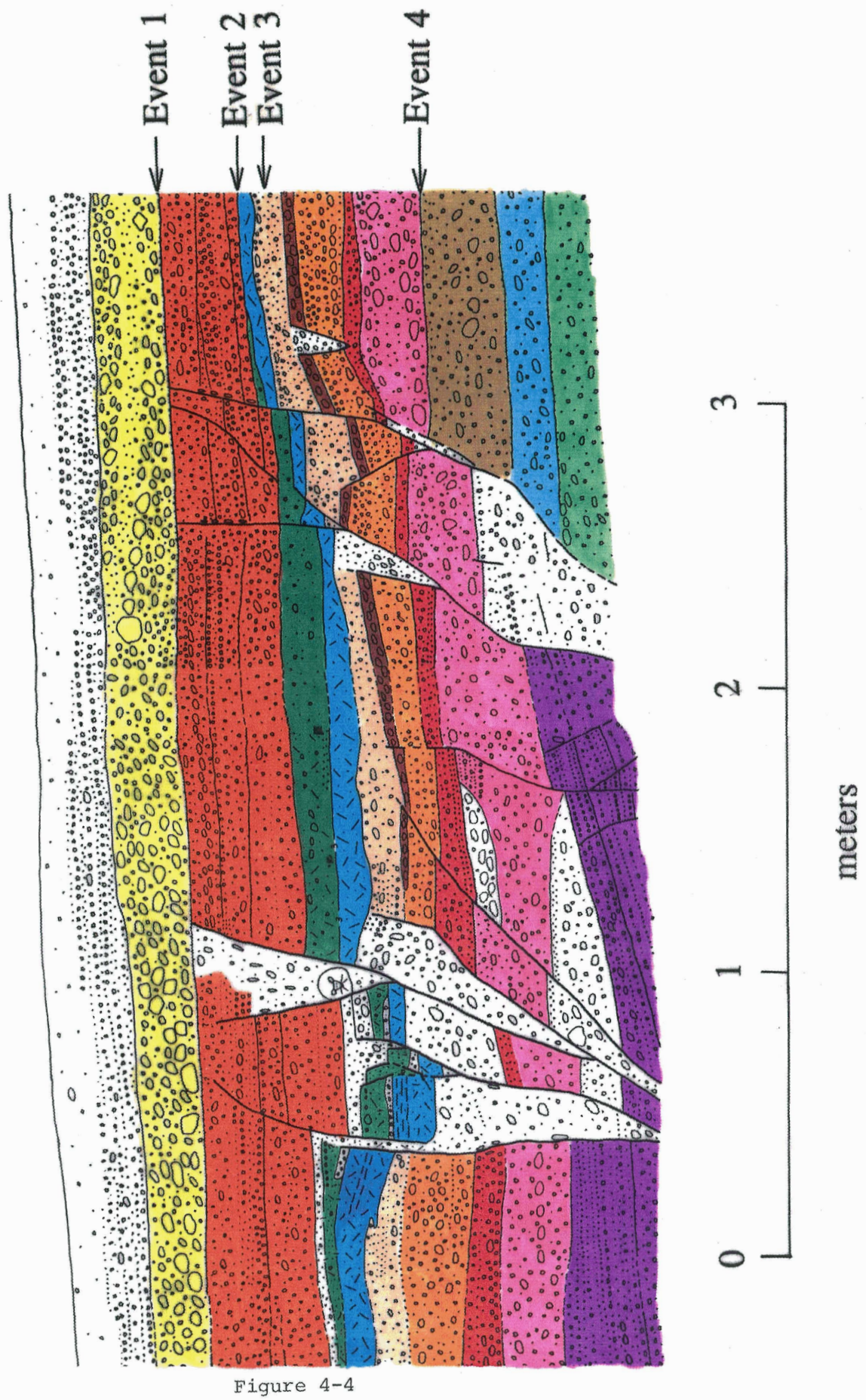


Figure 4-4

meters

juxtaposed against thinly bedded sands (unit 15) also supports a faulting event at this stratigraphic level. This relationship could be explained by strike-slip faulting on fault A and/or B prior to deposition of unit 10, which is the lowest unit that can be correlated across faults A and B.

CONSTRAINTS ON THE AGE OF THE LATEST EARTHQUAKE

Four faulting events are also present in Trench 2 (Figure 4-5), but it is not known whether these are the same four events that were found in Trench 1. The laterally discontinuous nature of alluvial fan sediments made certain correlation of stratigraphic units between the two trenches impossible. A charred twig, labelled T2E-2 in Figure 4-5, was found beneath the shaded gravel bed, which was faulted in the most recent earthquake. The twig is thus older than the most recent large earthquake on this part of the fault. The charred twig was dated at the University of Arizona by Accelerator Mass Spectrometry radiocarbon dating. The fraction of modern carbon contained in the twig was 0.9697, and the measured value of $\delta^{13}\text{C}$ was -23.75 per mil (A. J. T. Jull, written communication; Univ. of Ariz. sample #AA-5774). This yields a conventional radiocarbon age of 267 ± 60 radiocarbon yr B.P.

The program CALIB (Stuiver and Reimer, 1986) was used to calculate the calendric age of the sample, based on the dendrochronologic time scale. No error multiplier was included in this calculation because the error quoted by the NSF-Arizona Accelerator Mass Spectrometry facility is based on the overall reproducibility of results in that lab. The calendric date ranges that correspond to the radiocarbon

FIGURE 4-5: Cross section from the central part of the eastern wall of Trench 2. The shaded gravel unit was faulted in the most recent event. Radiocarbon sample T2E-2 (filled square) was found beneath this gravel bed and provides a maximum age for the most recent event.

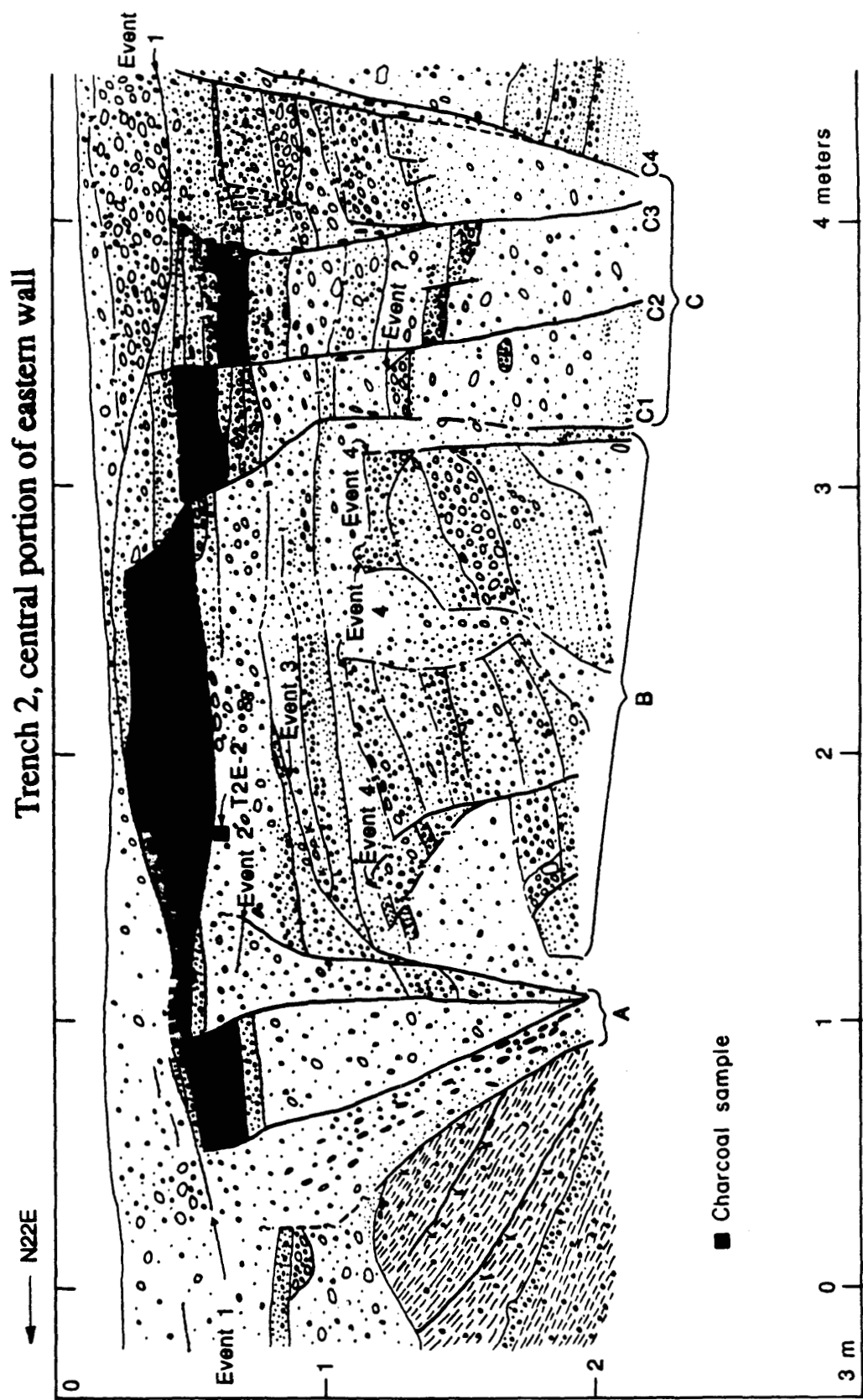


Figure 4-5

TRENCH 2, EAST WALL

224b



Figure 4-5

age of the sample are A.D. 1460 to 1680, A.D. 1733 to 1807, and A.D. 1935 to 1954.

The youngest of these 2σ ranges can be excluded on the basis of the historical dormancy of the Garlock fault (see below).

The age of this sample is a maximum age for the latest event, because an unknown period of time may have elapsed 1) between the death of the twig and its deposition, and 2) between deposition of the charred twig and faulting of the overlying gravel bed (shaded in Figure 4-5). The only way in which the age of this sample would not represent a maximum age for the most recent event would be if the charcoal fragment was not deposited contemporaneously with the unit in which it was found, but rather was emplaced later through bioturbation. Although there are no recognizable animal burrows in the unit from which sample T2E-2 was collected, the fairly massive, poorly sorted nature of this unit might make recognition of burrows difficult or impossible. Two fecal pellets(?) collected from a massive, poorly sorted unit exposed in the western wall of Trench 2 and beneath at least one earthquake horizon have a modern radiocarbon date, even though they were not located within a recognizable burrow. This emphasizes the importance of collecting radiocarbon samples from units with well-defined bedding so that post-depositional emplacement of the sample through bioturbation can be ruled out. Unfortunately, no carbon samples large enough to be dated were found in well-bedded units at this site. Although post-depositional emplacement of sample T2E-2 can not be ruled out, the unit from which this sample was collected is somewhat better sorted and has more depositional structure preserved than does the unit from which the modern

fecal pellets were collected. Therefore, it is less likely that unrecognizable burrows exist in the unit from which sample T2E-2 was collected. The fact that sample T2E-2 is a charcoal fragment also makes it less likely to have been emplaced through bioturbation than the fecal pellets. Thus, the 500-yr maximum age of sample T2E-2 most probably represents the maximum age for the most recent earthquake on the Garlock fault in Searles Valley.

It is also possible that more than one faulting event has occurred since deposition of sample T2E-2. The relation between this sample and a fault strand that may have ruptured in the penultimate event (labelled event 2 in Figure 4-5) is obscure. It is possible (though by no means required by the stratigraphic relations) that this penultimate event may also have occurred *after* deposition of sample T2E-2. It is also conceivable that other faulting events have occurred that are not recorded in this stratigraphic section because of a lack of deposition between any two earthquakes. Thus, at least one and possibly more than one large earthquake has occurred on the Garlock fault in the past 500 years.

Historical data indicate that the most recent event probably occurred before 1903 A.D. The most recent earthquake on the part of the Garlock fault in Searles Valley probably involved 2-3 m of left-lateral displacement (McGill and Sieh, 1991, and Chapter 3 of this dissertation), and thus was probably larger than $M_s = 6.7$ (the size of the smallest historical earthquake associated with 2 m of strike-slip displacement [Bonilla and others, 1984; Chang and others, 1947]). No earthquakes this large have occurred near the Garlock fault since 1903 A.D. (Hanks and others,

1975). Thus, the most recent slip event on the Garlock fault in Searles Valley must have occurred between about 90 and 500 years ago.

PROBABLE TIMING AND SIZE OF THE NEXT LARGE EARTHQUAKE

Let us compare these constraints on the age of the most recent faulting event on the Garlock fault in Searles Valley with the average recurrence interval for that portion of the fault to estimate the amount of time before the next event occurs. McGill and Sieh (1991, and Chapter 3 of this dissertation) estimate the average recurrence interval for large earthquakes on the portion of the Garlock fault in Searles Valley to be 200-750 yr. Although Roquemore and others (1982) found evidence for 6 Holocene faulting events in a trench across the Garlock fault at Christmas Canyon, implying a recurrence interval of about 1700 yr, this is a maximum estimate of the recurrence interval because that trench may not have had a complete stratigraphic record of the Holocene epoch.

By combining the range of plausible dates for the most recent event (1460-1903 A.D.) with the range of plausible values for the average recurrence interval (200-750 yr), the range of plausible dates for the next large earthquake on the Garlock fault in Searles Valley is from 1660 A.D. to 2650 A.D. Despite the large range of plausible dates for the next large event, this range spans the present, indicating that it is conceivable that such an event could occur within the next few decades. If we assume that it is equally likely that the next earthquake on the Garlock fault in Searles Valley will occur at any time between the present and 2650

A.D., this suggests that the probability of a large earthquake on this part of the fault within the next 30 years is about 5% (30 yr / (2650 A.D. - 1990 A.D.)).

The approach used above ignores the variability of individual recurrence intervals about the mean recurrence interval. For comparison, an adaptation of the methods used by the Working Group on California Earthquake Probabilities (1990) is outlined below. I assume that individual recurrence intervals are lognormally distributed about the mean recurrence interval with an intrinsic uncertainty of $\sigma_I = 0.21$ (Nishenko and Buland, 1987). The uncertainty in the mean recurrence interval is termed the parametric uncertainty and is denoted by σ_P . I have chosen to use $\sigma_P = 0.33$, which corresponds to about a 95% probability that the mean recurrence interval lies between 200 yr and 750 yr. I then assume that individual recurrence intervals are lognormally distributed about the mean recurrence interval (450 yr) with a standard deviation of $\sigma = \sqrt{(\sigma_I^2 + \sigma_P^2)} = 0.39$. Following the procedures of the Working Group on California Earthquake Probabilities (1990), this yields a conditional probability of a large earthquake on the portion of the Garlock fault in Searles Valley within the next 30 yr of 18%, if the latest earthquake occurred 530 yr ago, or of less than 0.1% if the latest earthquake occurred 90 yr ago. If it is equally likely that the latest earthquake occurred any time between 90 and 530 yr ago, then the conditional probability of an event in the next 30 yr is about 9%.

I present these probabilities merely to indicate that a large earthquake on the Garlock fault in the next 30 yr is plausible, given our current knowledge of the fault. I advise caution in the use of these probabilities, because they reflect both the

analytical uncertainties in the mean recurrence interval and date of the latest event and an estimate of the stochastic uncertainty in the length of individual recurrence intervals. As future studies reduce the analytical uncertainties in the mean recurrence interval and the date of the most recent event, this estimate of the probability of another event occurring in the next 30 years may change significantly. In addition, Sieh and others (1989) showed that patterns of large earthquakes on the San Andreas fault, for example, may not be well characterized by an average recurrence interval with a probability-density function centered on the mean.

The magnitude of the next surface faulting event on the Garlock fault in Searles Valley will probably be between $M_w = 7.2$ and $M_w \leq 7.8$. McGill and Sieh (1991, and Chapter 3 of this dissertation) delineated a number of plausible rupture patterns for the most recent large event along the Garlock fault. The moment-magnitudes for those patterns involving rupture of the portion of the fault in Searles Valley range from $M_w = 7.2$, for rupture of a 77-km-long segment from Trona Road to the Quail Mountains, to $M_w \leq 7.8$ for rupture of the entire fault (McGill and Sieh, 1991, and Chapter 3 of this dissertation). On the basis of empirical equations relating acceleration at a given site to moment-magnitude and distance of the site from the rupture (Joyner and Fumal, 1985), these rupture scenarios would produce, for example, accelerations of 0.29 g to 0.34 g in Ridgecrest (population 22,000), 0.04 g to 0.12 g in Lancaster (population 95,000), and 0.01 g to 0.04 g in Los Angeles. As mentioned above, a lower bound on the size of the next event in Searles Valley is $M_s = 6.7$, the size of the smallest, historical, strike-slip earthquake produced by 2 m of

displacement (a 1946 event in Taiwan; Bonilla and others, 1984; Chang and others, 1947). A $M_s = 6.7$ event centered on Searles Valley would produce 0.20 g acceleration in Ridgecrest, 0.02 g in Lancaster and 0.01 in Los Angeles (Joyner and Fumal, 1985).

COMPARISON OF THE WESTERN AND CENTRAL GARLOCK FAULT

A number of investigators have commented on the relative degree of activity of the western and eastern Garlock faults. Fault scarps and offset geomorphic features along the central and eastern Garlock fault appear younger than those along the western part of the fault, suggesting that the central and eastern parts of the fault may have ruptured more recently than the western part (Clark, 1970, 1973). The 530-yr maximum age of the most recent faulting event in Searles Valley is consistent with this hypothesis although it does not prove it. Paleoseismic work on the western Garlock fault near Twin Lakes (LaViolette and others, 1980) indicates a maximum age of 980 ± 195 yr BP for the most recent event along that part of the fault, twice as old as the maximum age of the most recent event in Searles Valley. Unfortunately, no useful lower bound can be placed on the age of either of these events, so it is impossible to determine their relative ages definitively at this time.

In addition to the suspicion that the central and eastern parts of the fault may have ruptured more recently than the western part, comparison of the recurrence intervals along various parts of the fault suggests that the central and eastern parts of the fault rupture more frequently than the western part. The interval between the

two most recent events at Twin Lakes on the western Garlock fault was >1550 yr (Laviolette and others, 1980), whereas the average recurrence interval along the central and eastern Garlock fault is estimated to be 300-1200 yr near Highway 395, 200-750 yr in Searles Valley, 200-1300 yr in Pilot Knob Valley, and 200-3000 yr in the Avawatz Mountains (McGill and Sieh, 1991, and Chapter 3 of this dissertation). The longer recurrence interval for the western part of the fault may be due to a lower slip rate (LaViolette and others, 1980), to a larger amount of slip per earthquake (Guptill and others, 1979), to partial release of stress by aseismic creep (Louie and others, 1985; Snay and Cline, 1980; Rodgers, 1979), or to some combination of these.

CONCLUSIONS

In conclusion, the most recent large earthquake on the Garlock fault in Searles Valley occurred between 1460 AD and 1903 AD (about 90 to 530 yrs ago). When compared with the range of possible recurrence intervals for this part of the fault, this indicates that the range of plausible dates for the next large event on this part of the fault extends from 1660 A.D. to 2650 A.D. Because this range of dates includes the present, I consider rupture of the Garlock fault plausible within the next few decades. On the basis of our current knowledge of the recurrence interval and date of latest event, the probability of a large earthquake on the portion of the Garlock fault in Searles Valley is about 5-9%, but this probability may change appreciably as our knowledge of the earthquake cycle on the Garlock fault is refined. Previous estimates of the likely sizes of earthquakes on the portion of the Garlock

fault in Searles Valley (M_w = 7.2 to 7.8) indicate that accelerations in towns near the fault (such as Ridgecrest) will be 0.26-0.34 g, those in towns somewhat farther away (such as Lancaster) will be 0.04-0.12 g, and those in Los Angeles will be 0.01-0.04 g. Finally, the 530-yr maximum age of the most recent event on the Garlock fault in Searles Valley is consistent with, but does not prove, the hypothesis that the eastern part of the fault has ruptured more recently than the western part.

REFERENCES

Bonilla, M. G., R. K. Mark and J. J. Lienkaemper, J. J., Statistical relations among earthquake magnitude, surface rupture length, and surface fault displacement, *Seismological Society of America Bulletin*, 74, 2379-2411, 1984.

Burke, D. B., and M. M. Clark, Late Quaternary activity along the Garlock fault at Koehn Lake, Fremont Valley, California, *EOS, Transactions of the American Geophysical Union*, 59, 1126, 1978.

Chang, L.-S., M. Chow, and P.-Y. Chen, The Taiwan earthquake of December 5, 1946, *Taiwan Geological Survey Bulletin*, 1, 17-20, 1947.

Clark, M. M., Some characteristics of the most recently active traces of the Garlock fault, *Geological Society of America Abstracts with Programs*, 2, 82, 1970.

Clark, M. M., Map showing recently active breaks along the Garlock and associated faults, California, *U.S. Geological Survey Miscellaneous Geological Investigations Map, I-741*, 1973.

Guptill, P., D. Collins, and E. Heath, E., Quaternary displacements on the south branch of the Garlock fault, Tehachapi Mountains, California, *Geological Society of America Abstracts with Programs*, 11, 81, 1979.

Hanks, T. C., J. A. Hileman, and W. Thatcher, Seismic moments of the larger earthquakes of the southern California region, *Geological Society of America Bulletin*, 86, 1131-1139, 1975.

Joyner, W. B. and T. E. Fumal, Predictive mapping of earthquake ground motion, *U.*

S. Geological Survey Professional Paper 1360, pp. 203-220, 1985.

LaViolette, J. W., G. E. Christenson, and J. C. Stepp, Quaternary displacement on the western Garlock fault, southern California, *in* Fife, D. L. and Brown, A. R., eds., *Geology and Mineral Wealth of the California Desert*: South Coast Geological Society, pp. 449-456, 1980.

Louie, J. N., C. R. Allen, D. C. Johnson, P. C. Haase, and S. N. Cohn, Fault slip in southern California, *Seismological Society of America Bulletin*, 75, 811-833, 1985.

McGill, S. F. and K. E. Sieh, Surficial offsets along the central and eastern Garlock fault associated with prehistoric earthquakes, *J. Geophys. Res.*, 96, 21,597-21,621, 1991.

Nishenko, S. P., and R. Buland, R., A generic recurrence interval distribution for earthquake forecasting, *Seismological Society of America Bulletin*, 77, 1382-1399, 1987.

Rodgers, D. A., Vertical deformation, stress accumulation and secondary faulting in the vicinity of the Transverse Ranges of southern California, *California Division of Mines and Geology Bulletin*, 203, 74 pp., 1979.

Roquemore, G. R., P. E. Smith, and E. W. Banks, Holocene earthquake activity of the eastern Garlock fault in Christmas Canyon, San Bernardino County, California, *Geological Society of America Abstracts with Programs*, 14, p. 228, 1982.

Sieh, K. E., M. Stuiver, M., and D. Brillinger, A more precise chronology of

earthquakes produced by the San Andreas fault in California, *Journal of Geophysical Research*, 94, 603-623, 1989.

Smith, G. I., Geology and volcanic petrology of the Lava Mountains, San Bernardino County, California, *U. S. Geological Survey Professional Paper 457*, 97 pp., 1964.

Smith, G. I., Holocene movement on the Garlock fault, *U. S. Geological Survey Professional Paper 975*, p. 202, 1975.

Snay, R. A., and M. W. Cline, Crustal movement investigations at Tejon Ranch California, *Natl. Oceanic and Atmospheric Administration Technical Report 87*, 32 pp., 1980.

Stuiver, M. and P. J. Reimer, A computer program for radiocarbon age calibration, *Radiocarbon*, 28, 1022-1030, 1986.

Working Group on California Earthquake Probabilities, Probabilities of large earthquakes in the San Francisco Bay region, California, *U. S. Geological Survey Circular 1053*, 51 pp., 1990.